UMD - ATLAS

Heavy Lift Helicopter

Alfred Gessow Rotorcraft Center
Department of Aerospace Engineering
University of Maryland, College Park
College Park, MD 20742

June 1, 2005

University of Maryland

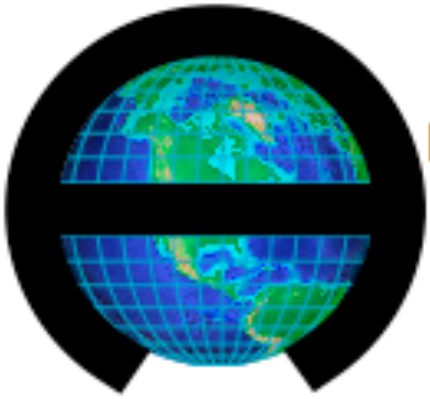

Alfred Gessow Rotorcraft Center
Department of Aerospace Engineering
University of Maryland, College Park
College Park, MD 20742

UMD - Atlas Design Proposal

In response to the 2005 Annual AHS International
Student Design Competition - Graduate Category
June 1, 2005

Benjamin Hein

Dr. Inderjit Chopra - Faculty Advisor

Eric Schroeder

Dr. V.T. Nagaraj - Faculty Advisor

Anne Brindejonc

Eric Parsons

Anirban Chaudhuri

Tim Beasman

Nicholas Rosenfeld

Eric Silberg

Acknowledgements

The Atlas design team would like to acknowledge the following people and thank them for their valuable assistance and guidance.

Dr. Vengalattore T. Nagaraj - Research Scientist, Dept. of Aerospace Engineering, University of Maryland, College Park.

Dr. Marat Tishchenko - Former Chief Designer, Mil Design Bureau.

Dr. Inderjit Chopra – Professor and Director of the Alfred Gessow Rotorcraft Center, Dept. of Aerospace Engineering, University of Maryland, College Park.

The Honorable Jacques S. Gansler, former Under Secretary of Defense for Acquisition, University of Maryland, Technology and Logistics, Roger C. Lipitz Chair in Public Policy and Private Enterprise.

Mark Robuck, Associate Technical Fellow, Drive systems, Boeing Rotorcraft.

Dr. J. Gordon Leishman - Minta Martin Professor of Engineering, Dept. of Aerospace Engineering, University of Maryland, College Park.

Dr. Fredric Schmitz - Martin Professor of Rotorcraft Acoustics, Dept. of Aerospace Engineering, University of Maryland, College Park.

LT Rich Whitfield, Squardon Quality Assurance Officer HSL41, SH-60B Instructor Pilot, USN.

Dr. Jayant Sirohi - Research Associate, Dept. of Aerospace Engineering, University of Maryland, College Park.

Paul Samuel, Joseph Conroy, Jinsong Bao, Anubhav Datta, Maria Ribera, - Graduate Students, Department of Aerospace Engineering, University of Maryland, College Park.

Table of Contents

List of Figures

List of Tables

List Symbols and Abbreviations

Active Control of Structural Response (ACSR)
Aeroflightdynamics Directorate (AFDD)
Aeronautical Design Standard – Performance Specifications (ADS-33E)
American Helicopter Society (AHS)
Angular Velocity (Ω)
Armor Piercing Incendiary (API)
Attitude Command Attitude Hold (ACAH)
Automatic Direction Finder (ADF)
Automatic Flight Control System (AFCS)
Autorotative Index (AI)
Auxiliary Power Unit (APU)
Best Endurance Speed (V_{BE})
Best Range Speed (V_{BR})
Blade Loading Coefficient (C_T/σ)
Built-In Test (BIT)
Center of Gravity (CG)
Command Display Unit (CDU)
Common Missile Warning System (CMWS)
Computer Aided Design (CAD)
Electromagnetic Interference (EMI)
Differential Global Positioning System (DGPS)
Disk Loading (DL)
Dynamic Antiresonant Vibration Isolators (DAVI)
Face Width (W)
Federal Aviation Regulations (FAR)
Flight Control Computer (FCC)
Flight Control System (FCS)
Flight Management System (FMS)
Fly By Wire (FBW)
Forward Looking Infrared (FLIR)
Fully Automated Digital Electronic Control (FADEC)
Future Combat System (FCS)
Heads Up Display (HUD)
Health and Usage Monitoring System (HUMS)
Heavy Lift Helicopter (HLH)
Helmet Mounted Display (HMD)
Hertz Index (K)
Horsepower per Load Path (P)
Hover Out of Ground Effect (HOGE)
In Ground Effect (IGE)
Inertial Navigation System (INS)
Infrared (IR)
Integrated High-Performance Turbine Engine Technology (IHPTET)
International Standard Atmosphere (ISA)
Joint Turbine Advanced Gas Generator (JTAGG)
Learning Curve Factor (LCF)
Line Replaceable Unit (LRU)
Liquid Inertia Vibration Eliminators (LIVE)
Magnetic Particulate Trap (MPT)
Magnetorheological (MR)
Maximum Gross Take Off Weight (MGTOW)
Mean Sea Level (MSL)
Multi-Function Display (MFD)
Multi-Mode Radar (MMR)
National Advisory Committee for Aeronautics (NACA)
National Aeronautics and Space Administration (NASA)
Never Exceed Speed (V_{NE})
Night Vision Goggle (NVG)
Number of Blades (N_b)
Number of Teeth on Pinion (N_p)
One Engine Inoperative (OEI)
Out of Ground Effect (OGE)
Pinion Pitch Diameter (d)
Pinion RPM (n_p)
Polar Moment of Inertia (J)
Primary Flight Control System (PFCS)
Production Quantity Factor (PQF)
Proportional Integral Derivative (PID)
Push To Talk (PTT)
Rate Command Attitude Hold (RCAH)
Rate Damping (RD)
Rate of Climb (ROC)
Reduction Ratio (m_g)
Request for Proposal (RFP)
Rotations Per Minute (RPM)
Runway Independent Aircraft (RIA)
Specific Fuel Consumption (SFC)
Standard Turn Rate (STR)
Quad Tilt-rotor (QTR)
Second Flap Frequency ($f_{2\theta}$)
Shape Memory Alloy (SMA)
Tactical Air Navigation (TACAN)
Threat Adaptive Countermeasures Dispenser System (TACDS)
Trailing Edge (TE)
Ultraviolet (UV)
Unit Load (U_l)
University of Maryland Advanced Rotorcraft Code (UMARC)
Unmanned Aerial Vehicle (UAV)
Versatile Affordable Advanced Turbine Engine (VAATE)
Vertical Takeoff and Landing (VTOL)
VHF Omnidirectional Range (VOR)
Volts, DC (VDC)
Weight (W)

RFP Compliance

RFP Requirement	Compliance Action	Reference
Shipboard compatible with L-class or CVN	Folded height and weight within CVN maintenance elevator limits	Section 7.2 & 8
Capable of transporting a 20-ton FCS vehicle	Internal clearance and drive path provided for FCS	Section 7.1
Capable of transporting at least two 463L pallets	Internal winch, floor rollers, and cargo bay hard points permit easy loading	Section 7.4
Intra-theater deployment of 1000nm without refueling	Range of 1079nm at 3000' density altitude without refueling	Section 15.4
Mission elements: 125nm outbound leg at VBR, 15 min loiter, 3 min HOGE (3000'), 125nm return leg at VBR, 2 min HOGE (sea level), 20 min fuel reserve (ISA+20°C)	Designed with adequate cruise speed, hovering capability, range, and endurance to complete mission	Section 4.3
Power-off/autorotation	Improved autorotation capability	Section 5.7
Powered rotor blade/airframe folding	Blade folding/tail folding allows for compact footprint, ideal for shipboard operations	Section 8
Load factor structural capability at MGW at least -0.5G to +2.5G	All structural members designed to withstand required load factor	Section 7.2
Capable of twice standard turn rate at cruise speed	Blade loading chosen such that 2x standard turn could be conducted at cruise speed of 145 kt	Section 4.4
OEI HOGE at 60% fuel and full payload, with no more than emergency power, sea level, ISA+20°C	Three engines provides OEI capability and also hover ceiling in excess of 12,500 ft	Section 14.1
Side-by-side cockpit seating for pilot/co-pilot, cabin seating for loadmaster	Cockpit layout designed for crew safety	Section 7.3
Accommodations for FCS crew of two	Cabin provides adequate seating for crew	Section 7.3
Combat countermeasures	IR jammers, chaff/flare dispensers, radar warning receivers included	Section 13
Equipment suite for flight operations in adverse weather/ night operations	All necessary equipment provided for navigation, communication, night ops, adverse weather	Section 11.1
Facilitate access for inspection/rapid repair of aircraft components	Work platforms in airframe, access panels ensure easy maintenance	Section 7.3
Engine drive system design and performance evaluation	Future engine technology substantiated, with detailed transmission design	Section 14.1
Discussion of manufacturing materials	Discussion of composite material selection and procedures for fuselage and main rotor structures	Section 5.1 & 7.5
Flight performance, stability and control, and handling qualities evaluations of the design.	Aircraft performance analysis discussion, also including hover and forward flight stability and handling qualities analysis	Section 9 & 15
Crashworthy Design	Skin designed for water landing impact absorption	Section 7.5
	Sponson mounted landing gear	Section 7.3
	Titanium transmission deck	Section 7.5
	Crashworthy fuel tanks	Section 7.5
	Crashworthy seats, with adequate seat stroke, 8"	Section 7.3
MIL-STD-1375 weight breakdown	MIL-STD-1375 weight breakdown	Appendix A
Optional discipline examined	Smart material actuated - active trim tab	Section 5.5

Atlas: Performance Summary and Design Features

Performance Data

	Design GW (MSL)	Full Fuel, No Payload (68,500 lb) (MSL)	Self-Deployment Mission (MSL)
Design Cruise Speed (kt)	150	160	145
Speed for Best Range (kt)	145	129	145
Speed for Best Endurance (kt)	81	60	81
Maximum Cruise Speed (kt)	176	172	176
Maximum Range (nm)	325	395	1160
Maximum Endurance (hr)	2.8	4.1	9.9
Vertical ROC (ft/min)	2600	5440	2600
Maximum ROC (ft/min)	4820	6050	4820
HOGE Ceiling (ft)	12,500	23,000	12,500

Vehicle Dimensions

Fuselage Length (ft)	94.8
Overall Length (ft)	135.0
Height – Hub (ft)	16.6
Wheel Height (ft)	
Fuselage Width (ft)	18
Horizontal Stabilizer Span (ft)	11
Fuel Capacity (gallons)	2170

Weights

Design Gross Weight (lb)	108,500
Empty Weight (lb)	55,300
Useful Load (lb)	53,200
- Max Usable Fuel (lb)	10,800
- Flight Crew (lb)	600
- Max Payload (lb)	40,000
- Fixed Mission Equip. (lb)	1,800

Engine Ratings

Number of Engines	3
One Engine Rated Power (hp)	7,916
One Engine Max Cont (hp)	6,253
One Engine Emergency (hp)	9,103
AEO Transmission Limit (hp)	23,487
OEI Transmission Limit (hp)	15,658

Main Rotor Specifications

Diameter (ft)	116
Number of Blades	7
Chord (Root) (ft)	2.91
Chord (Tip) (ft)	1.94
Solidity	0.111
Disk Loading (lb/ft^2)	10.6
Blade Twist (deg)	-12
Tip Speed (ft/s)	720
Shaft RPM	118
Shaft Tilt (deg)	5
Tip Sweep (deg)	Parabolic
Tip Anhedral (deg)	10
Root Cutout	11%
Airfoil Sections	SC-1095

Tail Rotor Specifications

Diameter (ft)	22.4
Number of Blades	6
Chord (ft)	1.46
Solidity	.25
Blade Twist (deg)	-8
Tip Speed (ft/s)	720
Shaft RPM	1909
Root Cutout	15%
Airfoil Sections	SC1095

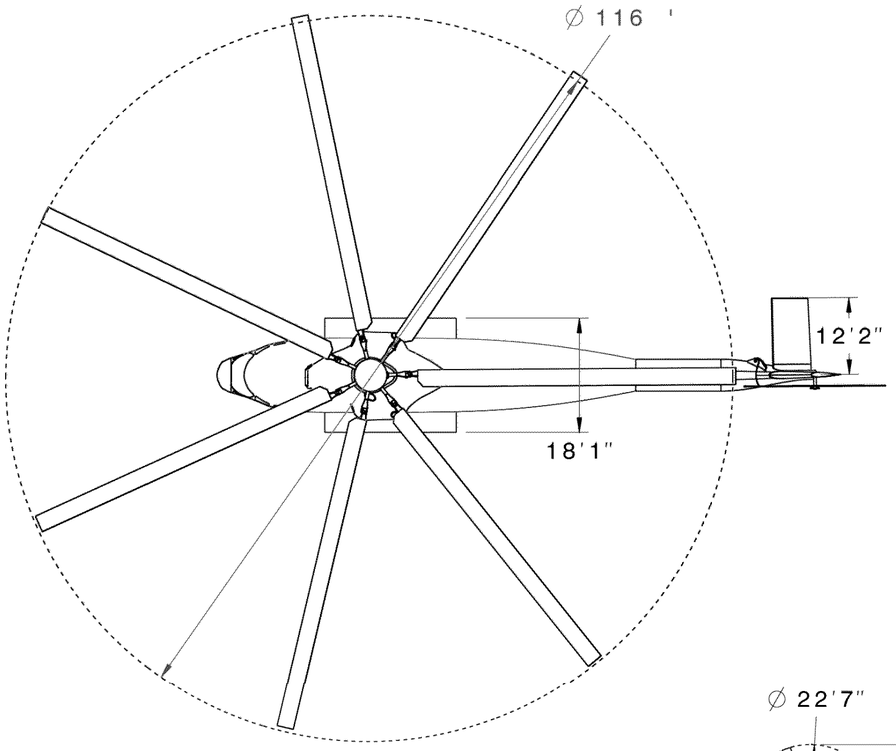

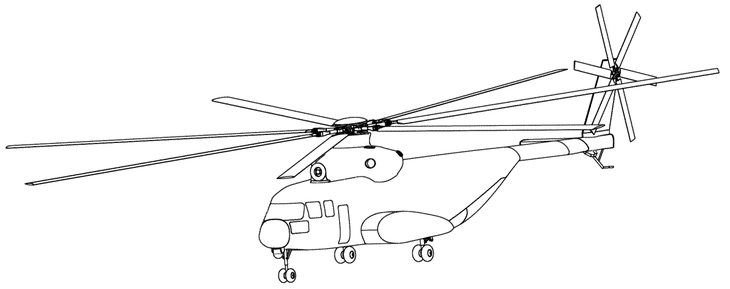

Configurations:

- Main rotor folded. CG at 4.0% of the main rotor radius
- Tail boom folded. CG at 1.0% of the main rotor radius
- Main rotor and tail boom folded. CG at 3.62% of the main rotor radius
- Fully loaded. CG at 0.8% of the main rotor radius
- Empty weight. CG at 1.3% of the main rotor radius

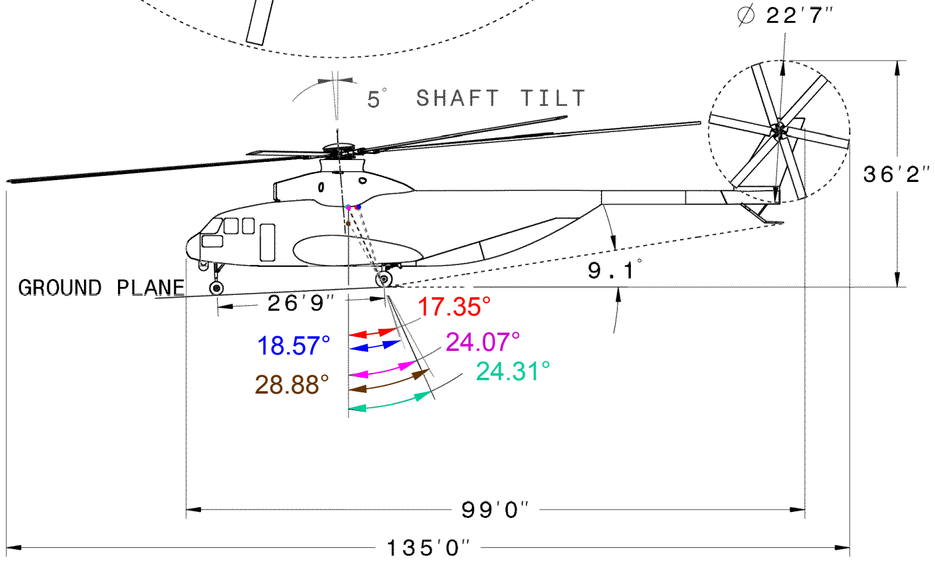

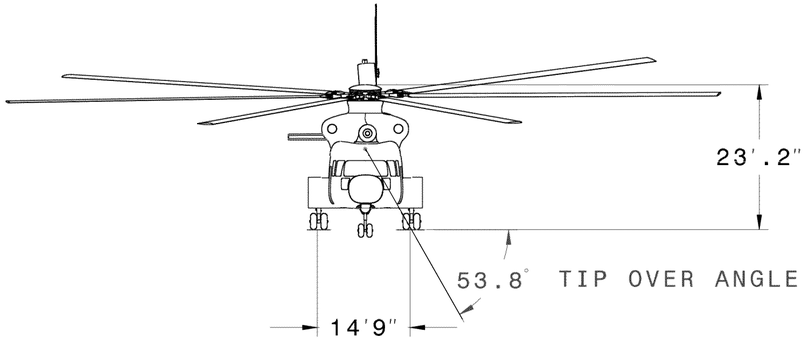

Atlas Four View Drawings

Section 1: Introduction

This proposal describes the design of the Atlas Helicopter, a ship based military helicopter designed to support logistics for an Army Future Combat System (FCS) light armored vehicle. The design was developed to meet the requirements of the 2005 Request for Proposals of the AHS/NASA Student Design Competition, which was sponsored by Boeing. The RFP addressed the military's need for a modern heavy lift VTOL design, able to transport a 20 ton payload over 250 nm range and capable of automatic blade and body folding that is necessary for naval shipboard operations. The objective was to develop a conceptual design of a military aircraft that maintains a balance of shipboard compatibility, cruise speed and payload handling with Initial Operational Capability in 2018.

The RFP states that the primary aircraft measure of merit is "the timeline for one aircraft to deliver four FCS combat vehicles versus the predicted acquisition cost of the aircraft," given as mission hours per acquisition cost in RFP clarifications [RFP05]. The value of the aircraft to the military is maximized by the lowest cost design with the highest productivity. Therefore, the proposal design philosophy is focused on the design of a low-risk military aircraft that is an innovative, low cost and highly reliable solution that pushes the VTOL cruise limitations.

In the proposed aircraft, all system design efforts were directed towards minimizing weight, manufacturing complexity and maintenance effort, using modern high-value technology. The shipboard compatible aircraft provides a substantial increase in performance over existing heavy lift helicopters, while minimizing operational and development risk. A realistic assessment of all major technical areas ensured an efficient aircraft designed to meet the *goals* of present and future military heavy lift VTOL missions.

1.1 Historical Considerations

In 1971, the United States military approved the specifications for Heavy Lift Helicopter (HLH) program. Boeing developed the tandem rotor XCH-62 HLH with a 22-ton external payload capability, but the program was cancelled in October 1974. The CH-53E, deployed in 1981, has the highest payload capacity of any western production helicopter in service. It is a ship-based aircraft, "designed to carry 32,000 pounds of cargo at cruise speed to a range of no less than 50

Table 1.1: Historical Survey of Heavy Lift VTOL Aircraft

Aircraft	Configuration	No. of Engines	Max Rated Power (shp)	MR Diam. (ft)	Max. Take-off Weight	Empty Weight (lb)	Range (nm)	Payload (lb)	Cruise Speed (kt)
CH-53E	conventional	3	14,800	79.0	73,500	33,373	100	32,000	150
Mi-26	conventional	2	11,400	105.0	123,450	62,170	423	33,069	137
CH-47SD	tandem	2	7,533	60.0	52,000	25,469	652	12,000	155
XH-62	Tandem	3	26,910	92.0	140,000	-	20	44,000	-
CH-54A	Conventional	2	9,600	72.0	47,000	19,234	200	20,000	91
K-MAX	synchropter	1	1,80	48.3	12,000	5145.5	300	6,000	80
V-22	tilt-rotor	2	6,150	38.0	47,800	33,140	515	20,000	250

nautical miles" [Glob05]. The Mi-26, introduced in 1983, was developed for a 270 nm mission with 15-metric tons (33,070 lb) of payload [Tish00]. It is the largest production helicopter in the world, with performance capabilities similar to the requirements of the RFP, but it lacks any shipboard operation capability. A survey of several heavy lift helicopters is seen in Table 1.1.

To properly address the problem presented in the RFP, an understanding of the fundamental objectives and design drivers was necessary. Input from several international helicopter designers identified the unique design issues associated with heavy lift rotorcraft systems. Valuable insight into defense acquisition methodology was provided by the Under Secretary of Defense for Acquisition, Technology and Logistics (1997 – 2001), the Honorable Jacques Gansler. The following points were stressed by these advisors. The short development timeline of 13 years, given by the RFP, demands a low risk aircraft configuration solution. Management of the development timeline, and the associated risk of cost inflation, is addressed by designing for modern manufacturing capabilities. The military operational financial risk is addressed in the design by maintenance considerations and reliability features. A viable military aircraft design, therefore, focuses on the minimization of risk and the overall cost associated with the aircraft development and operational program phases.

Section 2: Identification of Design Drivers

This discussion identifies and prioritizes the attributes desired for an aircraft that optimally satisfy the requirements of the RFP. The ability of an aircraft configuration to effectively complete the FCS vehicle transport mission and its impact on shipboard compatibility will be discussed for configuration selection, and also provides the targets for detailed design decisions made throughout the proposal.

2.1 FCS Transport Performance Capabilities

At present, there is no VTOL aircraft that has the heavy lift payload capabilities designated by the RFP while also satisfying the ability to "live on" an existing air-capable naval ship. The mission analysis investigates how each of the necessary aircraft capabilities influences the mission performance.

2.2 FCS Logistics Mission Requirements:

a) *Hover Out of Ground Effect:* For this capability, the aircraft must hover efficiently to minimize the required power. VTOL aircraft weight efficiency is limited by a One Engine Inoperative (OEI) hover performance because hover power is generally 20 – 50% higher than maximum continuous cruise power. Furthermore, hover in a naval environment requires high directional and roll control authority because of increased adverse conditions, combined with unsteady winds and ship-generated turbulence. From these conditions, it is noted that that shipboard landing maneuvers are the limiting factor for naval VTOL aircraft handling qualities [Prou86].

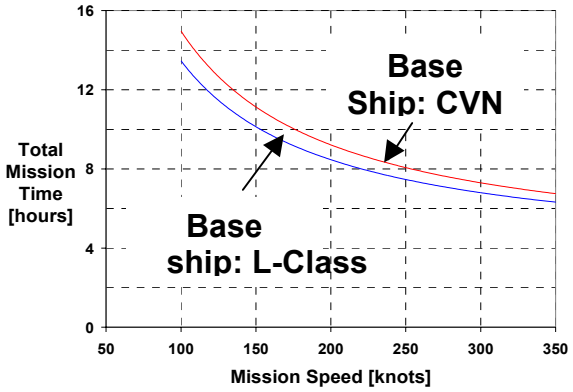

Figure 2.1: Timeline for one aircraft to deliver (4) FCS vehicles to objective and return to base

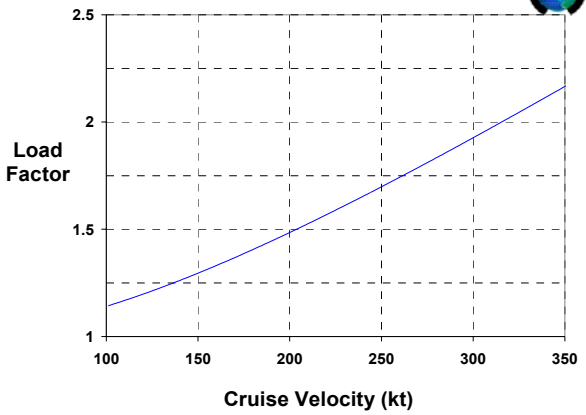

Figure 2.2: Load factor required to sustain twice the standard turn rate at cruise speed in level flight

b) Cruise: A high cruise speed will minimize the time spent delivering the FCS vehicle to its destination. The mission profile shows that 50-75% of the total mission time is spent in cruise (Fig. 2.1), a critical mission time parameter. During cruise, the aircraft is required to be capable of turning maneuvers at twice the standard rate (6°/sec) [RFP05]. Figure 2.2 shows the normal load factor for this maneuver as a function of cruise speed. Higher cruise speeds demand increasing load factors, an unusually stringent requirement for a cargo class of VTOL aircraft.

c) Shipboard Environment: Besides the hovering capabilities already discussed, the naval ship operation environment requires the heavy lift VTOL aircraft to fold within the ship maintenance elevator footprint and height [RFP05]. The folded size also determines the number of aircraft that can be stored on deck. When on deck or conducting take-off and landing operations, the rotors must maintain a large separation from the ship superstructure for safety. The presence of high humidity and salinity in the ocean environment reduces the lifecycle of unprotected components. Aircraft avionics must also be protected from ship generated electromagnetic interference (EMI).

2.2 Mission Profile

The RFP specifies that this aircraft be capable of hover out of ground effect (HOGE) at full payload for take-off at mean-sea-level (MSL), and 3000 ft density altitude. All mission segments are performed at ISA+20°C conditions. The mission profile for delivering 4 FCS vehicles from the L-class ship is shown in Table 2.2, where the some mission times are undetermined.

Leg	Time (min)	Range (nm)	Airspeed	Altitude	Task Description
1	15	-	-	MSL	Loading FCS vehicle and (re)fueling
2	10	0	-	MSL	Engine warm-up, pre take-off check
3		0	0	MSL	Hover OGE for take off from ship
4	climb	-	Best ROC	0–3,000 ft	Climb to cruise altitude
5	cruise	125	Cruise	3000 ft	Cruise to objective best range speed
6	15	0	Endurance	3000 ft	Loiter near for mission cueing
7	3	0	0	3000 ft	Hover OGE 3000’
8	unload	-	-	3000 ft	Unload vehicle
9	cruise	125	Cruise	3000 ft	Cruise to L-class ship
10	decend	-	Best ROC	3000–0 ft	Descend to sea level
11	2	0	0	MSL	Hover OGE for shipboard landing with 20 min loiter fuel reserve

2.3 Configuration Selection Drivers

The following list of parameters was taken into consideration when selecting the aircraft configuration attributes required to meet RFP mission requirements. The selected parameters influence the capabilities of the aircraft's hover and cruise performance, the maintenance and reliability, and also impact the vehicle cost.

Hover Efficiency (RFP): Low hover power is a key design condition because a heavy lift VTOL aircraft must maximize its weight efficiency to minimize acquisition cost for the mission. Aircraft with low rotor disk loading and high blade twist achieve better power-to-weight ratios in hover.

Maximum Cruise Speed (RFP): A high maximum cruise speed minimizes the mission time in cruise, which is an important element of mission productivity (work done per unit cost and mission time). High speed aerodynamics can limit rotors advance ratio. Aircraft propellers or rotors with smaller diameter will achieve higher cruise speeds.

Cruise Efficiency (RFP): Configurations that have higher lift-to-drag ratios can achieve higher efficiency at a given flight speed. Low cruising power can minimize the fuel weight fraction and extend range capabilities. Low drag fuselage, moderately twisted rotors and fixed-wings have better lift-to-drag ratios in cruising flight.

Hover Downwash Velocity (Shipboard Operations): Considerations of both shipboard operations and unprepared landing areas demand low downwash velocities. Also, lower velocity airflow will improve ship crew safety. Low downwash also avoids brownout situations in unprepared landing zones, which affect pilot visibility and may lead to hazardous conditions. Aircraft with large rotor diameters normally have lower downwash velocities.

Turn Rate (RFP): Turn rate capabilities define the maneuverability of an aircraft in forward flight. The RFP stipulates that the aircraft must execute a sustained turn at twice the standard rate at design cruise speed. A sufficient stall margin is required to perform a high load factor maneuver.

Yaw Authority (Shipboard Operations): Hovering in the presence of a ship superstructure demands good directional stability and control with quick response time to pilot inputs. The yaw control system should maintain directional authority over a range of atmospheric conditions that include gusts and side winds.

Folding Complexity (RFP/shipboard Operations): Airframe or rotor folding should be accomplished with a minimum number of parts and mechanical complexity. Aircraft components with folding mechanisms resistant to wear or failure minimize the associated weight penalty, maintenance time and cost.

Shipboard Clearance (RFP/Shipboard Operations): Existing air-capable naval ships have deck space restricted by both aircraft footprint and height. These clearance requirements in turn affect the aircraft performance.

Development Cost (RFP): For a small fleet size, the program development cost strongly influences the final acquisition cost per aircraft. Design configurations that have unresolved technical issues or complex manufacturing requirements will risk a longer development timeline, and would raise the program cost.

Mechanical Complexity (RFP/Shipboard Operations): Mechanically complex subsystems, such as power transmission or in-flight airframe articulation decrease total system reliability and increase maintenance effort and cost. Parts and subsystems that are virtually maintenance-free and are easy to access will lower the aircraft operating costs, which is a key feature in the acquisition process.

Technological Maturity (Military Operations): Unproven vehicle configuration features add great risk to development timeline and raise the risk of critical operational failure. Technologies that have a proven history of performance will lower the risk of a heavy lift aircraft in the development and operation period.

Loading Flexibility (Logistics Operations): Aircraft components, such as wings, empennage or propellers, should not present obstacles to payload loading/unloading operations.

Center of Gravity Range (Logistics Operations): A large CG range can allow a great deal of loading flexibility, and can minimize the risk of exceeding control limits.

Operational Flexibility (RFP): Design configurations with efficient performance over a wide range of flight speeds can perform multiple missions besides medium-range cargo transport.

Ground Crew Safety (Shipboard Operations): Propellers and rotors on an aircraft should be configured to avoid conflict with ship deck operations.

Maintainability (RFP): Military category aircraft subsystems are ideally designed to minimize the required maintenance-man-hours per flight-hour. Critical components that are susceptible to corrosion, fatigue or require complex maintenance procedures should be minimized.

Autorotative/Glide Performance (RFP): Conventional fixed-wing and rotary-wing aircraft have proven methods for recovery to a safe landing, in the absence of engine power. Aircraft that require conversion between multiple flight modes or have fuselage, wing or rotor interactions, raise the risk of losing an aircraft in the event of a power failure.

Section 3: Configuration Selection

The initial configuration selection was made through a qualitative decision matrix. Each of the previously developed design drivers is given a weighting factor depending on its impact to the design goals, shown in Table 3.1. The inherent capabilities and drawbacks of each configuration were investigated to determine their ability to meet specific design drivers. The scores were based on the team evaluation derived from an extensive historical literature survey and design experience. Configuration score are evaluated on a scale of excellent to poor, as seen in Table 3.2. The precision of the scoring evaluation was limited to half a point in order to emphasize the qualitative nature of the evaluation. The maximum possible weighted score is 140 points. The completed configuration selection matrix is shown in Table 3.3.

Table 3.1: Weight Factors	
Weight Factor	**Description**
3	Critical
2	Major
1	Minor

Table 3.2: Configuration Ratings	
Weight Factor	**Description**
4	Excellent
3	Good
2	Fair
1	Poor

Table 3.3 Configuration Selection Matrix

Configuration Selection Drivers	**Weighting**	**Conventional – Tail Rotor**	**Conventional – Fan-in-Fin**	**Conventional – with Wing**	**Conventional – Full Compound**	**Single Main Rotor Tip-Jet**	**Compound – Tip-Jet**	**Coaxial**	**Tandem**	**Synchropter**	**Quad Tilt-Rotor**
Max Cruise Speed	**2**	3	3	3	3.5	2.5	3.5	2.5	3	2	4
Cruise Efficiency	**3**	2.5	3	2.5	3.5	2	4	2	2	2	4
Hover Efficiency	**3**	4	4	3	3	3	3	4	4	4	2
Downwash Velocity	**1**	4	4	3.5	3.5	4	3.5	3	3	3	1
Folding Complexity	**3**	4	3.5	3	3	2	2	2	3	2	2
Shipboard Clearance	**2**	3.5	3	3.5	3.5	4	3.5	2	2.5	3	2.5
Development Cost	**3**	4	3	3.5	3.5	2	2	2.5	3.5	2.5	2
Mechanical Complexity	**2**	4	3.5	3.5	3	3.5	3	2.5	2.5	2.5	2
Technological Maturity	**2**	4	4	3	3	2	2	3	4	3	1
Loading Flexibility	**2**	3	2	2.5	2.5	4	3	4	4	4	4
CG Range	**1**	3	3	3.5	3.5	3	3.5	3	4	3	4
Operational Flexibility	**1**	3	3	3.5	4	2	3.5	3	3	3	2.5
Ground Crew Safety	**2**	3	3.5	3	3	4	3	4	4	4	4
Maintainability	**3**	4	4	3.5	3	2	2	3	3	3	2
Turn Rate (Cruise)	**2**	3	3	3.5	3.5	3	3.5	2.5	3	2.5	4
Yaw Authority	**2**	4	4	3.5	4	2	2.5	3	3	3	3
Autorotative/Glide Performance	**1**	4	4	3	3	4	4	3.5	4	3.5	2
Total Score	**140**	**124**	**118.5**	**111**	**114**	**96**	**103**	**100**	**112.5**	**101**	**92**

Single Main Rotor with Conventional Tail Rotor (124): A conventional single main rotor was found to be the most efficient heavy lift VTOL aircraft configuration. It provides a higher hover efficiency compared to other VTOL configurations. The advantages from minimum required engine power and gross weight give this configuration the lowest empty weight fraction, and lowest cost. A low value of gross weight leads to a small rotor radius, and therefore, lighter transmission. The conventional tail rotor delivers high-authority anti-torque and yaw control. Modern advances in rotor blade technology and reductions in airframe weight allow much higher cruise speeds than earlier conventional helicopters. This helicopter provides a low cost, low-risk, development program and high operational performance reliability.

Single Main Rotor with Fan-in-Fin (118.5): The single main rotor with fan-in-fin for anti-torque provides many of the advantages of the conventional tail rotor. However, because of scaling effects, the duct necessary for an effective fan-in-fin suffers a large weight fraction penalty and increased parasite drag. Because cargo helicopters are optimally loaded from the rear, the fan and duct design conflicts with the desire for a raised empennage. For a cargo helicopter that requires rear cargo loading, a complex and expensive development solution is required to design a lightweight fan-in-fin empennage.

Single Main Rotor with Wing (111): Compound lift designs nominally unload the main rotor in forward flight by using the more efficient fixed-wing to raise the lift-to-drag ratio in forward flight. This design has two fundamental flaws for a heavy lift VTOL aircraft. First, the wingspan required to provide significant offloading at 150 kt would be of on the same order as the rotor diameter. In hover, the download on the wing would be 8-12% of the gross weight, and a large source of drag in forward flight. Second, the rotor must still provide all the required propulsive forces. This results in a substantially greater nose down pitch attitude. Historically it has been shown that the compound wing rotorcraft affords little to no performance advantage in forward flight and has a lower weight efficiency than conventional helicopter for the same payload.

Single Main Rotor with Full Compound (114): By adding a turbo-prop and fixed-wings to a single main rotor, a compound helicopter produces a higher lift-to-drag ratio in high-speed forward flight. With the addition of turbo-prop propulsion, the main rotor can nominally be offloaded by approximately 80% in lift and 100% in propulsion. The unloaded rotor delays retreating blade stall to higher speeds, and the additional propulsion allows for a more level fuselage trim attitude. The primary drawback is the weight penalty from extra structural weight and increased airframe download. The empty weight typically rises by 20-30%. Furthermore, transmission weight issues arise because a rotor must maintain a low RPM, while a turbo-prop has a much higher RPM. Therefore, a highly complex power-sharing solution or cross-shafting transmission scheme is needed. Alternatively roughly 20,000 shp becomes redundant in both the main rotor and turbo-prop powerplants. The compound configuration, as a heavy lift VTOL platform, has a large degree of mechanical complexity and high empty weight fraction.

Single Main Rotor, Tip-Jet (96): A tip-jet driven main rotor can potentially provide weight savings by eliminating the anti-torque reaction. The torqueless drive system comes at a cost, mainly because small tip-jets have much higher specific fuel consumption than turboshaft engines. When used to drive the main rotor, tip-jets compromise the internal structure of the blade, and prevent the use of thin airfoils in the tip region of the blade to prevent internal losses. The extra fuel weight and lower lift-to-drag ratio of the main rotor more than offsets the transmission and tail rotor penalty that is accepted by conventional helicopters. Tip-jets also generate unacceptably high noise signatures, a severe penalty for any aircraft.

Full Compound Single Main Rotor, Tip-Jet (103): To retain the weight benefits of the reactionless drive system while still achieving efficient cruise flight, the tip-jets can be shut off and the aircraft operated as an autogiro. In this flight mode, the lift-to-drag ratio of the total system can be increased, allowing higher cruise speeds and better cruising efficiency. However,

from a military standpoint, there are several downsides to this configuration. First, as discussed, the internal structure of the blade is compromised. These blades cannot be removed easily because the additional propulsion housing and fuel-air system in the blade structure, which is a serious maintenance penalty.

Co-axial (100): A coaxial rotorcraft relies on dual rotors separated vertically on the same rotation axis. Generally, the interference losses from upper and lower rotor are roughly equivalent to the power losses of a conventional tail rotor. A heavy lift coaxial ideally has rotor blades approximately 70% the radius of an equivalent single main rotor. To avoid blade collisions, it is necessary that each rotor be allowed to flap up or down by a minimum of 5.2°. For a 50 ft radius blade, the two rotors must be separated by at least 9.5 ft. To meet the maximum RFP height restrictions, a mechanical actuated reduction in mast height would be required, which would significantly increase the mechanical complexity of the system. Since a conventional helicopter hub already accounts for one-third of the net flat plate drag area, the exposed coaxial shaft significantly increases the total parasite drag.

Tandem (112.5): The tandem rotor configuration has two rotors positioned along the longitudinal axis. While the CG range of the aircraft is significantly expanded by this solution, the advantage is somewhat diminished in the present mission because it has a well-defined payload position. Simple calculations for tandem rotors demonstrate drawbacks compared to a single main rotor with identical rotor area, tip speed and total number of blades. Even with an optimistic 20% overlap, the tandem rotor footprint is at least 26% longer. For equivalent blade loading, tandem rotor blades will have half the aspect ratio of the single main rotor, giving lower rotor figure of merit and higher control loads. Helicopters on the scale of the Mi-26 require a large number of blades, greater than six, to maintain a sufficiently large aspect ratio blade to minimize blade weight [Tish76]. For more than three blades per tandem rotor, the rotor overlap must be decreased, which further increases the overall length and footprint of the aircraft. Furthermore, the higher disk loading inherent to heavy lift helicopters would cause great interference effects on the rear rotor in forward flight, decreasing the cruise performance of the helicopter. Each of the two main rotor transmissions must also be designed to carry “more than 50 percent – usually up to 60%– of the total rated power” because of variations in load sharing with flight speed between rotors [Keys79]. Because the configuration also requires oversized gearboxes and cross shafting for OEI performance, the transmission suffers a large weight efficiency penalty. Overall, the tandem rotor helicopter does not optimally satisfy the RFP mission requirements.

Synchropter (101): The Kaman Aerospace K-MAX, is the heaviest synchropter in production, with a maximum payload of 6000 lb. This aircraft relies on dual two-bladed intermeshing rotors. Dual rotor aircraft, of the size required by the RFP, would require at least 8 blades to retain a sufficiently large blade aspect ratio and low blade loading. Intermeshing main rotors require a greater separation, as the number of blades increases, contributing more drag. As with the coaxial, this would restrict the cruise speed to a greater degree than for other configurations. Historically, the synchropter has also demonstrated a dynamic, high-speed flight instability.

Quad Tilt-rotor (92): The tilt-rotor is an innovative design concept that can theoretically achieve fixed-wing cruise speed while retaining VTOL capability. To retain stiff, small-diameter rotors (prop-rotors), it is necessary to employ a quad-rotor design rather than a dual rotor configuration currently in use. Much like the tandem configuration, the QTR has a larger acceptable lateral and longitudinal CG envelope. The configuration relies on four prop-rotors for thrust and control in hover, and also for propulsion in forward flight. Such rotors, with very high disk loading, require more than twice the power to hover compared to cruise, and create a large downwash velocity. This compromise to achieve high-speed flight gives the system extremely poor weight efficiency, and has the highest empty weight fraction of any of the configurations. A large amount of complexity is associated with transition flight modes. Even more complexity and weight derive from the large cross-shafted transmission for the four widely spaced rotors. These issues will significantly impair maintenance efforts and lower the overall reliability of the aircraft. The financial risk inherent in the development of the QTR places it out of feasibility for the short 13-year development timeline, as set by the RFP.

Section 3.1 Configuration Cost and Cruise Speed Analysis

From the preliminary analysis, it was found that total mission time is largely a function of cruise time. Cruise speeds of conventional helicopters are primarily limited by retreating blade stall and the onset of compressibility on the advancing balde. Higher cruise speeds have been achieved by tilt-rotor and compound helicopters. Figure 4.9 shows the acquisition cost of the aircraft that can fulfill the RFP mission. It is clear that the high speed solutions greatly increase aircraft cost. Figure 4.10 shows the reduction in total mission time per unit increase in cruise speed as a function of aircraft cruise speeds. This parameter is a measure of the benefit gained by increases in cruise speed. Below a cruise speed of 150 kt, the mission time reduction rate is two to six times higher than that for an equivalent cruise speed increase above 150 kt. This means that for speeds above 150 kt, the reduction in mission time with increase in cruise speed follows a law of diminishing returns. From the increase in cost, and mission-time reduction data, it was conclude that conventional helicopters provide the greatest return on investment for the RFP primary measure of merit (mission time per acqusition cost).

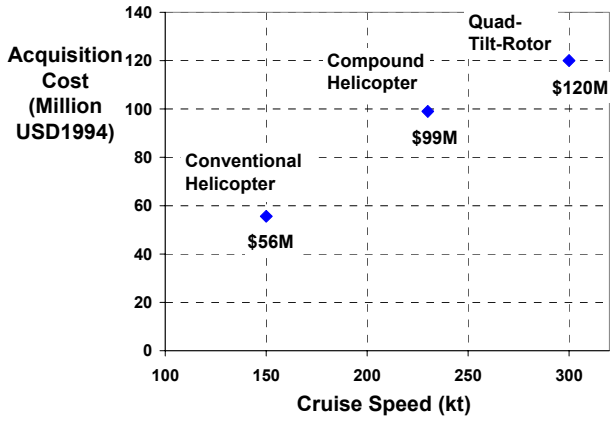

Figure 4.9: Acquisition cost for Heavy Lift - high speed VTOL aircraft

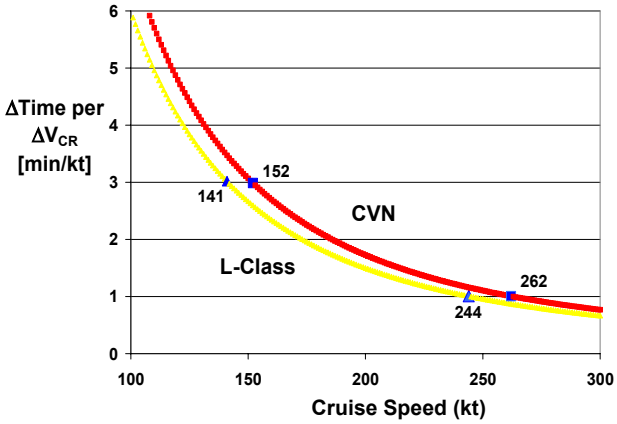

Figure 4.10: Mission time reduction per unit increase in speed for RFP mission

Section 4: Preliminary Sizing

4.1 Design Requirements

The primary mission defined by the RFP is the delivery of four 20-ton FCS vehicles and their crew to an inland combat landing zone. The vehicle will be deployed from an L-Class ship, 125 nm from the landing zone. All mission legs must be performed at ISA+20°C conditions. The cruise altitude was chosen to be 3,000 ft in accordance with the RFP. The engines are nominally sized to meet the OEI condition, where the helicopter is hovering out of ground effect (OGE) at MSL with 60% fuel and full payload.

4.2 Method of Analysis

For preliminary design analysis, the methodology developed by Tishchenko [Tish03] at Mil Design bureau and later modified at the University of Maryland is used for preliminary sizing. The analysis methodology uses an iterative process that is tailored to the payload and range requirements from the RFP. Modifications include updating the weight coefficients to reflect current production helicopters. The analysis begins by specifying the mission requirements of payload and range. Rotor data, including the blade loading, lift-to-drag ratio, figure of merit, propulsive efficiency, and tip speed are also input into the analysis. The initial analysis calculates the preliminary sizing characteristics, such as the main rotor diameter, disk loading, power required, fuel weight, empty weight, and gross weight. These data are used to recalculate the component sizes and weights using weight coefficients modeled after existing technologies and, where applicable, future technologies. After the component weights are calculated, the empty weight, takeoff weight, and fuel weight are recalculated, and the procedure is repeated until convergence is achieved. The analysis is performed for a single blade loading and range of numbers of blades, aspect ratios, enabling several configurations to be compared simultaneously.

4.3 Initial Sizing

For the initial analysis, a cruise speed of 150 knots was chosen as the design point. The OEI requirement resulted in a high single engine power requirement, and a parametric study was conducted to determine the optimum number of engines [Section 14.1.7]. A three-engine configuration was chosen as a result of this study. A large number of blades is needed on a heavy lift helicopter to minimize the main rotor diameter and weight while maintaining a high cruise speed and keeping the rotor vibration levels low [Tish76]. The Atlas was designed for the maximum number of blades that could be easily folded. A rotor with fewer than 8 blades minimizes the required folding articulation complexity. Thus, seven blades were chosen for the main rotor. From the results of the

Table 4.1: Preliminary Sizing of Baseline Helicopter

Number of Blades	7	Number of Engines	3
Aspect Ratio	20	C_T/σ (Blade loading Coefficient)	0.100
Main Rotor Diameter, ft.	102	Takeoff Power (hp)	17,790
Solidity	0.111	Uninstalled Power (hp)	26,684
Takeoff Weight, lbs.	106,325	One Engine Uninstalled power (hp)	8895
Empty Weight, lbs.	52,543	Disk Loading, lb/ft^2	13.5
Empty Weight Fraction	0.494	Acquisition Cost, $M	58
Fuel Weight, lbs.	11,299		

initial sizing analysis, a baseline helicopter with a 7-bladed, 102 ft diameter rotor was selected for further optimization. A full description of this helicopter is in Table 4.1.

4.4 Trade Studies

Trade studies were performed around the baseline configuration in Table 4.1 to assess the influence of variations in blade loading coefficient (C_T/σ) and blade aspect ratio on helicopter characteristics. The range of C_T/σ and blade aspect ratio was chosen based on existing heavy lift helicopters. The RFP specifies that the design must meet a maneuver condition of twice the standard turn rate (STR = 3°/sec) with full payload at cruise speed. As previously described, the maneuvering load factor increases with airspeed. A blade loading trade study was conducted to establish the blade loading limitations that allow the helicopter to perform the required maneuver at a given cruise speed. The tradeoff study employs a trim-performance code to assess the maximum level flight speed of the helicopter at the maneuvering load factor where stall occurs over any section of the blade. Inputs include the basic rotor geometry, airfoil data in the form of table look-up, and helicopter dimensions. The trim performance code uses a blade-element method to calculate the fuselage attitude, cyclic flapping angles, blade section angles of attack, and other trim parameters. The design airfoil (SC-1095) has a high lift coefficient, a low pitching moment, and high drag divergence mach number [Bous03].

Beginning with the preliminary design defined in Table 4.1, the stall speed was calculated from the performance trim code for maneuver blade loading ensuring that the sizing code cruise speed is less than the stall speed. The rotor C_T/σ was varied by changing the aircraft weight while keeping the same rotor solidity and diameter. The corresponding level flight C_T/σ was derived by dividing the weight by the load factor associated with that cruise speed (Fig. 4). This process therefore ensures that the level flight C_T/σ can meet the maneuver requirement at the given cruise speed. Therefore, the relationship between C_T/σ and cruise speed is found for level flight and maneuvering conditions. This data is used to determine a range of sizing configurations.

The "Level Flight" line in Fig. 4.1 represents the values of C_T/σ in trimmed level flight and the "Maneuver 2x Standard Turn" line represents the values of C_T/σ in the maneuvering condition. The analysis shows that for the preliminary design in Table 4.1, the level flight C_T/σ of 0.1 results in a maximum cruise velocity of 111 knots that satisfies the maneuvering requirement. To meet the target cruise speed of 150 knots, the value of C_T/σ in level flight

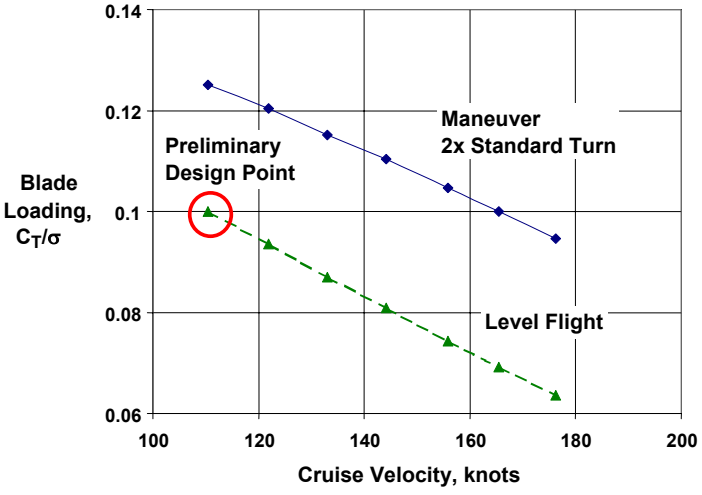

Figure 4.1: Variation of Cruise Velocity with Blade Loading

should be around 0.075. Lowering the level flight blade loading coefficient to 0.075 results in a significantly larger main rotor diameter and increased weight compared to the baseline design.

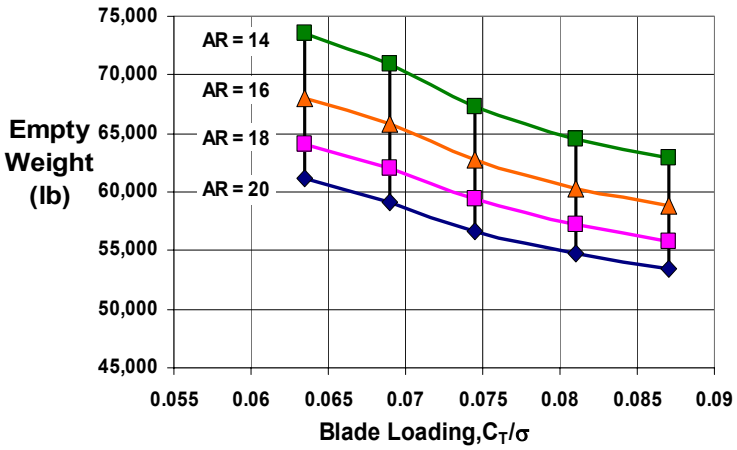

Figure 4.2: Empty Weight as a function of Blade Loading

The results from Fig. 4.1 were input into the sizing code to generate several configurations for each value of C_T/σ. A parametric study was conducted to find how the empty weight varies with blade loading and aspect ratio, and these results are shown in Fig. 4.2. No relative minimum occurs, though it is noted that the lowest empty weight is the product of the highest aspect ratio and highest C_T/σ configuration.

A similar trade study investigated the relationship between hover power required and C_T/σ for different aspect ratios. It can be seen that the hover power increases with increasing C_T/σ and decreases with increasing aspect ratio. For a given C_T/σ, an increase in blade aspect ratio corresponds to an increase in rotor diameter. In turn, the disk loading decreases, leading to a decrease in hover power required. The results are shown in Fig. 4.3.

Figure 4.4 shows the relative cost of a configuration as a function of C_T/σ and aspect ratio. The cost is computed as a function of installed power and empty weight. Once again, there is no relative minimum. The data show that the highest blade aspect ratio and highest rotor C_T/σ will have the lowest cost. This relation arises because, for a given solidity, a higher C_T/σ leads to a smaller main rotor diameter, effectively lowering the empty weight. A high blade aspect ratio produces a lower power requirement and lower empty weight. Thus, from a cost perspective, the highest aspect ratio and highest C_T/σ configuration is the best.

Cruise speed is the other primary design driver. A tradeoff study was conducted to find the variation of C_T/σ with respect to cruise speed, and the results are shown in Fig. 4.5. The cruise speed corresponds to the results of Fig. 4.1. From

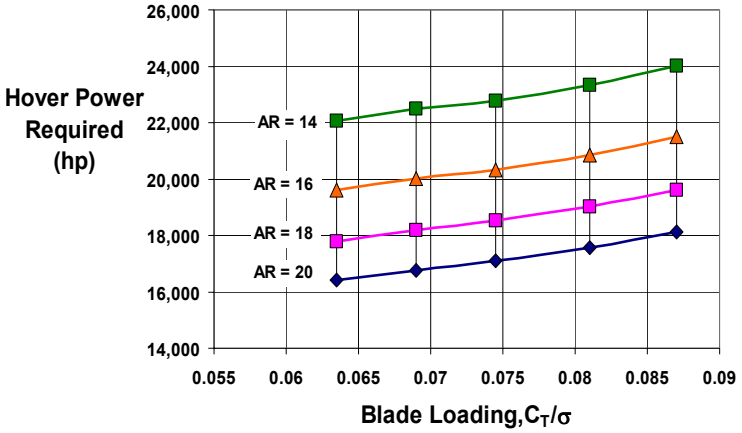

Figure 4.3: Takeoff power required as a function of blade loading

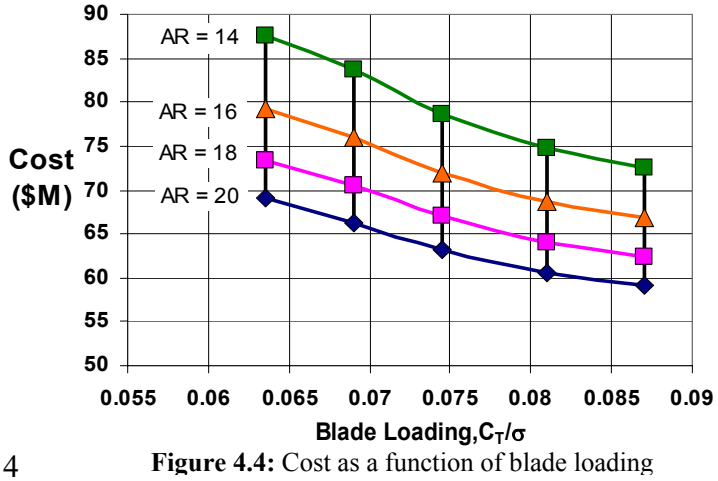

Figure 4.4: Cost as a function of blade loading

the Fig. 4.5, it can been seen that a high Ct/σ causes the rotor to stall at lower cruise speeds for a given aspect ratio. Additionally, a low aspect ratio for a given C_T/σ moves the rotor stall point to a higher cruise speed.

It was shown in Figs. 4.4 and 4.5 that rotor variations C_T/σ and aspect ratio do not point to an optimal configuration balance between low cost and high speed. The results from these figures are combined in Fig. 4.6. Thus, a compromise must be reached to choose the design C_T/σ. From Fig. 4.6, it can be seen that lower costs give proportionately lower cruise speeds. A clear choice to maximize cruise speed while minimizing cost is not evident, and so a further analysis is required. A different performance metric, productivity, is used as it simultaneously considers the best compromise between cost and time. Productivity is defined as [Tish05]:

$$\text{Productivity} = \frac{(\text{Payload})(\text{Range})}{(\text{Time})(\text{Cost})}$$

The mission payload and range remains constant for all size configurations. Therefore, maximizing productivity results from minimizing the product of time and acquisition cost. The metric is plotted against cruise velocity in Fig. 4.7. The product of time and cost has minimum values for C_T/σ of about 0.0745 and blade aspect ratio of 20. It was realized that productivity has a weaker dependence with C_T/σ around the minimum point in Fig. 4.7. Therefore, a productivity variation of 1% was allowed for a secondary design feature to be considered without significantly penalizing the productivity. A compact main rotor diameter optimizes the design for the shipboard requirement. A smaller main rotor diameter decreases the cost and empty weight, while marginally increasing the required takeoff power. The design cruise velocity is marginally decreased for a smaller main rotor diameter, but the savings in cost justify this tradeoff.

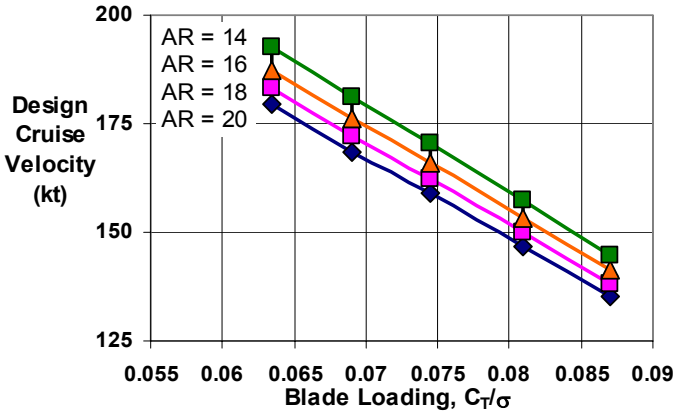

Figure 4.5: Cruise Velocity as a function of Blade Loading

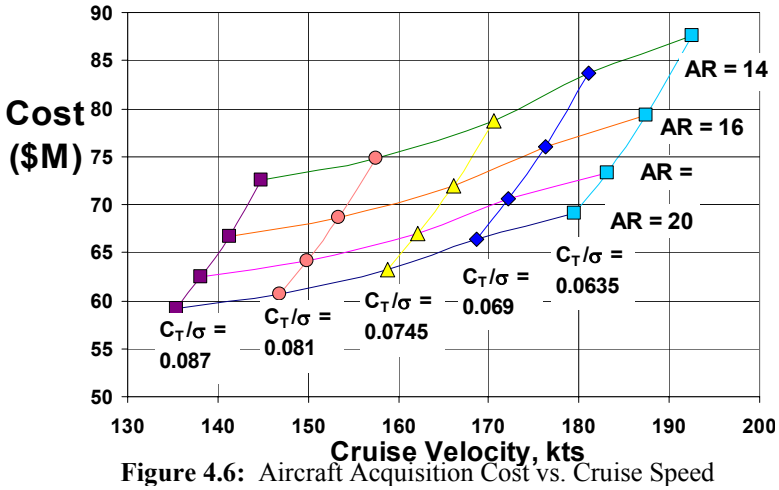

Figure 4.6: Aircraft Acquisition Cost vs. Cruise Speed

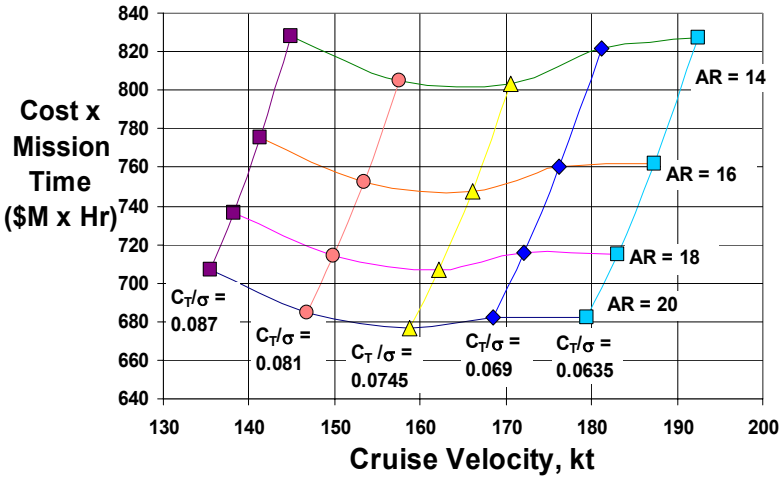

Figure 4.7: Denominator of Productivity vs. Cruise Velocity

Figure 4.8 shows the variation of main rotor diameter as a function of cruise velocity for a range of C_T/σ and blade aspect ratio. The results show that increasing C_T/σ from 0.0745 to 0.079 while keeping the aspect ratio at a constant value of 20 reduces the cruise speed (8 kt), main rotor diameter (4 ft), takeoff weight (1700 lb), and cost ($1.9 M). The cruise speed at this design point

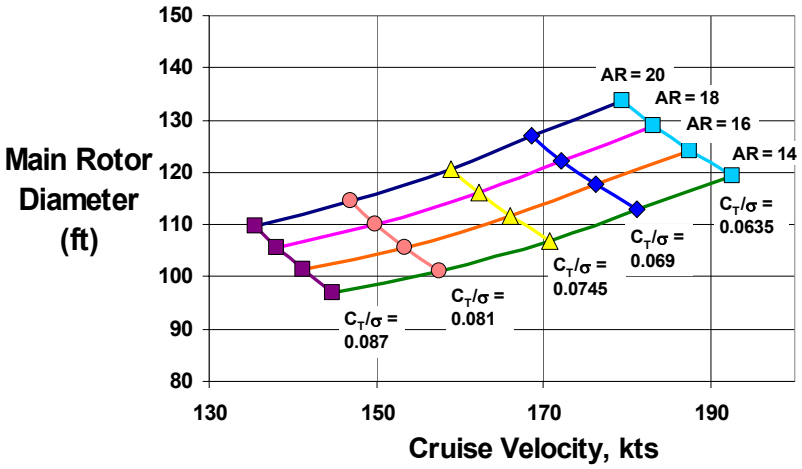

Figure 4.8: Variation in Main Rotor Diameter with Cruise Velocity

was 150 kt. By using C_T/σ =0.079 and a blade aspect ratio of 20, the most optimum balance of design attributes was ultimately determined, and the results are in Table 4.2.

Table 4.2: Final Dimensions

Number of Blades	7
Aspect Ratio	20
Main Rotor Diameter, ft.	116
C_T/σ (Blade Loading)	0.079
Solidity	0.111
Takeoff Weight, lbs.	108,470
Empty Weight, lbs.	55,232
Empty Weight Fraction	0.509
Fuel Weight, lbs.	10,843
Number of Engines	3
Takeoff Power, hp	15,827
Installed Power, hp	23,741
One engine Installed Power to meet OEI requirement, hp	7,914
Disk Loading, lb/ft^2	10.6
Acquisition Cost, $M	56

The final configuration maximizes productivity by minimizing the acquisition cost and utilizing at a small decrease in cruise velocity. This follows the design philosophy goals of a low-cost, low-risk configuration, while adhering to the sizing constraints in the RFP and meeting the maneuver requirement. Benefits of this design include a low empty weight and power required.

4.5 Mission Timeline Prediction

The primary mission segments are seen in Table 4.3. The ship-to-ship mission segment is seen in Table 4.5. Section 7.4 discusses the traditional loading methods employed by the Atlas design. The primary timeline driver is the cruising speed of the helicopter. Fully loaded, the Atlas has a 99% best range cruise speed of 145 kt, while the return trip relies on the fast cruise speed of 160 kt to reduce mission time, as discussed in section 16.3.1. The Atlas main rotor hub height is taller than the L-class maintenance deck elevator limit, so the initial and final leg of the mission involves the arrival and return to the L-class from the CVN. The total mission time to deliver 4 FCS vehicles and return to the base ship is seen in Table 4.5.

4.6 Preliminary Design Cost Analysis

The acquisition cost model of an aircraft is function of material and labor cost, as well as the production efficiency of the manufacturer (eq 4.1). This analysis uses the Harris-Scully helicopter cost model, a comprehensive historical analysis, to predict the first aircraft unit cost (Table 4.6) [Harr97]. This model is reliable forecasting tool of the first unit helicopter cost based on primary vehicle parameters (eq 4.2) using data from Table 4.6. The final fleet size stated by the RFP, was 200 aircraft. The Production Quantity Factor (PQF) quantifies the reduction in cost as a function of increase in production efficiency for a given final production quantity (eq. 4.4).

Table 4.3: Mission Timeline Evaluation for transporting 4 FCS vehicles to Objective Dropoff point

Segment	Time (min)	Range (nm)	Airspeed	Altitude	Task Description
1	15	-	-	MSL	Loading FCS vehicle and (re)fueling
2	10	-	-	MSL	Engine warm-up, pre take-off check
3	1	0	0	MSL	Hover OGE for take off from ship
4	1.2	1.6	81	0–3,000 ft	Climb to cruise altitude
5	51.7	125	145	3000 ft	Cruise to objective 99% best range speed
6	15	0	81	3000 ft	Loiter near for mission cueing
7	3	0	0	3000 ft	Hover OGE 3000’
8	9	-	-	3000 ft	Unload vehicle
9	46.9	125	160	3000 ft	Cruise to L-class ship
10	2	2.7	81	3000–0 ft	Descend to sea level
11	2	0	0	MSL	Hover OGE for shipboard landing with 20 min loiter fuel reserve

Table 4.4: Additional Mission time from CVN based aircraft

Segment	Time (min)	Distance (nm)	Airspeed	Altitude	Task
1	4.7	-	-	MSL	Fueling for 75 nm between L-class and CVN
2	1	0	0	MSL	Hover OGE for take off from ship
3	10	75	-	MSL	Cruise between L-class and CVN
4	2	0	0	MSL	Hover OGE for shipboard landing

Table 4.5: Additional Mission time from CVN based aircraft

	Min	Hours
4 FCS Transport Mission	597.2	9.95
CVN Basing Addition	35.4	0.59
Total RFP Mission Time	**632.6**	**10.54**

Acquisition Cost (2005) = (inflation)(Profit)(Overhead)(PQF)(First Unit Cost) (4.1)

First Unit Cost (1994) = $269(H)(Wgt. Empty)$^{.4638}$[Total Eng.(s) Rated HP]$^{0.5945}$(No. Blades)$^{0.1643}$ (4.2)

$$\mathbf{PQF} = \frac{1 + (\mathrm{LCF}) + (\mathrm{LCF})^{\log 3/\log 2} + \ldots + (\mathrm{LCF})^{\log \mathrm{N}/\log 2}}{\mathrm{N}} \quad (4.3)$$

H = (Engine Type)(Engine No.)(Country)(Rotors)(Landing Gear) (4.4)

The Atlas has a multi-engine gas turbine with retractable gear, US Military production, and one main rotor. An inflation rate of 30.44% was used to calculate the 2005 acquisition cost, from the 1994 baseline cost. If it is assumed that the PQF and the overhead rates roughly cancel, the acquisition cost for the helicopter is $72M (USD 2005) (Table 4.2). If an overhead rate of 1.2 and a conservative learning curve (LCF) factor of 0.95 are assumed (PQF=0.73), the acquisition cost is $63M USD (2005), shown in Table C.3. For the $63M helicopter, with a mission time of 10.4 hours, the **mission measure of merit is 0.165 hours/$M (USD 2005).**

Table 4.6: Aircraft H calculation factors [Harr97]

Engine Type	
Piston	1.000
Gas Turbine	1.794

Engine Number	
Single	1.000
Multi	1.344

Country	
US Commercial	1.000
Russia	0.362
France/Germany	0.891
US Military	0.883

Engine Number	
Fixed	1.000
Retractable	1.115

No. of Main Rotors	
Single	1.000
Twin	1.031

Table 4. 7: Atlas Predicted Acquisition Cost without production quantity and inflation

Year	Acquisition Cost ($M)	Inflation Rate
1994	56	-
2005	72	30.44%

Table 4. 8: Atlas Predicted Acquisition Cost with Production Quantity Factor Adjustment

Year	Acquisition Cost ($M)	Inflation Rate
1994	49	-
2005	63	30.44%

Section 5: Main Rotor and Hub Design

The main rotor was designed to meet the goals set forth in the RFP, and addresses such issues as low weight, low maintenance, and good performance, both in hover and cruise. This section addresses the features of the main rotor and hub, including blade characteristics, blade design, hub configuration, rotor control, blade dynamics, and autorotation characteristics.

5.1 Blade Aerodynamic Characteristics

The main rotor characteristics were selected as part of an iterative performance process to ensure acceptable hover and forward flight performance. Table 5.1 lists the key design parameters for the Atlas rotor (Pullout 5.1). Rotor performance relies heavily on the selection of proper airfoil profiles. The retreating blade requires an airfoil with high lift-to-drag and maximum lift coefficient to delay the onset of stall. The advancing blade, however, requires an airfoil with high drag divergence Mach number to delay compressibility effects at high forward speeds. A high L/D is also necessary for a low autorotation rate. To fulfill these requirements, the Atlas uses the SC–1095 airfoil.

Table 5.1: Main Rotor Characteristics

Diameter	116 ft
Number of Blades	7
Chord	2.89 ft
Solidity	0.11
Twist	-12° (linear)
Sweep	Parabolic (from 90%)
Anhedral	-10° (from 95%)
Taper Ratio	3:2 (from 90%)
Tip Speed	720 ft/s

Selection of tip speed must balance the effects of retreating blade stall, for which higher tip speeds are desired, as well as compressibility effects on the advancing blade, for which lower tip speeds are preferred. Other factors, such as noise and autorotative performance, require conflicting tip speeds as well. High tip speeds also increase the hub and blade root centrifugal force, increasing overall weight. Finally, a high tip speed lowers C_T/σ, an important consideration for heavy lift

rotorcraft. Taking all considerations into account, a tip speed of 720 ft/s was selected. The blade tip geometry was then modified to alleviate advancing blade compressibility effects.

The effects of blade twist on hover performance were studied using blade element momentum theory, with empirical corrections to account for tip loss and compressibility effects. Intelligent use of blade taper may be used to minimize profile power and improve hovering performance, giving a higher figure of merit. A taper ratio of 3:2 was, therefore, introduced over the outer 10% of the blade. Tip sweep is useful in alleviating compressibility effects on the advancing blade in high-speed flight. However, too much sweep introduces undesirable pitching and flapping inertial couplings. Furthermore, the optimum amount of sweep varies with spanwise location along the blade, as optimum sweep angle increases with radial location. Therefore based on a tip Mach number of 0.85 for the advancing blade, a parabolic tip sweep over the outer 10% of the blade was selected. An anhedral of 10° was also added to reduce aerodynamic hover tip losses, increasing the figure of merit. Anhedral also increases the axial separation of the tip vortices, reducing blade vortex interaction noise [Leis00].

Adding blade twist improves hover performance and minimizes vibrations and blade loads in forward flight. However, high twist decreases high speed cruise performance, as the twist leads to reduced or even negative lift on the advancing blade tip. After an extensive forward flight and hover performance tradeoff study a moderate blade twist of –12° was selected for the Atlas blades

5.2 Blade Structural Design:

Composite structures are used extensively in the construction of the rotor hub and blades of the Atlas. Their superior strength and stiffness characteristics allow the blades to be lighter, while their high fatigue properties, high damage tolerance, and soft failure modes increase structural integrity and safety. Another key factor, only possible with composites, is the introduction of couplings between bending and torsion modes. Furthermore, composites offer greater resistance to corrosion, important in the humid marine environments for which the Atlas is designed. Finally, composites are less demanding to repair and have a fatigue-life of up to five times longer than comparable metal blades. However, special care must be taken to prevent hydrolysis and deterioration from ultraviolet rays, which drastically reduce their strength.

Table 5.2: Properties of Possible Composite Blade Materials

Material	Density (lb/in^3)	Young's Modulus (Mpsi)	Cost (per lin. yard, 48" w)
S-2 Glass	0.072	6.24	$5.60
Kevlar 149	0.05	12.62	$16.50
IM7 Graphite	0.058	29.44	$21.50

5.2.1 Material Selection: S-2 glass, Kevlar 149, and IM7 graphite were all considered as possible blade construction materials (Table 5.2). S-2 fiberglass offers affordability and transparency to radar, but does not offer the specific strength or specific stiffness of graphite. Kevlar has excellent damage tolerance characteristics and is the lightest among lamination materials, but requires more involved bonding methods and is more susceptible to ultraviolet (UV) radiation. IM7 graphite was chosen because of its superior stiffness and strength characteristics, allowing for weight savings in both the hub and rotor blades.

All composite structural components were designed for ground operations static strength limits and design loads from -65°F to 190°F in wet conditions, and design fatigue strengths for 70°F in dry conditions.

5.2.2 D-Spar: A key blade component is the unistrap, consisting of unidirectional IM7 graphite/epoxy tape forming a "D" spar that winds around the hub attachment points, providing a continuous load path for the blade forces. Although more expensive, the use of prepreg eliminates resin squeeze during winding and provides more uniform structural characteristics. The D-spar/unistrap is sized for the centrifugal forces, lead-lag moments, and torsional moments acting on the blade. To meet AR-56 requirements for rotor braking loads (Section 3.3.2), the unistrap was also sized to resist loads corresponding to twice the maximum braking torque. At the hub attachment, two replaceable filament-wound composite sleeves, cold-bonded into position, transfer the load from the straps to the hub through two 1-½" tapered titanium shear pins. The sleeves provide superior bearing strength and resistance to fretting over a design where the tape would bear directly on the pins.

Analysis has shown that structural couplings in the blade have potential benefits of reduction in vibrations. Recently, Bao and Chopra [Bao03] have shown reductions of all 4/rev hub loads using a flap-bending torsion structural coupling introduced into the rotor blade: specifically 14, 22 and 18% reductions in the vertical shear, in-plane shear, and head moments, respectively, for a Mach scaled rotor. Also, the wind tunnel tests of the mach scaled rotors, demonstrated an increase in rotor performance at high speeds (5% power reduction) with couplings due to elimination of negative lift region.

A mixed coupled blade utilizing positive coupling over the outboard blade span (0.8R–1.0R), no coupling over the mid-span, and negative coupling over the inboard blade span (0–0.4R) was implemented on the Atlas blade spar. The top and bottom of the D-spar uses a plain weave IM7 graphite/epoxy layup of $[0_6/\pm35_4/\pm20_4/\pm35_8/\pm20_4]_s$ to achieve the desired coupling between flap-bending and torsion. The web uses the same plain weave graphite/epoxy fabric with an uncoupled lay-up of $[0_6/\pm35_2/\pm20_4/\pm35_4/\pm20_2]_s$ (Foldout 5.1). Tailoring of this coupling was arrived at using a comprehensive analysis UMARC to minimize vibratory hub loads at high advance ratios.

5.2.3 Torsion Wrap: A torsion wrap, constructed of graphite/epoxy fabric, encloses the D-spar and is tailored to provide coupling between bending and torsion in order to minimize vibratory hub loads (see Section 5.6). Ply overlap is 5/8 inch; the distance between overlaps is six inches at the root of the blade and four inches at the tip. The built-up spar and torsion wrap is then cured in a combined debulk/cure mold. The mold is constructed of six sections, each nine feet in length, and utilizes the vacuum bag technique as a cheaper alternative to match-die molding.

5.2.4 Core and Skin: The aft structure of the blade is made of Nomex honeycomb, carved on the upper side only to reduce manufacturing costs. This not only helps in maintaining the proper aerodynamic contour, but also helps in curing and increases shear stiffness as well. During the curing process, Nomex deflects and provides a backpressure against the skin, providing uniform bond pressure for the final blade cure [Sehg99]. The skin consists of a $[\pm45]_4$ layup of 4H satin

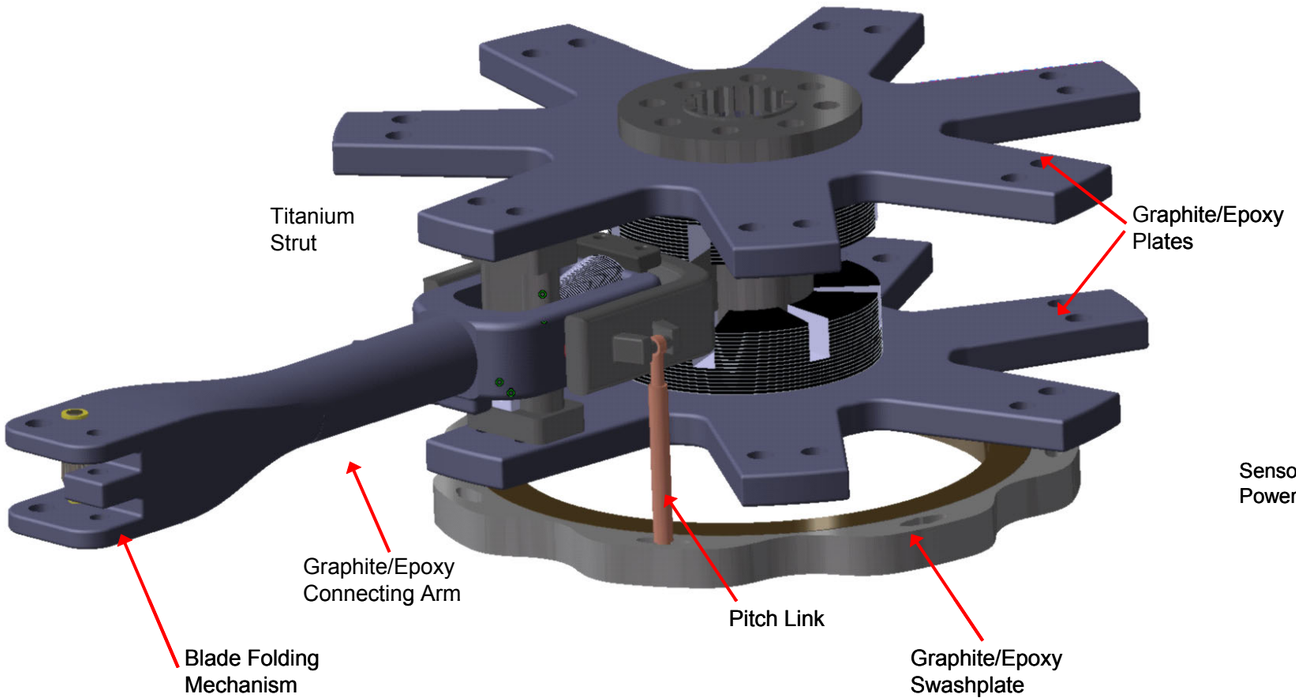

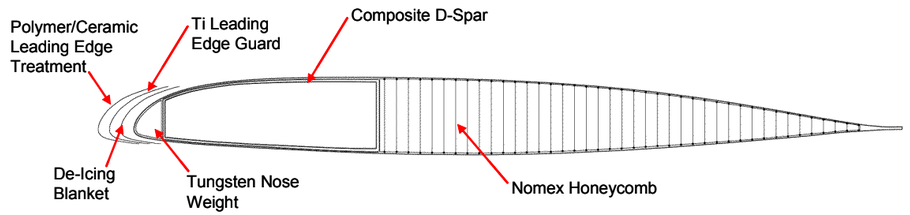

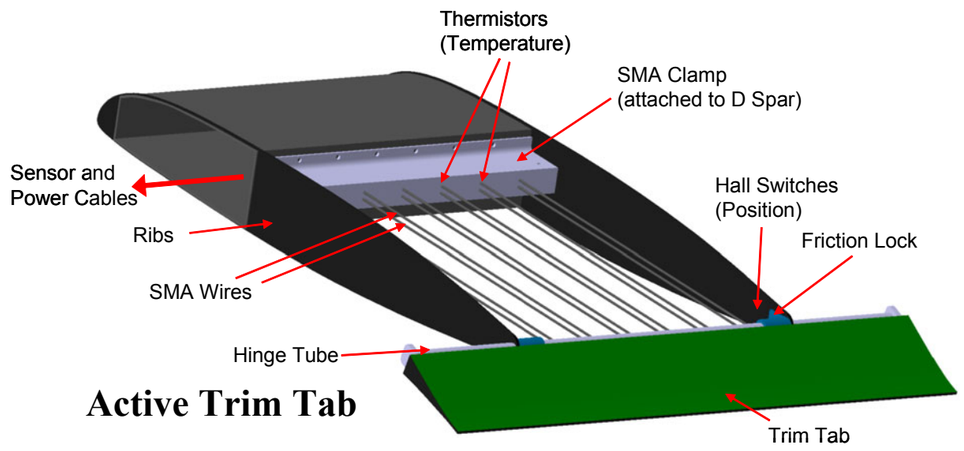

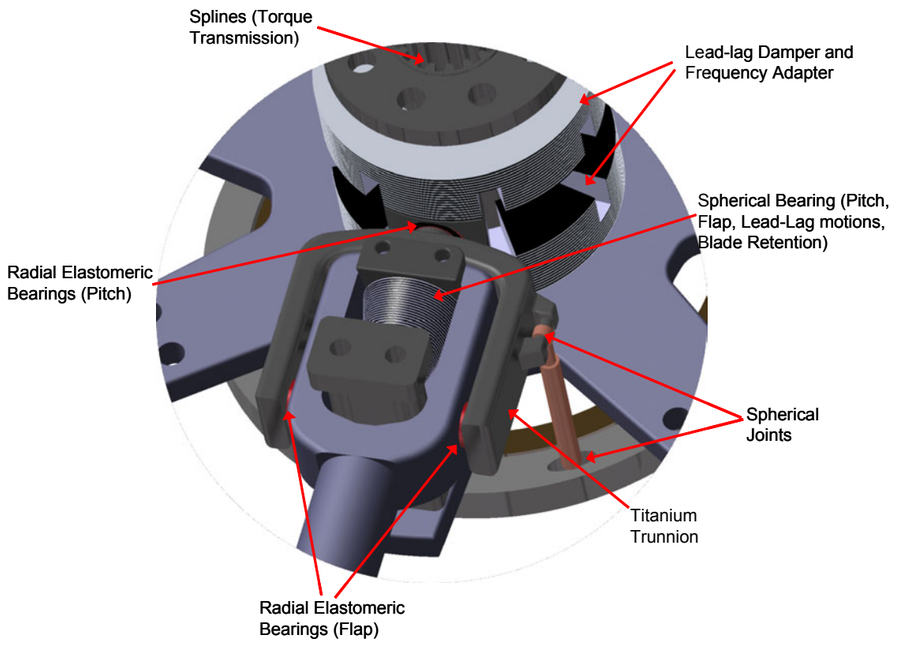

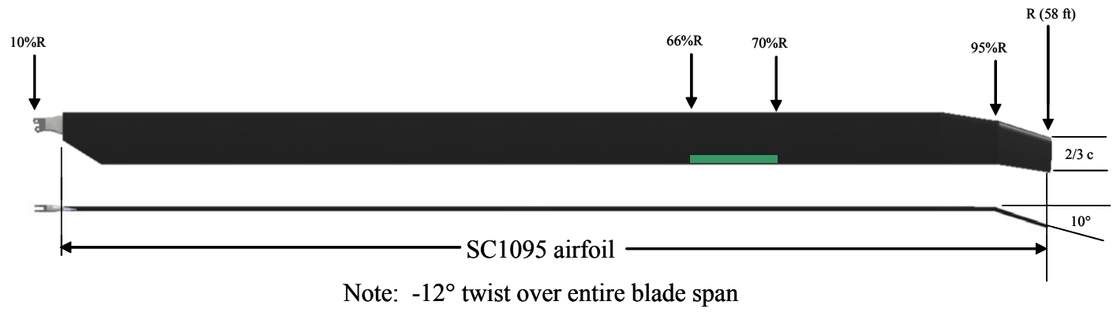

Foldout 5.1 – Rotor Blade and Hub Detail

graphite/epoxy and extends around the entire blade profile, eliminating the possibility of moisture entry in joints. The aft fairing at the root is tapered to 30° to reduce stress concentrations at the spar interface (Foldout 5.1). The bonded blade assembly consists of a cured D-spar and an uncured skin/Nomex core, thus eliminating a separate cure cycle for the skin. The uncured skin is then bonded directly to the cured spar, eliminating the mismatch and irregularities that would occur if the skin were cured separately, before the bonded assembly cure.

5.2.5 Abrasion Guard: Titanium, nickel-plated steel, and polyurethane elastomers were examined for the leading edge abrasion guard. Three types of surface treatment were examined: 1) Si_xC_y/DLC multi-layers deposited by chemical vapor deposition; 2) WC/TaC/TiC processed by electrospark deposition; and 3) polymer ceramic mixtures applied by means of an aqueous synthesis.

Chabot and Brescia [Chab93] demonstrated extensive softening of a polyurethane erosion guard after being exposed to hot/wet conditions that would exist for a naval helicopter, indicating hydrolytic reversion. Furthermore, indications in the testing pointed to more lot-to-lot variations in the polyurethane than in the metals. Moreover, while sand erosion characteristics of polyurethane were excellent, rain erosion resistance was relatively poor due to hydrolysis. This eliminates polyurethane for use on the ship-based Atlas. Nickel-plated steel, while more effective against sand abrasion than titanium, had a significant weight penalty over the titanium leading edge. Titanium did not perform as effectively as steel until a surface treatment was applied. Thus, three surface treatments were also evaluated for erosion protection [Rich03]. Erosion rate, strong adhesion, aerodynamically smooth coating, low residual stress, and ease of manufacture were considered. Each was tested in a wind tunnel facility using alumina and silica particles ranging in size from 9.5 μm to 200 μm at impingement angles of both 30° and 90° with a tunnel velocity of 604 ft/sec. Table 5.3 summarizes the results.

Of the three treatments, the one deemed most appropriate for the Atlas was the polymer/ceramic coating, consisting of nano-scale ceramic particles in either a urethane-based or sol-gel derived polymer matrix. In this combination the hard ceramic coating experiences less wear at high impingement angles, complementing the soft metallic coating. which experiences less wear at low impingement angles. The coating showed excellent adhesion characteristics, and erosion rates

Table 5.3: Summary of Leading Edge Surface Treatments

Treatment	Erodent	Impingement Angle (deg)	Average Erosion Rate (mg/g)
Uncoated baseline Ti	Alumina	30	1.206
WC/TiC/Co	Alumina	30	0.49
Si_xC_y/DLC	Alumina/Silica	30	1.24
Polymer/Ceramic	Alumina	30	0.045
Uncoated baseline Ti	Alumina/Silica	90	1.51
WC/TiC/Co	Alumina	90	0.16
Si_xC_y/DLC	Alumina	90	0.092
Polymer/Ceramic	Silica	90	0.054

demonstrated an order of magnitude improvement over the baseline titanium (Ti-6A1-4V) substrate. The coating can be applied at low temperature using conventional methods, such as spraying or dipping, and is quite cost effective. The polymer/ceramic coating over a titanium base was therefore selected for use on the Atlas rotor blades.

To reduce manufacturing costs, hot-sizing technique is used to form the titanium abrasion guard. The titanium sheet is placed between heated male and female metal-forming dies in increments of approximately 30 inches, until the entire leading edge is formed as one piece. It is then chemically milled to remove scale, and cleaned to prepare it for bonding. This process ensures contour repeatability, reduces chemical milling time, and increases production rates. The guard is bonded to the D-spar during the final blade assembly cure.

5.2.6 Balance Weights: Tungsten mass ballast weights, covered in a jacket of neoprene, are molded into an inner cavity forward of the D spar to move the center of mass near the quarter-chord location. Forward and aft balance weight pockets are included for spanwise and chordwise dynamic balance. An anti-node mass at 50%R is added to tune the second flapwise frequency to 2.8/rev, reducing vibrations. The tip of the blade also incorporates leading and trailing edge projections with cavities for balance weights (mass and dynamic tuning of the lead-lag frequencies), with a removable nickel cap in the high-wear tip area for easy access. The tip weight fittings consist of composite tubes integrally cured in place during the final blade assembly. Removable tungsten tracking weights fit in the tubes.

5.2.7 Lighting: A self-powered formation light is installed in the tip, powered by tritium-3, a self-generating light material. A variable intensity pilot selectable tip formation light is installed on the upper surface as well, powered by the 28 VDC electrical system of the helicopter.

5.2.8 Lightning Protection: The blades of the Atlas are designed for all weather flight capability. An electrically insulated heating element (de-icing blanket) is bonded beneath the erosion strip (Foldout 5.1). The blades are designed to withstand a 200 kA lightning strike with get-home capability [Alex86]. They are also designed to withstand multiple 50 kA strikes, with only minor repair needed. The main lightning protection of the blades is the titanium abrasion guard, which protects the graphite spar from delamination. Aluminum (copper) mesh screens, integral with the blade skins, carry a strike over the fairing to the nosecap. A titanium strip connects the abrasion guard to the hub lightning ground cable.

5.2.9 Survivability: Blades are ballistically tolerant to 7.62 mm armor piercing incendiary (API) projectiles, while all control system parts are tolerant against 12.7mm API threats. Spar damage is visible through cracking of the titanium erosion cap (non-critical for flight) before structural degradation of the blade occurs.

To ensure quality control, all incoming materials for blade manufacture are visually inspected. Major subassemblies (leading edge, aft fairings, spar) are both visually and ultrasonically inspected before blade assembly. The completed blades are visually, ultrasonically, and x-ray inspected to ensure acceptable blade quality.

5.3 Hub Design

The hub was designed to minimize drag, reduce parts count and maintenance, and maximize fatigue life. Consideration of the operational environment of the Atlas strongly influenced the hub design, and a special effort was made to eliminate as many corrosive sensitive components as possible. Although a bearingless design was initially considered for its simplicity, it was deemed infeasible for a rotor of this size. After careful considerations, an advanced hingeless elastomeric design was conceived that emphasizes low parts count and low maintenance.

5.3.1 Hub Operation: The hub consists of two composite star plates connected by a titanium strut (Foldout 5.1). Elastomeric bearings were selected to provide the necessary flapwise, edgewise, and feathering motions. Elastomeric bearings offer smooth performance, gradual and failsafe degradation over time, and are maintenance free. Furthermore, they are unaffected by sand and dirt and offer an inherent reduction in vibration and increased stability because of the damping augmentation of the elastomers.

Blade retention is accomplished through compression of a spherical elastomeric bearing positioned at the centerpiece of each blade (Foldout 5.1). The inboard face of the spherical bearing is bonded to a bearing adapter fitting, which is connected to the top and bottom star plates. Centrifugal forces are transferred to the hub member as a compressive load in the bearing as the yoke of the extension spar bears against the innermost bearing adapter. An elastomeric lead-lag damper and frequency adapter, located inboard of the spherical bearing, is constructed of a radial elastomeric bearing and elastomeric damper pads, affording a very compact design (Foldout 5.1).

A titanium trunnion is connected to the blade through radial bearings on each side at the flapping axis (Foldout 5.1). This allows the blade to flap freely. Out-of-plane (flap) motions are achieved through cocking deformations of the spherical bearing about its center of radius, which is located at 3.5% of the blade radius. The radial bearings are sized to transmit in-plane moments to the lead-lag damper. The trunnion extends through the radial bearing in the lead-lag damper.

Elastomeric members are constructed of alternating layers of modified natural rubber/silicone and stainless steel shims approximately 0.040 and 0.025 inches, respectively, bonded together [Lord05]. Feathering motion (pitch) is accomplished by twisting the spherical bearing, which is torsionally soft. The radial bearing in the lead-lag damper allows unrestricted feathering motion while orienting the blade and connecting the blade to the lead-lag damper (Foldout 5.1). The alignment of the radial and spherical bearings defines the pitch axis. The radial bearing, in which the inboard end of the trunnion is located, is itself positioned in an elastomeric shim. In-plane (lead-lag) motions are accomplished through the spherical bearing undergoing cocking deformations about its center [Hunt97]. The lead-lag damper, located inboard of the spherical bearing, is necessary to tune the natural frequency of the lead-lag oscillation and attenuate dynamic edgewise motions in order to meet blade stability requirements in ground resonance and in-flight air resonance.

Damping is provided through elastomeric damper pads (Foldout 5.1) connecting the hub and the radial bearing [Bryn98]. The damper pad is a toroid that wraps around the driveshaft and extends five inches in the radial direction around the titanium centerpiece. It is five inches in thickness on each side of the radial bearing, and each contains 17 layers of elastomer, each with a thickness slightly less than one-quarter inch. To size the damper, an average dynamic shear modulus of 100 psi (at 20% dynamic strain) was used for the elastomer [Lord05]. The area of the pad and number of elastomer layers were chosen such that the lead-lag angle was restricted to four degrees and the elastomer undergoes no more than 20% shear strain, which equates to an in-plane displacement of ±1inch. The lower half of the damper pad is continuous around the driveshaft, connecting all of the blades. This may have beneficial effects in regard to coupling of the lead-lag motions of the blades.

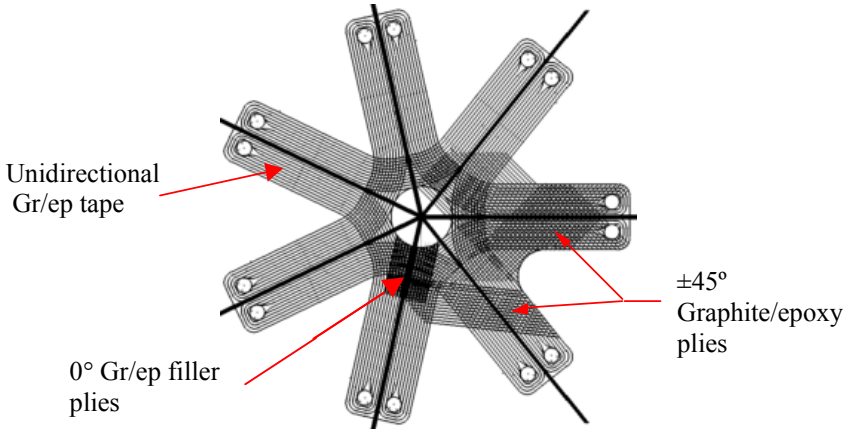

Figure 5.1: Upper and lower hub plate composite layup

5.3.2 Hub Construction: The hub plates are constructed out of a laminated structure composed of unidirectional IM7 graphite/epoxy tape and graphite/epoxy ±45° plies, while graphite unidirectional filler plies fill in the center sections (Fig. 5.1). Prewound composite bushings, located in each arm, provide attachment points for the titanium strut. Each star plate is 2.5 inches thick, and is designed such that principal strains are below 3000 με. No more than four layers of the same orientation are stacked in the same direction. A hybrid manufacturing approach was used for hub layup, where layup of the unidirectional tape layup is completely automated. A human operator is needed only to ensure smooth operation and to halt the machine for filler ply insertion.

Torque is transmitted to the main rotor through 13 splines (1”width x 1” height) in the driveshaft designed for twice the maximum torque rating of the main gearbox, as per AR-56 regulations (Section 3.3.1). By eliminating one tooth of the spline, the assembly of the hub is foolproof. The entire hub self aligns to the driveshaft flange. The driveshaft has an outer diameter of 10 inches and an inner diameter of 8 inches. Multiple grease ports and purge valves around the azimuth of the drive shaft ensure easy maintenance. Rotation of the main bearing is not necessary during lubrication, allowing lubrication to be carried out in storage. A split rubber boot prevents foreign material from entering the main bearing and contact surfaces.

A composite extension spar wraps around the spherical bearing and extends to 10% of the blade radius. The spar is sized to resist the centrifugal forces and bending moments acting on the blade. The rotor blade is attached to the end of the spar to accommodate blade folding. Centrifugally actuated droop stops are attached to the composite hub; when the rotor slows down, springs extend them into position. A blade locking mechanism, located on the front of the strut connecting the

star plates, locks the rotor blade into a fixed position to aid blade folding. The device consists of a small electric motor and a gear drive mechanism that drives a pin, in the axial direction, into the extension spar, preventing any motion of the blade. This aids blade folding, as it eliminates the moments that would act on the swashplate and pitch links (see Section 7).

The titanium struts that connect the composite star plates and the trunnions that join the rotor blades to the lead-lag damper are formed through investment casting. This process allows for very close tolerances, intricate detailed parts, and requires very little machining after the parts are cast, reducing manufacturing costs. While the inboard location for the flap and lead-lag axes allows for a compact hub, it limits the rotor control power to low positive g maneuvers. However, the rotor provides adequate maneuver ability for twice the standard turn rate at cruise speed, meeting the RFP requirements.

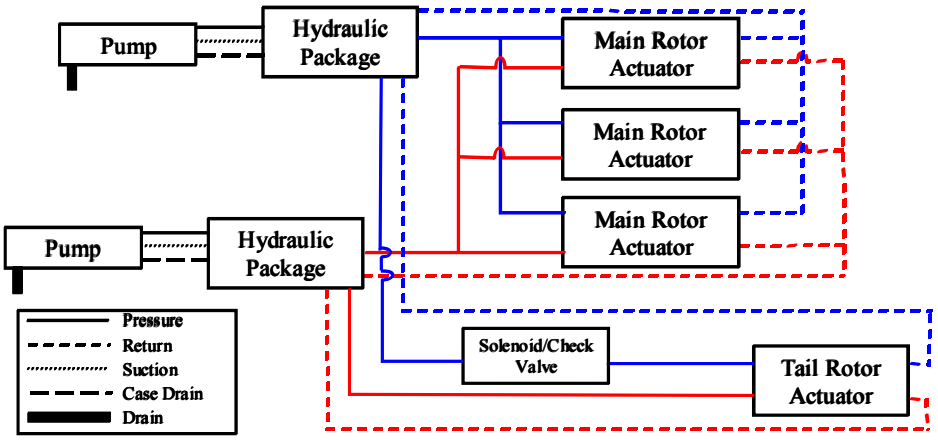

Figure 5.4: Flight Control Hydraulic System

5.4 Rotor Control

5.4.1 Trailing Edge Flaps: A feasibility study was conducted to determine whether a swashplateless rotor would be practical for primary rotor control of the Atlas. This configuration is desirable because it eliminates the high drag associated with the swashplate and control mechanisms, and a weight savings by eliminating the complex servo-hydraulic actuation systems. During the study, many different concepts for a swashplateless system were examined. These include: blade camber control, blade twist control, blade pitch control, tilting shaft concept, active trailing edge (TE) flaps, and active servo flaps. Because of the lower control deflection requirements, lower drag penalty, and availability of compact, high energy density smart actuators, plain moment flaps were chosen for the design feasibility study. A propulsive trim model of a helicopter in level flight condition, with trailing edge moment flaps, was developed and a parametric study of flap configuration was performed using a simple

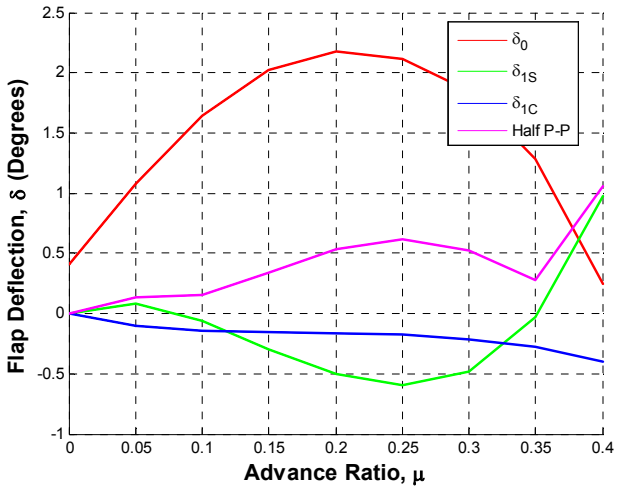

Figure 5.3: Flap Actuation Power

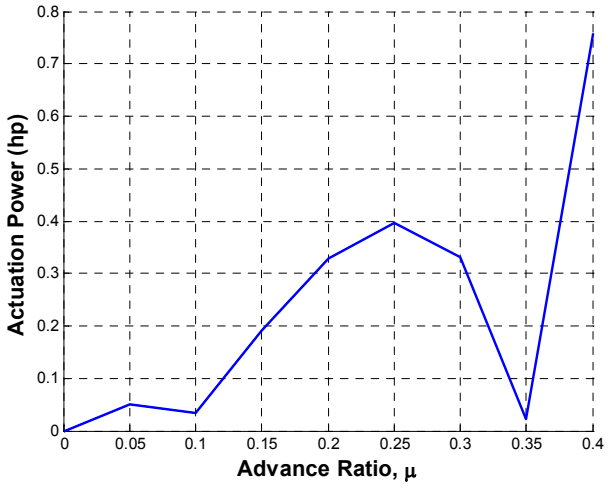

Figure 5.2: Flap Deflections for Trim

analysis developed specifically for this study to determine the optimal configuration for the design requirements. The trim results of this analysis were correlated with a correlated case prediction from UMARC [Shen04].

From the analysis, a trailing edge flap primary control system was designed. A torsional frequency of 1.85/rev was chosen to minimize actuation requirements while maintaining stability. Once a preliminary design was completed, it was optimized for high-speed flight. The effects of flap parameters such as blade index angle, blade twist, flap chord, flap length, and flap spanwise locations were examined for low flap deflections, hinge moments, and actuation power.

The results from the study demonstrate that trailing edge flaps for primary control, actuated with smart material, is feasible for the Atlas. But, considering the development schedule and the desire to minimize risk and cost, it was decided that the use of active trailing edge flaps was not prudent. Issues related to stroke and integrity of smart actuators for the dynamic environment of rotorcraft need to be investigated systematically before their implementation in full-scale systems.

5.4.2 Swashplate Design: The above considerations led to the choice of a conventional swashplate on the Atlas to minimize costs and maximize reliability. However, in view of the corrosive salt-water environment in which the Atlas will be operating, steel was not deemed a suitable construction material. In view of its expense and difficulty in machining to the precision required for a swashplate, constructing it entirely out of titanium was eliminated as a possibility. Instead, the Atlas will utilize a hybrid titanium/composite swashplate system [Bryn98]. It consists of an outer tubular ring, constructed of braids of tri-axial IM7 graphite fibers interwoven with unidirectional graphite plies, and an inner tubular ring, made from braided ±45° graphite fibers (Foldout 5.1). A titanium support ring is fastened to the inner edge of the rotating swashplate. Receiving bolts connect the support ring to the rotating ring through bearing retainer flanges. Apertures formed in the outer and inner rings receive the pitch link ends, which extend to the hub and connect to an extension on the titanium trunnion. Rotating scissors mounted between the rotating swashplate and the rotor head transfer the rotary motion from the rotor to the rotating swashplate, while stationary scissors prevent the swashplate from rotating due to frictional torque. Main rotor servos extend between the two sets of scissors.

Power to the de-icing blanket and active trim tab are transferred to the rotating frame using a fiber brush slip ring. Although power can be transferred to the rotor through non-contacting means, these methods require a rotating transformer or heavy magnets, increasing the weight of the system. Use of fiber brushes has a number of advantages over conventional composite brush or monofilament slip rings. They require no lubricant, thus reducing maintenance, experience less wear debris generation than composite brushes, and produce much lower electrical noise than composite brushes. Multiple contact points per brush ensure a negligible loss of power [Moog04].

Dual hydraulic systems for the main rotor control actuators are installed to ensure reliability. Each is designed to handle the control loads for minimum basic flying, while together the systems can handle loads for the entire flight spectrum.

This setup increases reliability and reduces weight over a system where each can handle the entire spectrum of control loads and one is kept as a stand-by in the event of a failure of the main system.

Each of the hydraulic systems is connected to the tail rotor actuator through lines running in the tail boom. One of the systems has a solenoid valve and a check valve in the tail rotor actuator pressure line; this is to ensure continuous operation of the main rotor actuators in the event of a tail rotor failure or damage to the hydraulic lines. The Atlas can then land under emergency auto-rotation.

5.5 Active Trim Tab

The Atlas also includes an active trim tab, which allows for automatic, in-flight blade tracking. Tracking is necessary because of the inherent differences in the blades from the manufacturing process, which lead to imbalance problems, as well as dissimilarities caused by the operating environment. Existing tracking adjustment typically requires manually bending aluminum trim tabs or heating and cooling a thermoplastic tab for track adjustment. Pitch link and tip mass adjustments are also used. The entire tracking cycle is time-consuming and labor intensive and results in significant down time. Moreover, in many cases blades are balanced as a set; if one blade is damaged, the entire set of blades must be replaced. One method of overcoming this inherent dissimilarity problem is by tightening manufacturing tolerances on blade construction, minimizing the differences in the blades. This, however, increases rejection rates and thus manufacturing costs as well.

A promising approach is to utilize active trim tabs that allow for in-flight rotor blade tracking. This not only allows manufacturing tolerances to be relaxed, reducing production costs, but also decreases the length and man-power intensive steps involved in conventional tracking. Although the use of active tabs has not yet been used on a production helicopter, it has been demonstrated on a model rotor. One-per-rev vibrations can also be substantially reduced, diminishing crew fatigue, increasing component life, and further reducing maintenance downtime and cost for the Atlas. Active tabs also mitigate imbalances caused by ballistically damaged rotor blades, an important combat consideration for the Atlas.

Most smart materials, such as piezoelectric bimorphs, piezostacks, electrostrictives, and magnetostrictives, have low maximum strain. For actuation with these materials, one would need a stroke amplification mechanism, which would add a significant weight penalty and mechanical complexity of the system. Shape memory alloy (SMA), on the other hand, provides the ideal smart material for trim tab actuation due to its high maximum strain capability (6–8%), large block force, and high energy density. Since blade tracking is a slow process SMA actuation appears appropriate. Moreover, shape memory alloys can be operated using low voltage systems, eliminating the weight and expense of a transformer. For these reasons, SMA has been investigated by a number of researchers for use in rotor tracking [Stra04][Epps01] [Sing02].

The actuator design for the Atlas is similar to those tested at the University of Maryland [Epps01][Sing02], consisting of an upper and a lower set of Nitinol SMA wires (Foldout 5.1). The wires are initially plastically strained, with one end fixed at the blade spar and the other end attached to the tab hinge tube (Foldout 5.1). The tracking tab is rigidly

attached to this tube, and comprises the rear 10% of the airfoil. This internal tab design minimizes the aerodynamic drag penalty of a tab past the trailing edge. The wires are thermally isolated from each other such that there are no coupling interactions between them. To activate the tab, one set of wires is heated, causing them to contract as they recover a portion of the initial plastic deformation. This causes the hinge tub to rotate, simultaneously deforming the other set of wires. This system allows for bidirectional actuation, as the behavior can be reversed by heating the opposite set of wires [Sing02].

As rotor tracking is only intermittently performed, the trim tab requires a locking system (Foldout 5.1). This maintains the tab position, once it has been set, without the need for continuous power or control input. A shaft collar around the hinge acts as passive friction brake, calibrated to prevent tab motion up to a preset braking moment. Thus, the hinge moments created by the SMA wires must overcome the friction of the brake as well as the force from the opposing SMA wires and aerodynamic loads.

The maximum actuation moment increases with the number of wires that provide actuation, and this design uses twelve wires in each set. The width of the tab is 24 inches, centered at 68% rotor radius. Its maximum stroke is set to ± 5°, determined by the length the SMA wires. An accuracy of ± 0.1° is possible using closed loop PID feedback control. This design can achieve duty cycles around 20 cycles per hour, much higher than could be achieve with SMA torsion tube designs. The trim tab actuator and the required structural enhancements add approximately two pound to the rotor blade. The Atlas is designed for operation in temperature from –60 to 160F, hence, a higher percentage of nick-based nitinol will be used that increases the transformation temperatures beyond the operating range.

Control electronics are attached to the D-spar. Hall effect sensors and thermistors monitor the positions and temperatures, respectively, of the SMA wires as well as the ambient temperature. The complete system for the active trim tab consists of: an out-of-track vibration monitor/display in the cockpit, a tracking tab control unit, slip rings to transfer power to the rotor, electrical cables running through the D-spar in the rotor blade, and the tracking tab itself. As the tracking tabs are not a critical flight system, the same slip rings used for de-icing may be used. The tabs are compatible with the Atlas's 28 VDC electrical system to maintain a simple electrical interface.

For operation, once the pilot is in the desired mode (ground, hover, forward flight) the system is switched on. Vibration levels are measured by accelerometers on the hub, and airframe and are fed back to the control unit. A control algorithm then cycles through the tab settings on the control unit until the setting with the lowest vibration levels is found. A closed loop PID feedback control algorithm controls the tab position, measures the deflection angle of the response, and sends actuation signals to the actuator. After the desired setting is determined, the tab is locked into position [Hess01].

5.6 Vibration Control

The high vibration levels that afflict helicopters are primarily due to the periodic variations in inertial and aerodynamic loads of the main rotor system. Such loads increase with forward speed, and cause not only discomfort for the crew, but also

increase fatigue of structures and increase maintenance costs. Current helicopters are limited to maximum vibrations levels of 0.1g in the fuselage. Military helicopters in recent years have adopted a limit of 0.05g [Math01].

The Atlas possesses many attributes that will inherently reduce vibrations. The large number of blades will decrease vibratory hub loads, as will be the placement of blade frequencies, such as the second flap frequency at $f_{2\theta}$=2.8/rev. Furthermore, the bending-torsion coupling introduced in the blade construction significantly decreases vibratory hub loads. The use of active tracking tabs, as previously discussed, is very effective in limiting vibrations to only N_b/rev harmonics of blade loads. However, to meet the objective of a maximum vibration level of 0.05g, a dedicated vibration control scheme is needed on the Atlas. To this end, a number of control schemes were examined.

Passive control schemes, such as pendulum absorbers, Dynamic Antiresonant Vibration Isolators (DAVI) and liquid inertia vibration eliminators (LIVE) may be tuned for maximum vibration reduction at a specific frequency. LIVE isolators, for instance, have been used successfully to eliminate up to 94% of blade passage frequency (N_b/rev) vibrations [Smit99]. Moreover, passive schemes require no power and little maintenance compared with active control schemes. However, the effectiveness of passive schemes degrades with any change in operation conditions [Math01].

Higher harmonic control, individual blade control, and active flap control were all considered for the Atlas. However, each of these designs must be employed in the rotating frame, increasing the complexity of the system, as this requires transferring an immense amount of data from the rotating frame to the fixed frame. Airworthiness requirements are also affected, as these systems may adversely impact the primary flight control system. Furthermore, these systems would significantly increase the production and maintenance costs of the Atlas, as there is still much research to be conducted before their implementation on a production helicopter. Active control of structural response (ACSR) was considered, but would require large, heavy actuators and an additional 250 horsepower to implement on the Atlas. Although this system was examined carefully, it was not regarded as the best choice for the Atlas.

In light of this, vibration control on the Atlas is accomplished through a combination of LIVE mounts on the main rotor pylon and semi-active tuned mass dampers to minimize vibrations locally in key areas of the aircraft such as the cockpit and crew area. The semi-active dampers make use of magnetorheological (MR) to vary damping and stiffness characteristics, keeping vibrations in critical areas to a minimum at all flight conditions. Such MR dampers can be controlled with low power and voltage, contain few moving parts, and are cost effective compared to other solutions [Alde03].

LIVE mounts are used in the gearbox support pylons, to isolate the rotor from the fuselage. Sensors monitor the levels of vibration in the fuselage and provide feedback to the control scheme. Generally, such sensors are placed in the tail boom or tail rotor transmission, the cockpit instrument mountings, the cabin floor, and around the pilot. It has been shown that optimal sensor locations may be derived using a coupled gearbox-fuselage model and the Fisher information matrix , which eliminates redundant sensors [Venk99]. With the optimal locations determined, a closed-loop controller for vibration

may be developed that varies the damping and stiffness of the MR damper to minimize vibrations in the cabin, crew area, and instrumentation. The vibration system implemented on the Atlas is designed to meet AR-56 requirements in Sections 3.6.1 and 3.6.5, keeping vibrations levels below 0.05g for all frequencies.

5.7 Rotor Dynamics

5.7.1 Dynamic Analysis

The University of Maryland Advanced Rotorcraft Code (UMARC) was utilized to obtain the blade natural frequencies and fan plot of the Atlas. The blade was modeled as 20 discrete elements, each incorporating different blade stiffness and masses, shown in Fig. 5.5. The blade stiffness was optimized to appropriately position the blade frequencies. The rotor fan plot in Fig. 5.6 demonstrates the blade frequencies are well placed with respect to the rotor harmonics at the operational RPM. The first seven natural frequencies are given in Table 5.4.

Table 5.4: Main Rotor Blade Natural Frequencies

Mode	Flap	Lag	Torsion
First	1.16	0.72	5.15
Second	2.7	9.54	5.81
Third	6.16	-	-

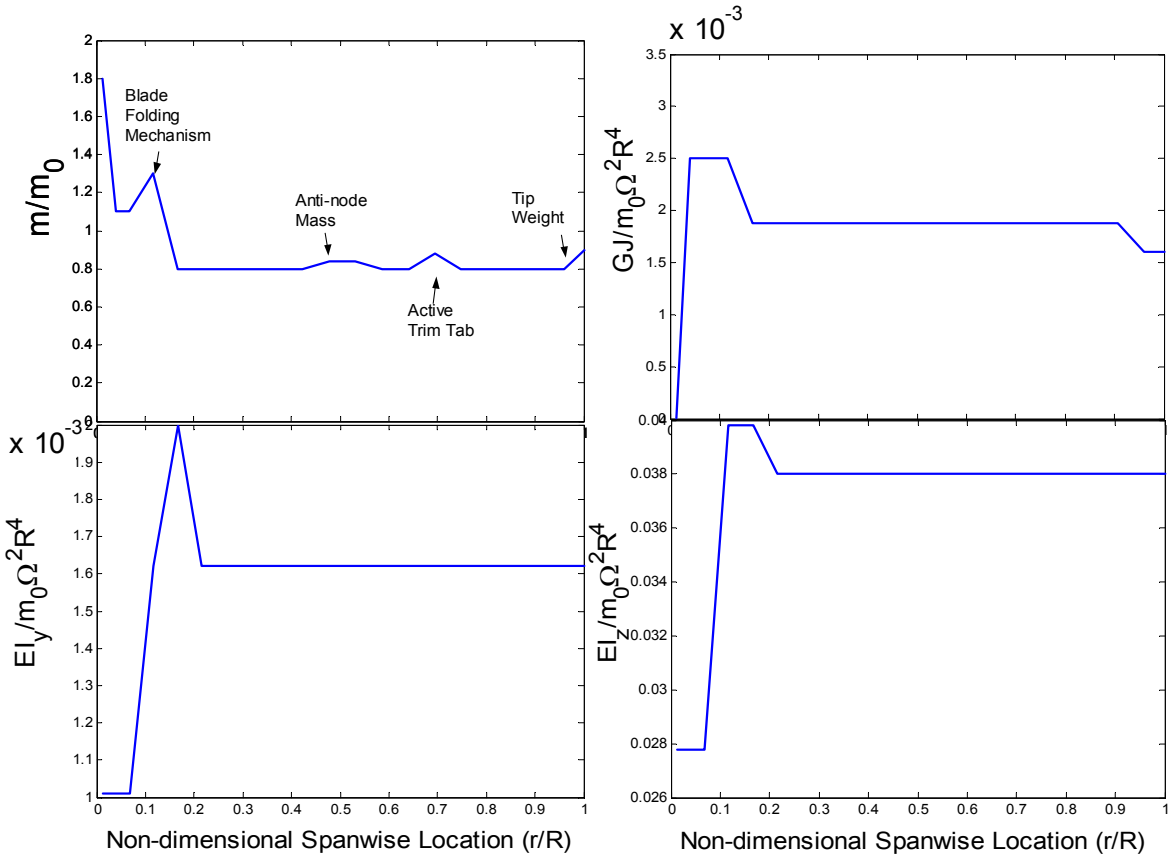

Figure 5.5: Blade Stiffness and Mass Distribution

5.7.2 Aeroelastic Analysis: A detailed aeroelastic analysis was performed to ensure the rotor was free from any aeromechanical instability (Fig. 5.9). A pitch-flap flutter analysis (Fig. 5.7) indicates that the critical c.g. offset to avoid pitch-flap flutter and pitch divergence is far behind the quarter chord at nearly 31% of the chord from the leading edge. Ballast weights in the blade tips were used to move the c.g. ahead to 22% of chord. This provides adequate margin to avoid pitch-flap flutter and divergence.

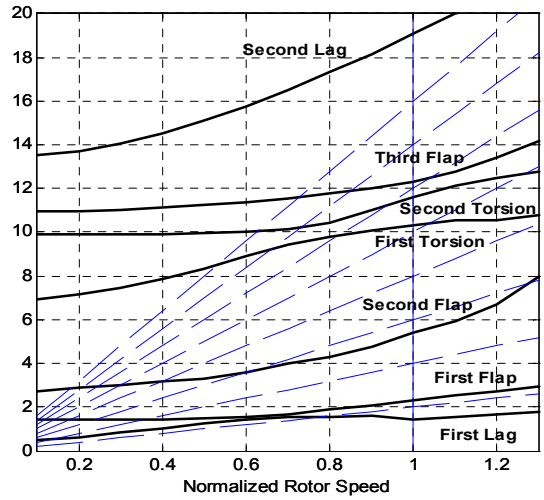

Figure 5.6: Fan Plot

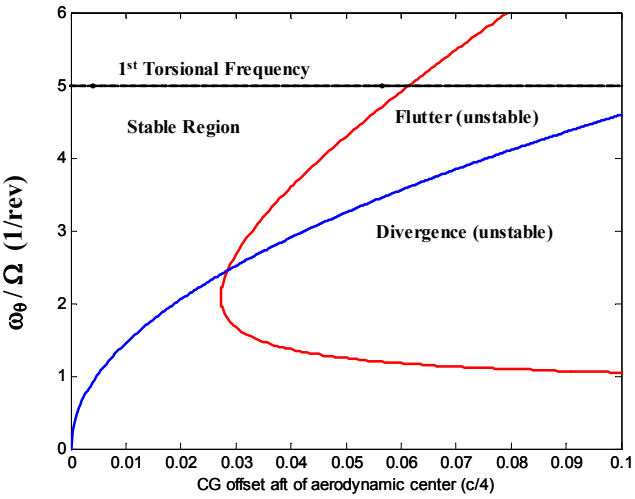

Figure 5.7: Pitch-Flap Flutter/Divergence

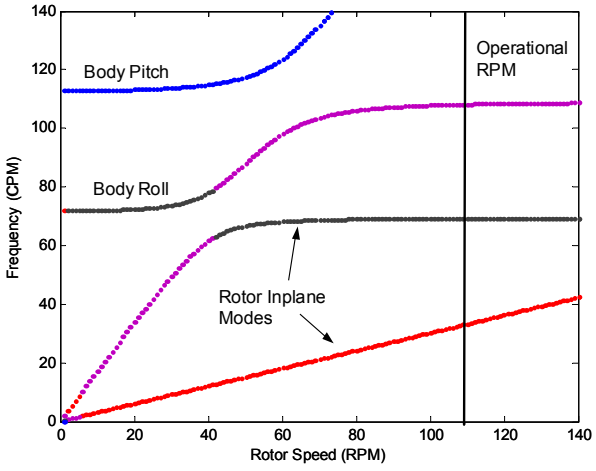

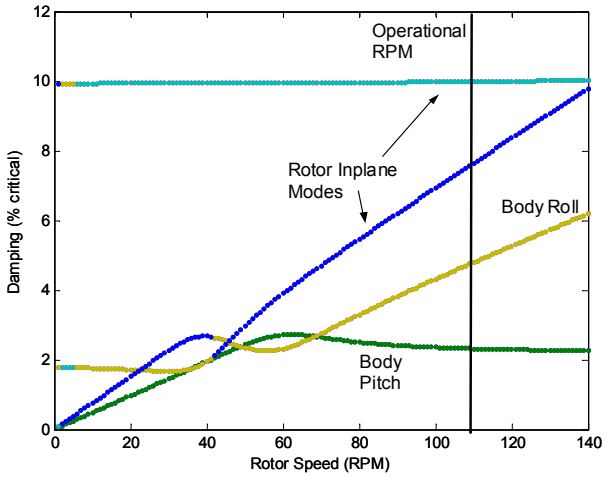

Figure 5.8: Ground Resonance Analysis

5.7.3 Ground & Air Resonance: Soft-in-plane rotors, such as the hingeless design implemented on the Atlas, are susceptible to interactions of rotor flap and lag modes with the fuselage pitch and roll modes. Therefore, a comprehensive ground resonance analysis was performed to ensure no instabilities existed. It can be seen from Fig. 5.8 that all modes,

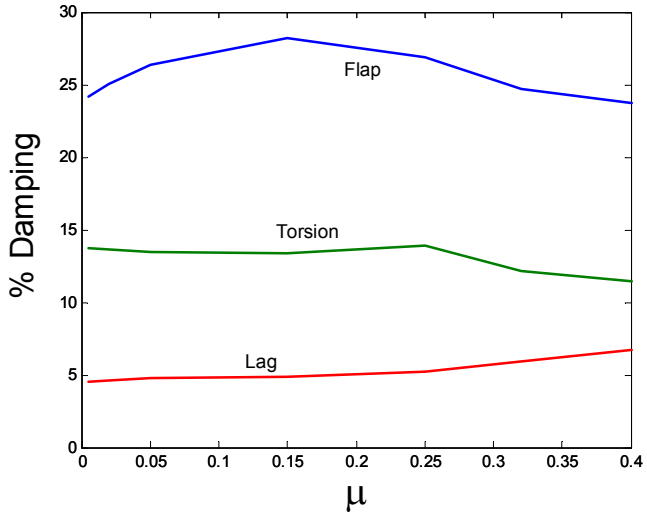

Figure 5.9: Flap/Lag/Torsion Analysis

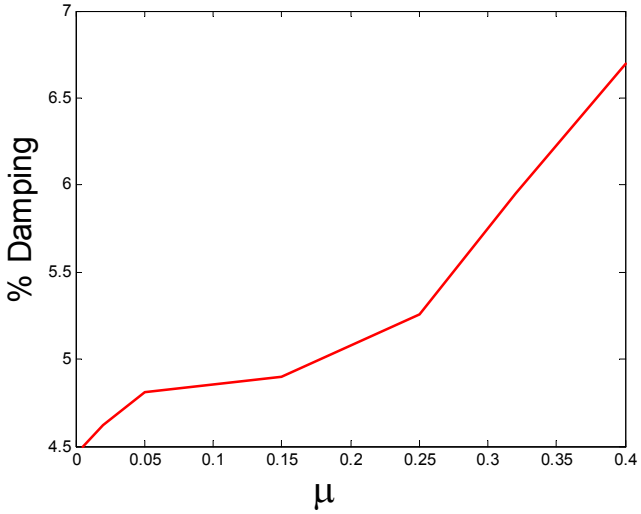

Figure 5.10: Air Resonance Analysis

including rotor in-plane modes, are stable and adequately damped. A comprehensive air resonance analysis was performed (Fig. 5.10), and it can be seen that all modes remain stable.

5.7.4 Autorotation

Autorotation is a critical component of helicopter design; as it provides the only means of safe landing in the event of an emergency. Table 5.5 compares the autorotative index of the Atlas with helicopters of similar size. The Sikorsky definition was used for the comparison, given by: $AI = \frac{J\Omega^2}{2W \cdot DL}$ where J is the polar moment of inertia of the main rotor. The Atlas has good autorotation characteristics compared to current heavy lift designs.

Table 5.5: Comparison of Autorotation Index for Heavy Lift Helicopters

Helicopter	GTOW (lb)	Polar moment of inertia (slug-ft^2)	Rotor speed (RPM)	Disk Loading (lb/ft^2)	Autorotation index (ft^3/lb)
Atlas	108,500	182,800	114	9.32	12.9
Mi-26	123,000	198,000	132	14.26	10.8
CH-53E	73,500	51,800	177	14.99	8.1

Section 6: Anti-Torque System

6.1 Anti-torque comparison

From the initial configuration selection (Section 3), a conventional tail rotor was chosen for the Atlas. Fan-in-fin tails are also used because of their increased safety to ground personnel. However, on a heavy lift helicopter the tail rotor is at a height that presents no danger to ground personnel. Fan-in-fin concepts, while ideal for smaller helicopters both for their increased safety, and reductions in noise and weight, are not viable on a helicopter of this size. The duct of fan-in-fin does not scale linearly with gross weight. A significantly larger duct weight component moves the c.g. unacceptably rearward. The thick duct profile also causes excessive drag in forward flight.

6.2 Tail Rotor Detailed Design

Sizing of the tail rotor is accomplished by the use of the sizing code discussed in Section 4, summarized in Table 6.1. Diameter of the rotor is a fixed ratio of the main rotor diameter, based on data from Tishchenko [Tish76]. A low value of C_T/σ is necessary for the tail rotor to prevent the onset of stall. Blade solidity was chosen to provide the thrust for the C_T/σ necessary for anti-torque during hovering at sea level. An iterative scheme was implemented to determine the chord and number of blades. The vertical fin uses a NACA 23012 airfoil set at a positive incidence so the tail rotor is somewhat offloaded in forward flight. To reduce the penalties associated with vertical fin blockage, a pusher rotor was implemented on the Atlas. The direction of rotation is aft at the top to minimize main rotor/tail rotor interactions.

Table 6.1: Tail rotor properties

Diameter (ft)	22.4
Chord (ft)	1.45
Distance between tail rotor and main rotor hub (ft)	70.0
Number of blades	6
Tip speed (ft/s)	722
Solidity	0.25
Power required (hover)	2137 hp
Blade airfoil	SC1095
Type	Pusher
Direction of rotation	Aft at the top

6.3 Tail Rotor Structure

The tail rotor hub uses a bearingless design to take advantage of their cleaner aerodynamics and reduced parts count. The primary hub structure consists of three identical stacked composite yokes. This arrangement reduces manufacturing complexity over a single six-arm design. Their smaller size also permits easier transportation than a single six-arm yoke.

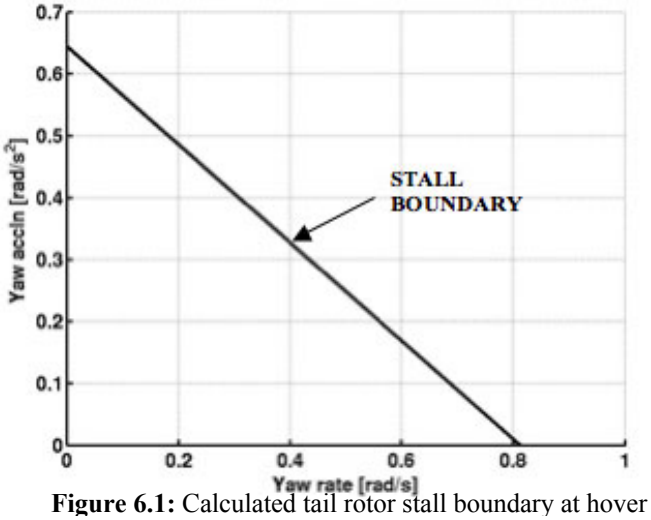

Figure 6.1: Calculated tail rotor stall boundary at hover

The arms of each yoke accommodate flapping and feathering flexures, in-plane motions, and also serve to transmit torque from the driveshaft to the blades. The flapping flexure is the most inboard component of the yoke, with the equivalent hinge offset at four percent radius. The feathering flexure is located outboard of the flapping flexure and is tailored not only to provide feathering motions, but for dynamic stability as well. The yokes extend to 15% of the blade radius.

The yokes are constructed of continuous filament-wound unidirectional IM7 graphite/epoxy tape that winds around composite blade attachment sleeves at each end of the yoke. Plies of ±45° graphite/epoxy are added between layers of tape to provide the required flapping and feathering flexures as well as strengthen the blade attachment area. Torque is transmitted from the driveshaft through bushings that run through each of the yokes and attach to a flange on the mast. As with the main rotor hub, the elimination of one of the bushings eliminates the possibility of incorrect assembly of the hub, which requires no special tools for assembly. A spider, located outboard of the stacked yoke, performs the collective pitch change for the tail rotor. Tail rotor blades use the same construction as the main rotor blades. The D-spar of the tail rotor blades, however, does not employ bending-torsion coupling. This simplifies tooling and composite layup, reducing manufacturing costs.

6.4 Tail Rotor Performance

During a hovering turn, the tail rotor is required to compensate for main rotor torque, provide yaw acceleration and accommodate tail rotor precession effects [Lynn69]. Figure 6.1 shows the stall boundary for the tail rotor based on the thrust requirements during a low speed yawing maneuver. Based on this, the maximum limiting combinations of yaw rate and yaw acceleration that can be carried by the helicopter in hover may be determined.

Section 7: Airframe and Landing Gear Design

7.1 Cargo Bay Cross-Section

The primary mission of the Atlas is to transport the Future Combat System (FCS), which is designed to fit within a C-130 cabin cross-section as shown in Fig. 7.1. Cabin accommodations are provided for two FCS vehicle crew. As the FCS

crew are considered as passengers, a 14-inch safety aisle is required between the cargo and airframe for emergency exit access; a six inch airframe clearance around the payload is included in the safely aisle [Engi71][AirF00]. Taking this into consideration, total FCS dimensions are estimated as: 91" W x 102" H x 240"L. The Atlas cargo floor area is 119-inch wide and 268-inch long to allow sufficient space for securing the FCS vehicle. An additional requirement in the RFP stipulates the aircraft must transport two 463L cargo pallets (88x96-inches and 108-inches height). A tradeoff study was conducted to determine the feasibility of carrying three pallets, as the payload weight would still remain less than the FCS vehicle. Three pallets require an area of 136-inches by 296 inches. The structural floor weight is the heaviest component of the central fuselage weight, and because the increased length of the cargo area in the three-pallet configuration increases floor component weight by 29.6%. Such an large increase in structural weight of the helicopter is not acceptable. For these reasons, the Atlas will use the 2-pallet configuration.

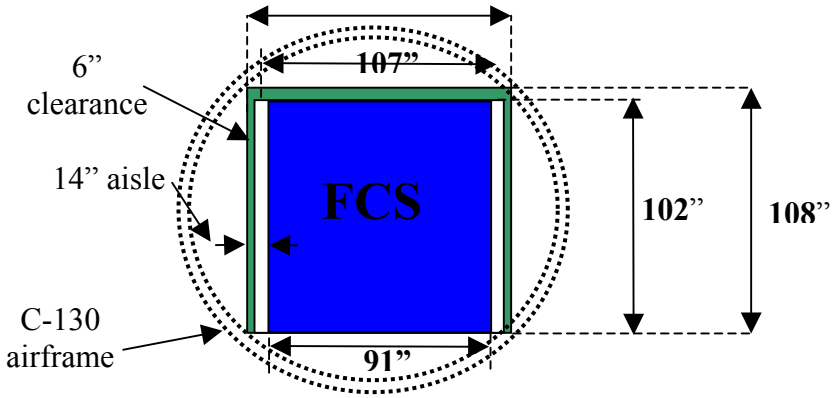

Figure 7.1: C-130 cross-section with FCS vehicle dimension assumptions

7.2 Airframe Design

The structural design of the Atlas is comprised of three primary modules: the cockpit, the cargo bay, and the empennage. Primary bulkheads are designed to efficiently support the transmission deck and maintain a crashworthy airframe. Additional secondary bulkheads maintain aircraft cross-section, skin cutouts, the cargo door, and the empennage. The minimum height of the Atlas, determined by the mast height necessary for blade/airframe clearance and the large cargo bay necessary to transport the FCS, exceeds the height of the hangar deck of the L-Class ship. However, the aircraft, in its stowed configuration with blades and tail empennage folded, fits in the CVN maintenance deck with 20 inches of clearance.

7.2.1 Structural Details: All structural members are designed with a load factor varying from –0.5g to +2.5-g and also a safety factor of 1.5 over the design loads. As shown on the structural layout (Foldout 7.1), thirteen primary bulkheads provide the proper flight and ground maneuver load paths, as well as interconnect the airframe modules. The first primary bulkhead connects the nose and the cockpit, and supports the radar avionics. The second primary bulkhead and supports the cockpit floor and nose gear load. The third connects the cockpit to the cabin. The fourth through eighth bulkheads carry the transmission deck loads from the main rotor to the airframe. The fifth and sixth bulkheads are the primary support from the

Foldout 7.1 - Structural Layout

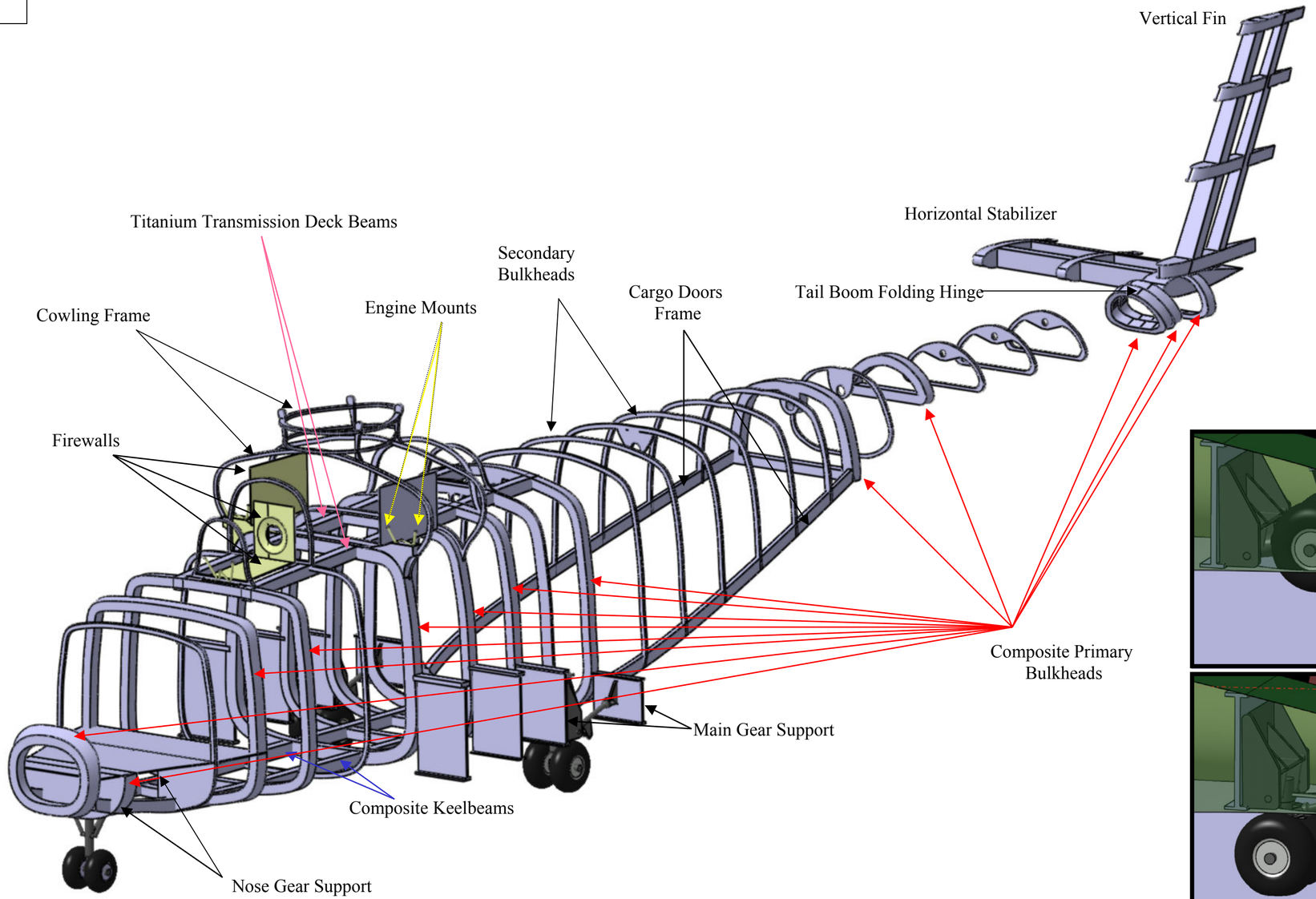

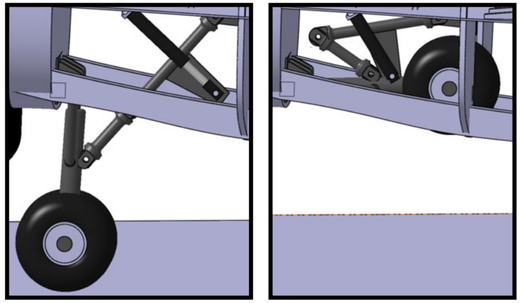

Nose Gear Retraction

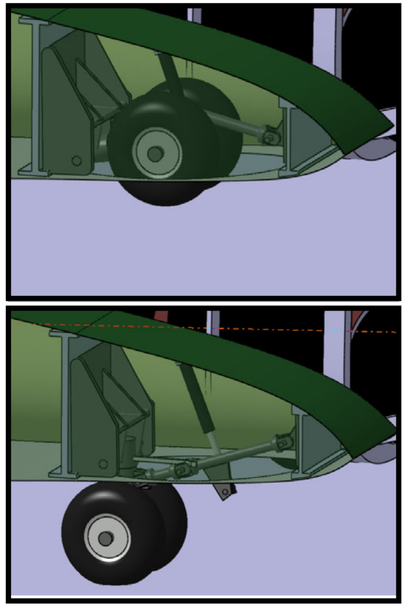

Main Gear Retraction

transmission deck to the airframe, while the seventh bulkhead supports the main gear load path. The eighth primary bulkhead, placed at the rear of the cargo area, supports transient loads during cargo loading and unloading. The ninth bulkhead supports the rear cargo-door frame. The empennage is connected to the rear cargo section by the tenth primary bulkhead. The eleventh and twelfth primary bulkheads provide support to the tail-boom folding hinge. The final primary bulkhead supports the tail rotor, horizontal and vertical fin loads. Clamshell doors are attached to an inclined support bolted to the eighth and ninth bulkheads.

7.3 Airframe Layout

7.3.1 Cockpit: Pilot and copilot seats are can be adjusted longitudinally to fit crewmembers from the 5th percentile and to the 95th percentile of the population [Engi74]. Armored seats were chosen for safety considerations. Seat stroke and damping are controlled by a cutter mechanism, which absorbs energy in a crash by shaving metal from a seat support as the seat compresses. Seats are floor-mounted and crashworthy, satisfying FAR part 29/27 requirements [MB01]. Port and starboard windows in the nose allow the pilot to see downward during shipboard approaches and set-downs.

7.3.2 Cabin and Cargo Bay: The cabin area, between the cockpit and cargo bay, contains three seats for the loadmaster and two FCS crewmembers. The 29.7 lb seats are unarmored to save weight. Cabin seating arrangements for the loadmaster and FCS vehicle crew are symmetric to the centerline of the fuselage. Life jackets are provided for each person on board, beneath the seats. The cockpit and cabin floor is positioned 27 inches higher than the cargo bay level, providing space for nose gear retraction and avionics systems.

The cargo area is configured such that the main rotor shaft axis, with 5º forward tilt, passes through the CG of the payload. A nonstructural fairing covers the engines and transmission. Engine cowlings are hydraulically actuated and may be used as work platform for the rotor. “Kick-in” steps on the outer fuselage offer easy access to the engines and transmission access panels.

7.3.3 Doors and safety exits: The Atlas is equipped with three exit doors. The first is located on the port side at the rear of the cabin; the second and third are placed at the rear of the loading area. All are large, hinged on the forward side, and located on the lower level for safe entry and exit to and from the helicopter. These doors, as well as the cockpit and cabin windows, can be jettisoned in the event of an emergency, as described in 14CFR29.783.

7.3.4 Sponsons: The sponsons contain the fuel tank volume and main gear. Assuming a fuel density of 6 lb/gal, the fuel capacity is 1,737 gallons. Fuel tanks are located in the sponsons along the sides of the cargo bay, with their CG located on the main rotor shaft axis. This location simultaneously improves crash safety and reduces the height of the aircraft. The main landing gear are semi-retracted and secured in the rear portion of the sponsons. This gear configuration increases the lateral distance between the main landing gear, improving tip-over angle. A streamlined airfoil profile is used for the sponsons, which are secured through spars attached to the fourth and fifth primary bulkheads.

7.3.5 Empennage: The tail boom is sized to support the tail rotor, and vertical and horizontal stabilizer bending loads. The stiffness is tailored such that its natural bending modes do not coincide with the main rotor and tail rotor harmonics. The tail boom cross-section has a flat bottom to maximize FCS vehicle clearance near the loading ramp. The top surface of the tail boom provides walkway access to the base of the vertical fin from the transmission cowling, while kick-in steps on the leading edge of the vertical fin facilitate tail rotor and gearbox maintenance.

7.4 Cargo Loading

7.4.1 Loading Considerations: Great concern was taken to ensure that the FCS has adequate clearance under the tail boom. Automatic loading, positioning and securing methods were considered to minimize loading time. Although such methods may reduce loading time, they were rejected due to unnecessary weight penalties, mechanical complexities, and maintenance issues associated with them. Sufficient internal clearance and drive paths are provided such that the crew can drive the FCS vehicle into the cargo bay (Foldout 7.2). The FCS is then secured to the cargo bay using chains to the cargo bay hard points. Pallets are loaded using a forklift and an internal winch. Appropriate nylon tie-down devices (15,000 lb. rating) secure the load to cargo bay hard points (Foldout 7.2). Such straps, meeting Mil-Spec requirements, are commercially available.

Loading and refueling may be accomplished concurrently, reducing turnover time between missions. With ten tie downs to secure, and if a time of two minutes per tie-down per person is assumed, it will take three crew members (load master and two FCS crew) seven minutes to secure the FCS vehicle in the cargo bay. With another two minutes allotted for driving the FCS into the cargo bay (nine minutes total), the loading process will be accomplished in less than the 15 minutes required for fueling. Although automatic loading can reduce loading time, the mission time would remain unchanged.

7.4.2: Airframe Loading Structures: Clamshell doors and a ramp, both hydraulically actuated, are located at the rear of the fuselage to provide cargo loading. Clamshell door curvature is simplified to minimize manufacturing cost and structural complexity. To support the 20-ton payload weight during loading, the ramp is constructed of a sandwich structure, consisting of an aluminum foam core between two layers of steel. The ramp surface is knurled to increase traction. Two braces on the ramp outer surface support cargo loading operations. Both nose gear and main landing gear include pneumatics; extending the nose and retracting the main gear create a level path for cargo loading.

7.5 Manufacturing

7.5.1 Airframe Materials: Bulkheads and keel-beams are structurally simplified to allow for low cost manufacture, final assembly, and maintenance. Carbon composite is substituted extensively for traditional metal skin and stringers, saving approximately 30% weight over a traditional layout of equivalent strength and stiffness [Beau05]. The fuselage skin is carbon composite construction, with IM7 graphite and 8552 epoxy matrix. The composite sandwich replaces the traditional skin and stringer construction, eliminating fasteners and simplifying manufacturing assembly. In the maritime operational environment of the Atlas, the corrosion resistance of graphite is also a primary advantage, reducing maintenance and

Foldout 7.2 – Inboard Profile

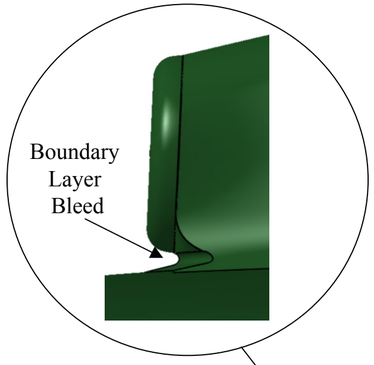

View of Vehicle Loading from Rear

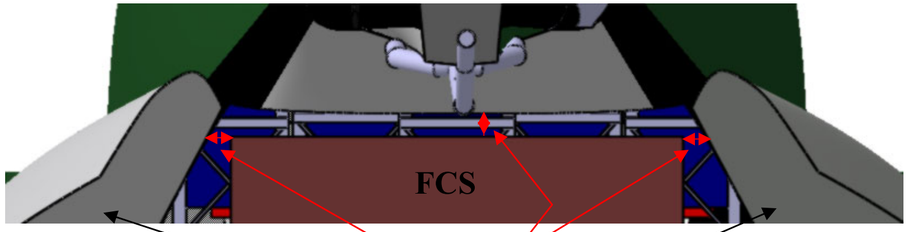

Alternate Missions

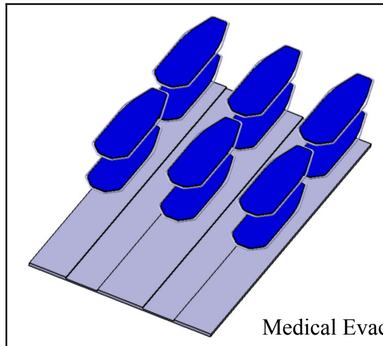

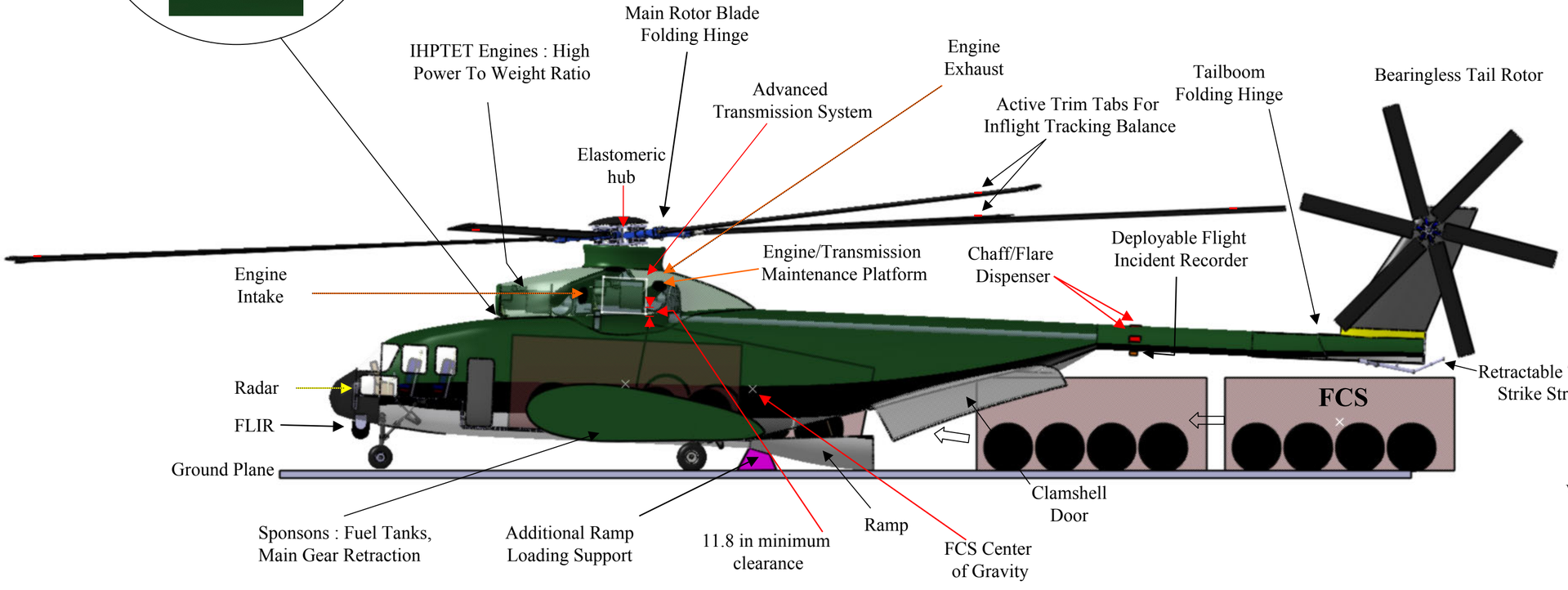

463L Pallets Loading

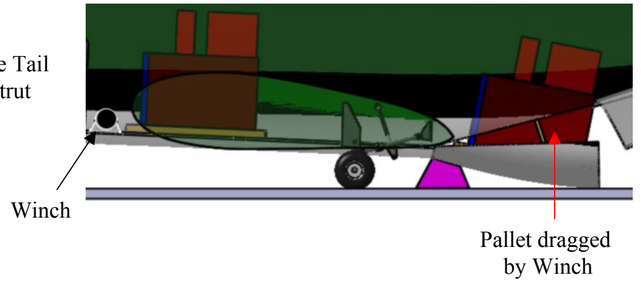

operating cost. Aluminum mesh installed during the skin layup, provides lighting protection and prevents the composite skin from delaminating. Static discharge wicks are placed are placed on the sponsons and tail boom to dissipate electrical charge into the air. The cockpit and cabin underbelly skin are both reinforced with light-weight Electromagnetic Polymer armor, which provides ballistic armor for the crew, and also protects the helicopter from loose debris stirred up by the rotor downwash during hover. The nose of the helicopter is made of E-glass epoxy to allow transmission and reception of the radar signal.

Primary bulkheads of the Atlas are constructed principally of IM7 graphite/epoxy. Composites were chosen due to their resistance to fatigue and cracking. Titanium reinforcements, inserted during layup, are added at the skin attachment locations to reduce the likelihood of tearout. Although a fully integrated composite airframe is not yet in production, the technology to do so is becoming more mature. The bulkheads and skin for the Atlas are fabricated separately and joined later in manfuacturing. The transmission deck and firewalls are made of titanium alloy plate, offering heat and fire resistance. Titanium plate was chosen over aluminum lithium or composites for its superior heat and oil corrosion resistance [UMCP04].

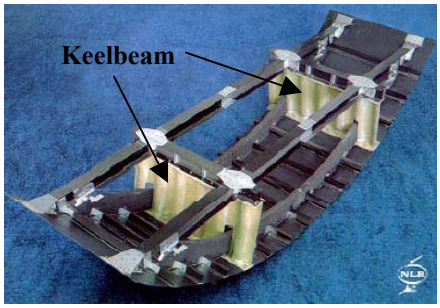

Figure 7.2 Sine-wave keel beams

7.5.2.1 Airframe Structures: The web of each keelbeams is designed to collapse in a high buckling mode, increasing the amount of energy absorbed in emergency landings. Bulkheads are designed to collapse progressively under high inertial loads to minimize the transfer of crash energy to the crew seats.

Keelbeam are constructed as sine-wave beams (Fig.7.2) connected by cruciforms, which are soft in compression to avoid high peak loads during a crash and maintain stability between the sine-wave beams. During a crash, energy is absorbed by crushing the sine-wave beams, constructed of graphite-kevlar fabrics. Kevlar is used to maintain the post crash structural integrity [Ubel02].

In case of a crash on land, the landing gears dissipate approximately 50% of the crash energy. However, in the event of an impact on water, the skin must transfer the crash loads to the keel beams, which absorb the largest amount of energy. It is therefore essential that skin integrity is maintained. *Poly-Ethylene fabric* (*Dyneema*) was shown to be the only reinforcement capable of resisting large deformation without fiber breakage while transmitting the load to the sub-floor structures. For the Atlas, a sandwich structure of Dyneema, carbon fiber, and Kevlar is used for the skin on the underside of the helicopter. Its core is a corrugated plate made of three layers Dyneema embedded in epoxy resin, and is combined with two layers of Kevlar fabric. The three-layer core was found to give the maximum energy absorption and smallest total deflection during dynamic tests compared to other configurations [Ubel02].

7.5.2.2 Fuel Tanks: Fuel tanks are designed to be both crashworthy and puncture resistant, and to meet AR-56 military requirements. Tanks meeting these requirements are commercially available. An additional liner is added in the tank with the capability to expand upon contact with fuel preventing leaks in the event of bullet penetration. Layers of light, fire-resistant polyurethane foam are placed outside the liners to prevent the tank from catching fire. Furthermore, the fuel tank pipe joints are self-sealing. A pressure relief valve accounts for the change in density as altitude increases. A static discharge port is also present to prevent the generation of sparks during refueling.

7.6 Landing Gear Design

The two different types of landing gear currently used on helicopters are skid type gear and wheeled gear. (nose-wheel or tail-wheel, retractable or non-retractable). Skid type gear is limited for use on helicopters with a gross take-off weight less then 10,000 pounds and, therefore, is not considered for use on the Atlas. A tricycle retractable landing gear configuration was chosen to accommodate the Atlas's rear loading design. A trade-study was performed to determine if the benefit of reduced drag outweighed the additional weight, cost, and mechanical complexity of a retractable gear system. The results of this study showed a 4% reduction in cruise power and more importantly a large reduction in the nose down pitching moment in forward flight with a retractable landing gear, and as such was implemented on the Atlas.

The longitudinal locations of the gear with respect to the rotor mast are based on distribution of the static reaction loads with the helicopter at gross take-off weight. In static conditions, the nose gear carries up to 20% of the load. The angle between the main gears and the most aft position of the aircraft center of gravity is 17.5 degrees, which is higher than the minimum value of 15 degrees required by turnover conditions [Curr88, Rosk04, Niu88]. To ensure good handling requirements for ship-based operations, the lateral tip-over angle is restricted to 54 degrees [Will89]. A wide wheel track was obtained by attaching the main gear to the sides of the fuselage. The Atlas has a wheelbase of 26.8 ft (8.1m), wheel track of 16 ft (4.9m) and the main gears are "toed-in" by 1-degree for smooth turning. The nose-wheel has a steering mechanism that allows swiveling up to 60 degrees on either side using either the rudder pedals or a hand-wheel; this mechanism is disengaged prior to retracting the gear. The Atlas uses carbon composite torque links, which are lighter, and stronger then conventional steel torque links [Thui99].

7.6.1 Tires and wheels: Each gear used two tires with a low inflation pressures to allow for landings in unprepared fields. The main gear uses Goodyear Type H31x13-12 (20 plies) with a rated load of 26,000 lbs and inflation pressure of 155 psi, while the nose gear uses Goodyear Type H25.5x8.75-10 (14 plies) with a rated load of 12,750 lb and inflation pressure of 101 psi [Airc02]. The wheels are made of forged aluminum alloy and are equipped with carbon brakes to get higher energy absorption and thermal resistance with low weight [Chai96].

7.6.2 Magnetorheological (MR) Fluid Based Landing Gear: Based on the mission profile, the Atlas is expected to land under varying conditions at different gross weights and on unprepared landing sites. Passive shock absorbers are point

designs for the "worst-case" landing scenario and therefore are not optimized over the range of landing conditions experienced by the helicopter. Landing impact has been recognized as a significant factor in structural fatigue damage, and passenger/crew discomfort, therefore, a smart landing system with adaptive damping characteristics proportional to the landing velocity is desirable [Berg98].

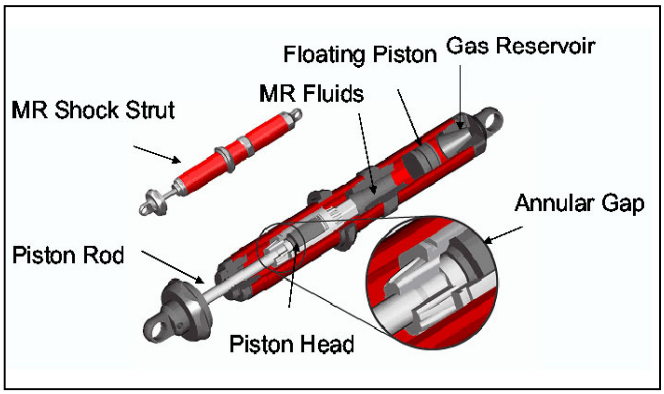

Figure 7.3: Schematic of an MR fluid based shock absorber

Magnetorheological fluids are known to have continuously controllable rheological properties, fast response times, and have been used in structural dampers, automobile suspensions systems, helicopter lead-lag dampers and similar applications. The yield stress of the MR fluid in the presence of a magnetic field produces additional damping, which helps to dissipate a large amount of impact energy and prevent it from affecting the main structure. Considerable research has been carried out to develop shock dampers and design controllers [Choi03] for continuous damping in response to impact velocities.

It is proposed to use a MR-based shock absorber in the landing gear system. A schematic of a flow-mode MR shock strut is shown in Fig. 7.3. The shock strut consists of gas and hydraulic reservoirs, similar to conventional oleo-pneumatic devices. The piston head divides the hydraulic reservoir, which is filled with a controllable MR fluid, into upper and lower chambers. The fluid moves in between chambers through an annular valve. A gas chamber is located above the upper chamber to compensate the changing fluid volume because of the movement of the piston rod. When a magnetic field is applied to the controllable fluid, additional damping force is generated in the annular valve by the field-induced yield stress. This damping force can be controlled continuously by adjusting the intensity of the applied magnetic field based on velocity feedback.

For safety reasons, the landing gear should operate successfully even in case of loss of power or failure of control strategy. The sizing for a conventional shock absorber were used for the MR shock strut design because it produces the same damping force as a passive oleo-pneumatic shock absorber in the absence of magnetic field. However, to obtain MR effect in a conventional strut, several components need to be added (e.g. coils to generate a magnetic field, flux return paths using magnetic material). These components add to the weight of the overall system. In our case, the additional weight is estimated to be 8% of the weight of an oleo-pneumatic shock absorber.

7.6.3 Shock strut sizing: The MR shock struts were sized by determining the equivalent required size of a conventional oleo-pneumatic shock absorber. Oleo pneumatic shock absorbers dissipate impact energy by forcing oil through an orifice and into a pressurized chamber. The oleo shock strut sizing was used to estimate MR shock strut design. In conformity with structural design requirements for helicopters operated by the Navy Section 3.4.2.4 of [AR5670], the maximum stroke of the

shock absorber was calculated from the energy dissipation required from a 12ft/sec vertical landing impact at the helicopter gross take-off weight. The energy absorption efficiencies of the tires and the shock absorber are taken as 0.47 and 0.85 respectively, and tire deflections are assumed to be one-third of the respective radii. An additional stroke of 1 in. was added to the calculated value to account for uncertainties and provide a margin of safety.

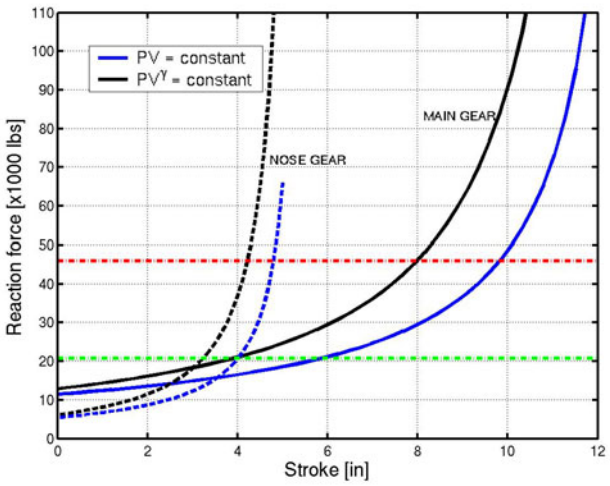

Figure 7.4: Force-stroke diagram of shock

The static pressure in the shock absorbers when supporting the gross weight of the helicopter is 1800 psi. The minimum length of the overlap section is 2.75 times the piston diameter while the external diameter of the strut is 1.3 times the piston diameter. The compression ratios are chosen as 4:1 (static: extended) and 3:1 (compressed: static). Load-stroke curves under isothermal and polytropic compression [Curr99, Milw53], shown in Fig. 7.4, used to determine the strokes under different loading conditions. The results are listed in Table 7.1

Table 7.1: Shock absorber dimensions (in inches)

	Piston diameter	External diameter of shock strut	Maximum stroke	Overall length
Main gear	5.8	7.6	12	28
Nose gear	4.0	5.2	5.0	16.0

7.6.4 Retraction scheme: To minimize the drag in forward flight, the main and nose gears are retracted backwards into the sponsons (behind fuel tanks) and fuselage (underneath the cockpit) respectively. The main undercarriage is not fully retracted into the sponsons and a part of the tires is left exposed because of space limitations. A drag link attached to a spar on the sponson and a hydraulic actuator is used to raise and lower the gear. The gear in its retracted and extended configuration is shown in Foldout 7.1. A positive downlock and an uplock are provided to prevent any unexpected motion of the gear and sensors are used to indicate the gear location to the pilot. An emergency blow down system is equipped on the gear to lower it in the event of a hydraulic failure.

Section 8: Folding Systems

8.1 Overview

As required by the RFP, the Atlas has an automated folding system that reduces its maximum dimensions for shipboard operations. The folding system is composed of a main rotor folding mechanism and tail boom folding mechanism. Both mechanisms are powered by hydraulics and centrally controlled by the folding program in the onboard computer. Feedback from various speed and position sensors on each mechanism allows the computer to correctly sequence and control the

folding procedure. The folding program allows for 3 folded configurations. The “fully folded” configuration is used for helicopter storage and provides the maximum reduction in overall helicopter dimensions. The “main rotor only” folded configuration leaves the tail rotor unfolded so that it does not block the rear loading door. This option is useful if the helicopter is being stored in a land-based hangar where there are no height restrictions. The “tail boom only” folded configuration is particularly useful for tail rotor maintenance. As seen in on Foldout 8.1, the tail boom folds forward and down reducing its overall height, making it more easily accessible. In this configuration, the main rotor blades are not folded and do not block access to the folded tail boom as they do in the “fully folded” configuration..

Once a folding configuration is selected, the folding progress is displayed on the MFD. If any faults or mechanical failures are detected during the folding process, the procedure is paused until maintenance is performed. The hydraulic system is designed so that even in the event of a folding system failure, the aircraft can be manually folded for relocation below deck to the maintenance hangar for repair. An “Emergency Stop” option is provided at all times during the procedure.

8.2 Automatic Main Rotor Blade Folding

To meet the requirement for automatic main rotor blade folding, the Atlas utilizes the onboard 3000 psi hydraulic system along with small hydraulic motors capable of supplying the torque required for this application. The main rotor system is seven bladed and by positioning one blade along the longitudinal axis of the fuselage, only six blades need to be folded (Foldout 8.1). The main rotor is equipped with an electronic speed sensor to measure its RPM and a position sensor to determine its azimuth position. During shut down, these sensors are monitored and when the rotor speed becomes low enough, the computer will initiate the application of the rotor brake. Through feedback of position and speed data, the rotor brake will stop the main rotor so that it is correctly indexed with the number 1 blade positioned over the tail boom and aligned with the longitudinal axis of the fuselage. After the rotor is correctly indexed, the rotor parking brake will be applied to prevent the rotor from wind milling.

It is necessary to offset the hinge from the rotor hub to prevent interference of the front rotor blades with the hub. Each folding hinge is offset 10% from the center of the rotor by using an extension spar as shown in Foldout 8.1. The inboard end of each spar attaches to the elastomeric bearing on the hub and the outboard end of each extension spar connects to the blade attachment point. The hydraulic motor and blade lock mechanism are located on the outboard end of this spar. Hydraulic lines and electrical lines run through the center of this spar (Foldout 8.1) to a 12-port hydraulic manifold and electrical connector mounted on the hub. This extension spar is manufactured from composite materials and has been sized to carry the flight loads as well as the large torsion loads created when in the folded position.

There is one rotary hydraulic motor and one hydraulic locking mechanism located at the hinge point for each of the 6 blades that require folding. When in the folded position, the blades transmit large torsional loads to the extension spar through pitch links and to the swashplate. The swashplate is not designed to handle these loads. After the rotor is parked,

Foldout 8.1 - Folding Systems

Folded Configurations

"Fully Folded" Configuration

"Main Rotor Only" Folded Configuration

"Tail Boom Only" Folded Configuration

Main Rotor Folding Mechanism

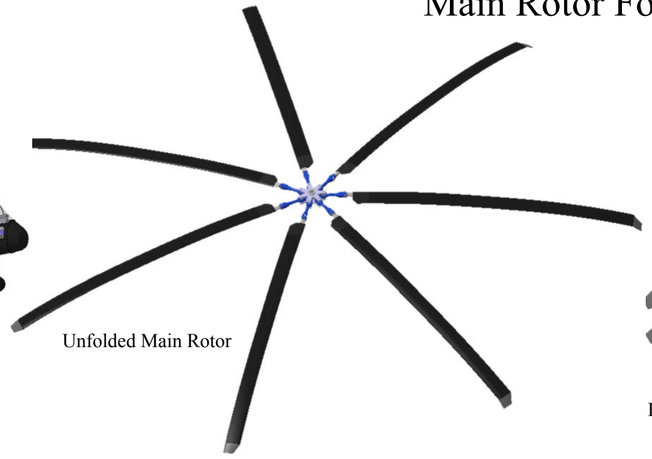

Unfolded Main Rotor

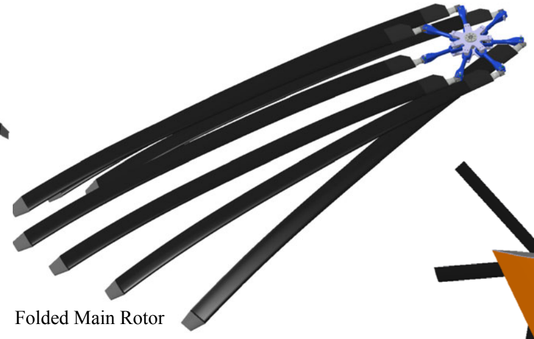

Folded Main Rotor

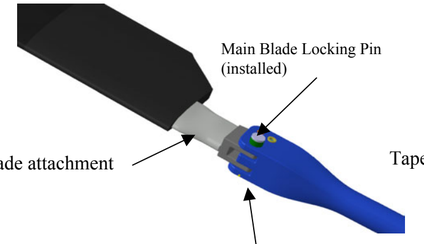

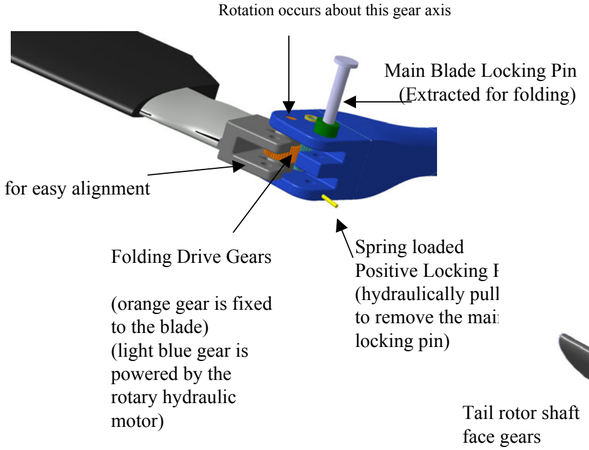

Tail Folding Mechanism

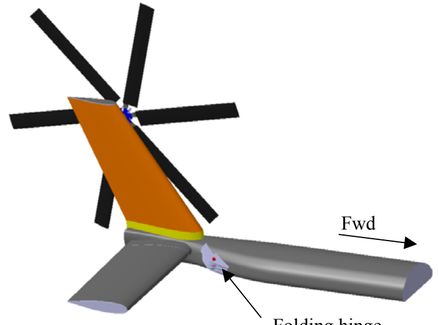

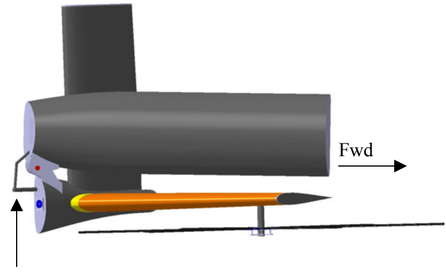

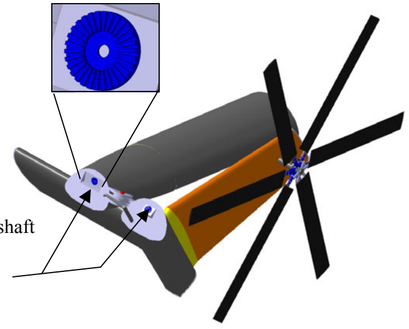

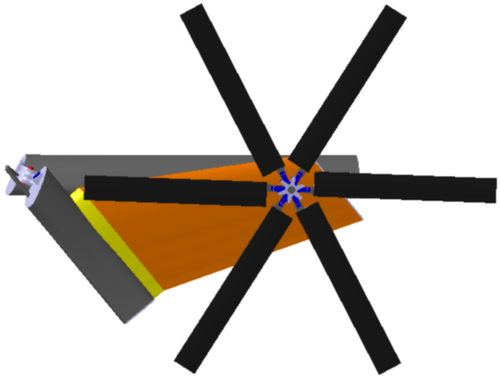

the extension spars are locked to the rotor hub by pins that are inserted by small electric motors. These pins transmit the loads to the rotor hub and alleviate swashplate loading. Even though blade number 1 does not require folding, it is constructed and attached in the same way as the other 6 blades to maintain inertial symmetry. The only difference is that a dummy hydraulic motor and locking mechanism of equal weight will be placed on blade 1.

The hydraulic motors and locking mechanisms are located in the rotating frame; whereas, the hydraulic pumps are located in the fixed frame. Typically, a hydraulic slip ring would be required to transmit this hydraulic pressure from the fuselage to the main rotor. However, because the blade folding motors only require hydraulic pressure when the rotor system is parked and indexed, hydraulic pressure is transmitted to the rotor through hydraulic lines, which connect the rotor hub to

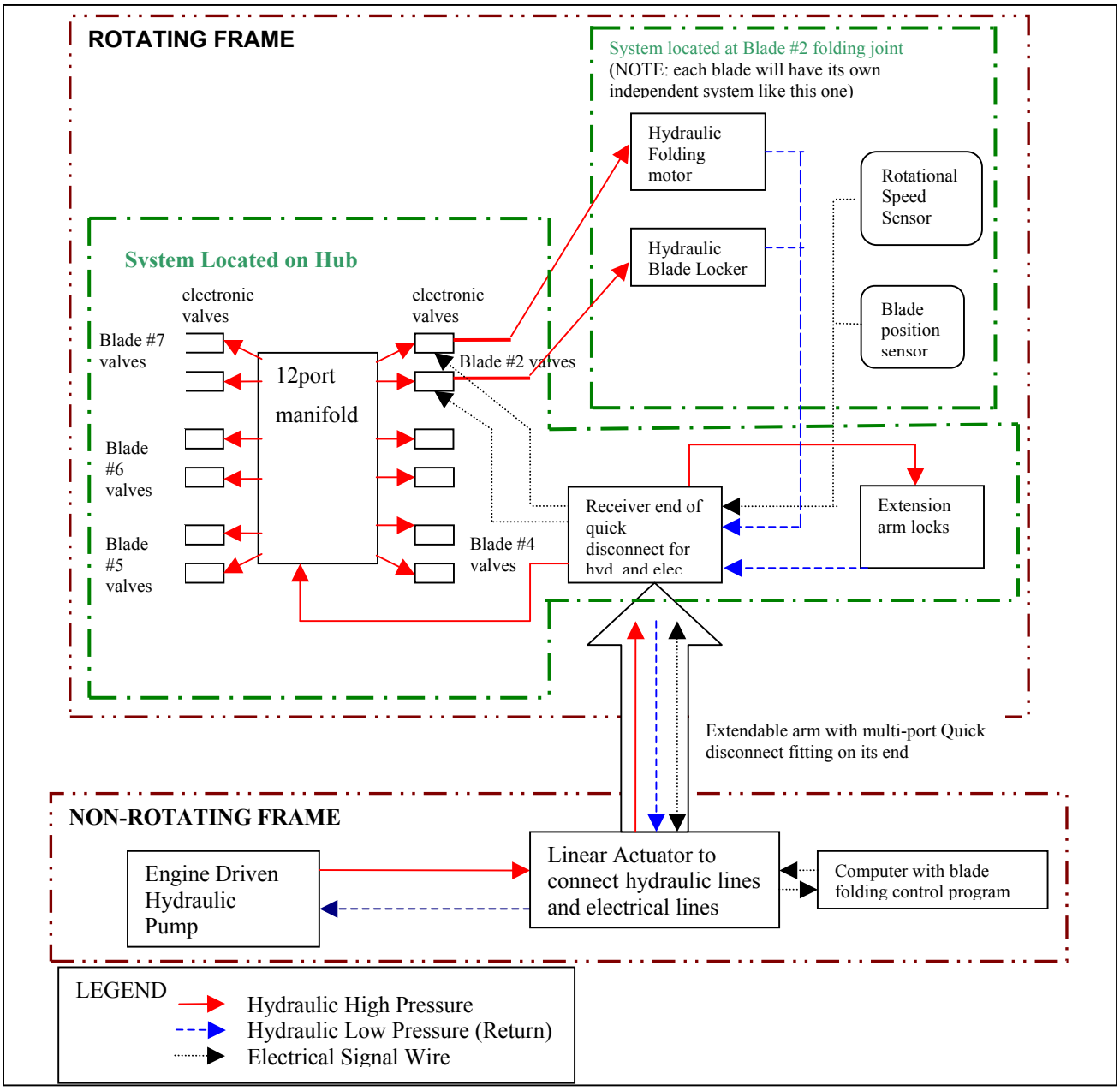

Figure 8.1: Hydraulic and Electronic Folding System Diagram

the fuselage after the rotor hub is parked. Then, the pilot will activate a switch and a linear actuator that is located on the fuselage below the rotor, will extend upwards along with a flexible hydraulic line. The linear actuator will insert the end of the hydraulic line into a hydraulic quick disconnect fitting located on the rotor hub. Hydraulic quick disconnect fittings are commercially available for systems up to 5000 psi and can be connected/disconnected with virtual no air inclusion or spillage of hydraulic fluid [Snap05]. These fittings meet MIL specs and are typically used for inspection of hydraulic systems. A guide hole on the rotor hub and a tapered guide pin on the end of the linear actuator will ensure correct alignment of the fittings. Using this type of system has the benefit of eliminating the hydraulic slip ring assembly, which are prone to leakage and require additional maintenance. In addition, the system ensures that there is no possibility of folding the blades unless the rotor is stopped and properly positioned. An electrical connection between the rotor hub and fuselage is also required so that the blade folding process can be fully automated. The same linear actuator will also be used to connect a multi-conductor wire to the main rotor hub from the fuselage in the same manner. The hydraulic line, which attaches the rotor hub to the fuselage after the rotor is stopped, delivers hydraulic fluid to the 12-port manifold, which is located on the rotor hub. This manifold has computer controlled hydraulic valves attached to each of the 12 manifold exit ports. These valves independently control the hydraulic pressure that is delivered to the hydraulic motor and hydraulic lock mechanism located at the folding joint of each blade. Each of the 6 folding blades is equipped with sensors at their hinge axis to monitor the individual blade position and rotational speed about the folding hinge, fed into the onboard computer. The onboard computer uses the sensor data and a folding control program to control the 12 hydraulic valves and control the blade folding process. The hydraulic and electric wiring diagram in Fig. 8.1 shows the locations and interconnections of each device.

A bi-directional hydraulic motor is mounted at each of the 6 folding hinges. The hydraulic motor supplies torque to the hinge axis through a gear set that provides mechanical advantage and reduces the required hydraulic motor size. The hydraulic motor needs to provide approximately 350 ft-lbs of torque to fold and unfold the blades. The torque requirement is based upon the blade mass, bearing friction, and any drag created by high wind operations which must be overcome to fold or unfold the blades. Small commercially available low speed, high torque hydraulic motors are easily capable of supplying this torque [Whit05]. Additionally, a hydraulic locking mechanism is also located at the folding joint to lock the blades in place when they are unfolded. The locking mechanism consists of a 1.5-inch diameter pin, which is hydraulically extracted and inserted into a hole that passes through the triple lap joint between the blade attachment and the extension spar (Foldout 8.1). The pin has a 2-degree taper, which will ensure the blade is properly seated when inserted. It is very important for the blade to be rigidly attached to the extension arm with no play in the joint. When the pin is inserted, a perpendicular spring-loaded pin positively locks it. The spring drives this pin into a detent on the main pin preventing it from pulling out. During extraction of the main pin, this positive lock pin is retracted using hydraulics.

The outboard end of the extension spar has been specially designed to provide a guide for the blade attachment during the unfolding procedure. During this procedure the blade must align itself properly without binding and align the pinholes. Tapering the ends of the blade attachment and chamfering the ends of the extension spar accomplish proper alignment of the blade. As the blade folding joint closes, the tapered tabs slide in and align the blade. The blade position sensor will indicate when the blade is properly seated in the joint. The hydraulic locking mechanism will insert the lock pin into the hole and the positive lock pin will insert to lock it in place. Note the full folding procedure in Fig. 8.2.

When fully folded, blades 2 and 7 rotate 40 degrees about their folding hinge axis so that they are parallel to blade 1. Next, blades 3 and 6 rotate 105 degrees about their folding hinge axis. The folding hinge axis on the extension spar and blade attachment for blades 3 and 6 is angled at 7 degrees from the vertical axis. This couples the rotation with downward vertical movement so that blades 3 and 6 fold underneath blades 2 and 7. Finally blades number 4 and 5 will fold back approximately 140 degrees. The hinge axis for blades 4 and 5 is angled at 11 degrees from vertical so that they fold back and down lower then blades 3 and 6. Blade number 4 cannot fold quite as far back as blade 5 because clearance must be left for the trailing edge of blade 4. Foldout 8.1 shows the blades in the fully folded position where the maximum lateral dimension is 40ft between the tips of blade 5 and 4 and a description of the folding and unfolding procedure.

Folding Procedure:

1. After landing the pilot will begin the shut down procedure.
2. The pilot must de-clutch the rotor in order to leave one engine running to power the hydraulic pump.
3. After de-clutching the rotor the rotor RPM will begin to decay
4. Once the rotor speed decays to 70% the rotor brake will be begin to be applied.
5. Using the rotor position and speed sensors, the rotor brake will stop the rotor in the correct indexing position.
6. Once the sensors indicate that the rotor is properly indexed, the pilot will be able to set the rotor parking brake.
7. Next the pilot will access the blade folding program and select the desired folding configuration
8. After selection, the linear actuator will extend from the fuselage to the rotor hub connecting it to hydraulic and electrical power.
9. After the hydraulic lines and electrical lines are connected the actuators will level the swashplate and install extension spar locks.
10. The lock pins are then hydraulically extracted to allow blade folding
11. After the pin has been extracted, blades 2 and 7 will begin folding. The blade speed and position sensors are monitored and the folding motors are controlled through this feedback.
12. If the “fully folded” option was selected, the tail boom will be folded at this time.
13. Next blades 3 and 6 and then blades 4 and 5 fold.
14. After all blades are folded the engine is shut down and the ground crew will tie down the blades to the fuselage using the attachment points on the blade tips and fuselage tail section.
15. Finally the ground crew can move the aircraft for parking.

Unfolding Procedure:

1. Ground crew unties the blades.
2. The engine is started.
3. Blades are unfolded and locked in the reverse sequence.
4. After blade sensors indicate that all blades are correctly locked, the pilot will disconnect the hydraulic and electric lines by retracting the linear actuator back into the fuselage.
5. After the linear actuator is fully retracted the pilot will be able to release the parking brake and pitch link locks.
6. After sensors indicate that the parking brake and pitch link locks are disengaged the pilot will check for freedom of movement of the cyclic control to ensure that the pitch links are free.
7. Starting procedure can continue as normal.

Figure 8.2: Blade Folding Procedure

8.2 Automatic Tail Boom Folding

The maximum unfolded height of the helicopter is 40 ft from the ground to the top of the tail rotor. A folding tail boom is necessary to meet the maximum folded height requirement of 25 ft for CVN operations. The tail boom of the Atlas is hinged 30 inches forward of the vertical fin leading edge. This hinge axis is angled 25 degrees forward from the vertical axis so that the tail boom folds forward and downward reducing the maximum height of the tail rotor. The folding hinge is located externally to reduce the complexity of the folding hinge. An internally located simple single-pivot hinge would not be able to achieve the range of motion required for tail folding. The use of an external hinge reduces the folding hinge complexity and size with a negligible drag penalty because the aerodynamic boundary layer at this location is thicker than a hinge itself.

The entire tail boom folding procedure is automated by the onboard computer system and is coupled with the automatic main rotor blade folding procedure, powered by hydraulic linear actuators. If the "fully folded" configuration is selected, then the tail boom must be folded after main rotor blades number 2 and 7 are folded. The folding program automatically sequences the main rotor and tail boom folding procedures so that they do not interfere with one another.

Once initiated, the tail boom folding procedure begins by engaging a tail rotor parking brake that will ensure that the tail rotor will not windmill after the tail rotor drive shaft is disengaged. Next the hydraulic tail boom lock mechanism will be disengaged and small hydraulic rams will rotate the tail boom about its hinge axis. The tail rotor drive shaft is split into two at the hinge joint and face gears are used to transmit power between the shafts (Foldout 8.1). As the tail boom begins to fold, the face gears will disengage. These face gears will remain in the same orientation with respect to one another because the rotor parking brakes have locked both the main and tail rotors. Flexible electrical and hydraulic lines are installed at the folding portion of the tail boom. A safety catch ratcheting assembly is located on the hinge. This assembly will hold the tail boom in its folded position and also prevent the tail boom from colliding with the fuselage in the event of a hydraulic failure during the folding or unfolding procedure. Once the tail boom position sensors have determined that the tail boom is in its fully folded position, the main rotor blade folding procedure will proceed as expected.

The unfolding procedure is the reverse of the folding procedure and will be carried out after main rotor blades 3, 4, 5 and 6 have been unfolded and locked in place. As the boom unfolds, the spring-loaded face gears will be pressed together by the springs ensuring that they are properly and securely meshed. After the boom has unfolded, the hydraulic locking mechanism will lock the boom and the tail rotor parking brake will be released.

Section 9 - Handling Qualities and Stability

ADS-33E (Aeronautical Design Standard – Performance Specifications) is a method of objectively defining the handling qualities of a helicopter, comparing pilot feedback to the helicopter's open loop vehicle dynamics. ADS-33E defines three ratings: Level 1, 2, and 3, Level 1 being the most desirable.

The AFDD (Ames) suggests certain ADS-33E requirements be tailored for cargo helicopters, as many maneuvers do not apply [Keys98]. The moderate aggression slalom maneuver is of particular interest for shipboard operations. Determined through flight tests, minimum roll attitude bandwidth for Level 1 is 2.3 rad/s, and up to 3.5 rad/s for high sea states. While the Atlas's estimated bandwidth near hover is 2.2 rad/s, the FCS can improve performance through closed loop control. As flight tests indicate a phase delay greater than 80ms can result in pilot induced oscillations, phase delay introduced must be minimized [Padf96, Tate94].

9.1 Stability

As a large cargo aircraft, stability must be understood both loaded and unloaded. Stability derivatives were computed using first principles-based methods described by Prouty [Prou86] for both conditions at hover and 150 kt cruise speeds (Fig. 9.1). As is typical, the yaw damping and phugoid modes are slightly unstable in hover. Dutch roll is also slightly unstable for the Atlas. As forward speed increases, all modes stabilize.

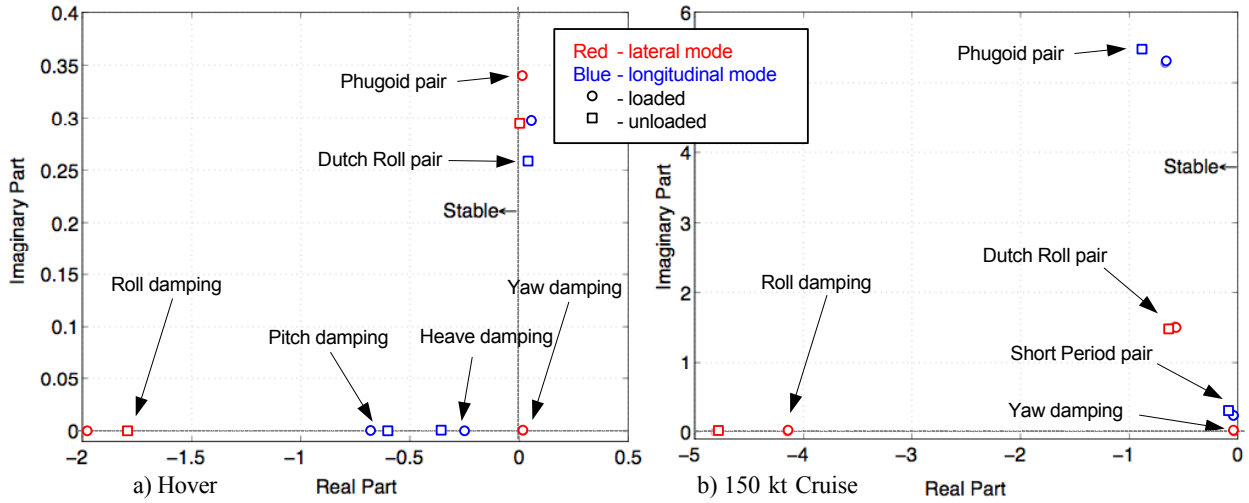

Figure 9.1: Hover and cruising flight stability modes

9.2 Effect of Design Elements

9.2.1 Hinge Offset: Unsteady winds common at sea must be accounted for when defining the FCS. Heaving motions can yield "low-g" conditions, unloading the rotor. In this situation, the sole source of moment control is flapping hinge offset. To evaluate control effectiveness in this condition, a metric compares control moment of the loaded to the unloaded case. The ratio is computed using rotor characteristics and hover blade loading (eq. 9.1.1a and 9.1.1b). This analysis implies that the Atlas's 3.5% flap hinge offset produces 42% of the loaded control force when unloaded. This is used to tailor the flight control system for adequate control, regardless of load.

$$\frac{\left[\frac{dM_{CG}}{d\beta_{1c}}\right]_0}{\left[\frac{dM_{CG}}{d\beta_{1c}}\right]_{hover}} = \frac{1}{1+K} \quad (9.1.1a)$$

$$K = \frac{\frac{4}{3}\frac{h_{MR}}{R}\frac{\gamma}{C_{l\alpha}}C_T/\sigma}{e/R} \quad (9.1.1b)$$

9.2.2 Horizontal Tail: The effects of the horizontal tail were studied for areas of 55, 65, and 75 ft^2, and incidence angles of 0°, -3°, and -5°. The zero payload condition was found to be limiting for the never exceed speed (V_{NE}), as V_{NE} is governed by swashplate limits of 10°. This trade study revealed that 0° and 55 ft^2 yield the highest V_{NE} of 177 kt. However, the 5° forward shaft tilt gives a nose up attitude in hover and low airspeed, so the stabilizer must be at a minimum of –5° for speed stability. This yields a V_{NE} of 172 kt unloaded and 175 kt at design gross weight.

Section 10 - Flight Control System

The Atlas's Flight Control System (FCS) is an advanced design to maximize safety, utility, and performance. It provides effortless control to the trained pilot, maximizes the flight envelope and ensures that the aircraft does not exceed its limits.

The FCS consists of a digital fly-by-wire (FBW) system with triple redundant Flight Control Computers (FCCs) and an analog backup channel in the event that all FCCs fail [McLe90]. Redundant data paths from the FCCs to the actuators, physically separated, minimize the possibility of losing connectivity. This redundancy allows for failures without impacting flight performance or safety. The FCS's is functionally divided into two parts: the Primary Flight Control System (PFCS) is responsible for primary control and commanding the actuators and the Automatic Flight Control System (AFCS) is responsible for stabilization, response tuning, and automated flight. See Fig. 10.2 for a schematic of the flight control system.

10.1 Primary Flight Control System (PFCS)

The PFCS determines the control outputs to the actuators based on inputs from pilot controls and the AFCS. Additionally, by monitoring flight conditions, the PFCS ensures that the Atlas's handling limits are not exceeded. Of note, the PFCS limits load factor to prevent blade stall. Normally, the system operates in "Standard Mode" tuning the aircraft response to improve handling qualities to Level 1 and 2. "Emergency Mode" provides quicker response, maximum control authority, and removes envelope limitations for evasive action, but is not appropriate for normal operations. Force feedback continues to communicate limits to the pilot in Emergency Mode, while permitting limit exceedance [Mass88].

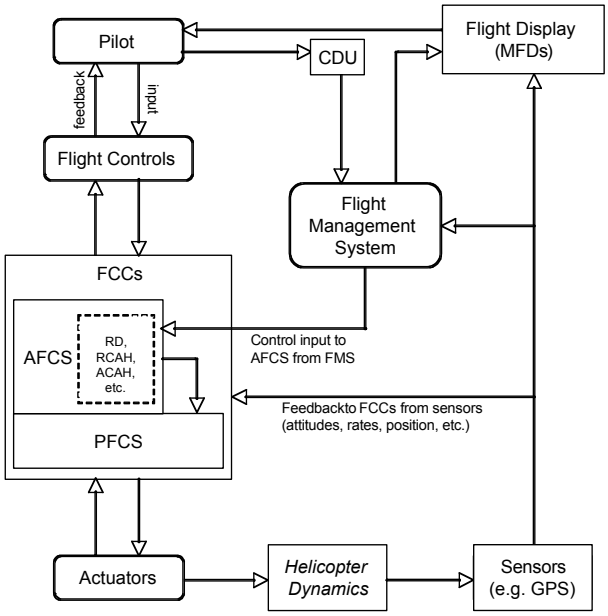

Figure 10.2: Schematic of Flight Control

10.2 Automatic Flight Control System (AFCS)

The AFCS provides stability augmentation and automated control to reduce pilot workload. Stability modes include Rate Damping (RD), Rate Command Attitude Hold (RCAH), and Attitude Command Attitude Hold (ACAH). Automated flight modes include automatic position hold, flight-track following, and optionally, full autonomy. RD is the simplest, damping

out attitude changes not explicitly commanded. RCAH translates control position into rate, commands the PFCS to achieve that rate, and maintains attitude when the input is removed. RCAH further aids the pilot by eliminating cross coupling dynamics. ACAH translates cyclic control position into attitude and commands the PFCS to hold the desired attitude. The collective and pedals operate in RD or RCAH mode when the cyclic is set to ACAH.

Automatic position hold uses input from the navigation system to maintain hover over a point. Flight-track following commands the course, altitude, and speed as determined by the Flight Management System, a computer providing flight direction, described in the Avionics section below [UMCP04, Kubo01].

The AFCS operates outside of the PFCS, providing inputs to the PFCS essentially identical to those provided by the pilot. Therefore, if the pilot disables the AFCS, the PFCS is unaffected.

Adding the optional capability for autonomous operation requires programming the FCCs and FMS with the requisite logic. Most of the added expense, however, would involve the testing and certification for autonomous flight. This capability would bring new meaning to "self-deployment" and would allow delivery of an FCS to a volatile area without endangering a flight crew, especially useful if an FCS were to become disabled.

Section 11 - Cockpit and Cabin Systems

11.1 Flight Crew Station and Controls

Careful consideration of control location, actuation, protection, and state indication is necessary for the safe operation of any aircraft, especially in the combat environment (Foldout 11.1, Figs. 11.1 and 11.2). The Atlas's controls are grouped into functionally similar sets and placed according to their frequency of usage and necessity. Critical switches are protected by a lockout mechanism that requires pulling the switch outwards before actuating. The landing gear, folding, and ramp switches are so protected and located under the center display. The landing gear switch is illuminated according to switch position and gear status (Foldout 11, Table 11.1).

11.1.1 Primary Flight Controls: As the Atlas's flight controls utilize FBW technology, the cyclic, collective, and pedals are mounted to force-feedback units connected to the FCCs. The PFCS normally determines appropriate feedback, as a function of control loads sensed by the actuator controllers. The AFCS determines feedback in RCAH and ACAH modes. Feedback is normalized to the standard control forces in MIL-SPEC AR-56 (Foldout 11 Table 11.2).

The cyclic grip (Foldout 11, Fig. 11.3) includes general flight, communications, and emergency controls. With an FBW system, trim is arbitrary; zero force can be set to any stick position. In RCAH and ACAH AFCS modes, center stick is neutral. In other modes, the pilot can set neutral to the current stick position with "Trim to here". The hat switch adjusts cyclic trim incrementally, and "Trim reset" returns trim to startup values. In certain AFCS modes, the hat commands airspeed or turn rate changes. Also available are PTT (Push-to-Talk), frequency toggle, AFCS mode/AFCS override, Emergency

Table 11.1: Landing Gear Switch Functionality

		Gear Position			
		Up	*Moving*	*Down: Locked*	*Down: Not Locked*
Switch Position	*Up*	dim	blinks green	blinks red and green	blinks red
	Down	blinks red	blinks green	steady green	blinks red

Table 11.2: Control Loads

Control	*Maximum Control Force (lb)*
Longitudinal Cyclic	100
Lateral Cyclic	100
Rudder Pedal	300
Collective	150
Brake	300

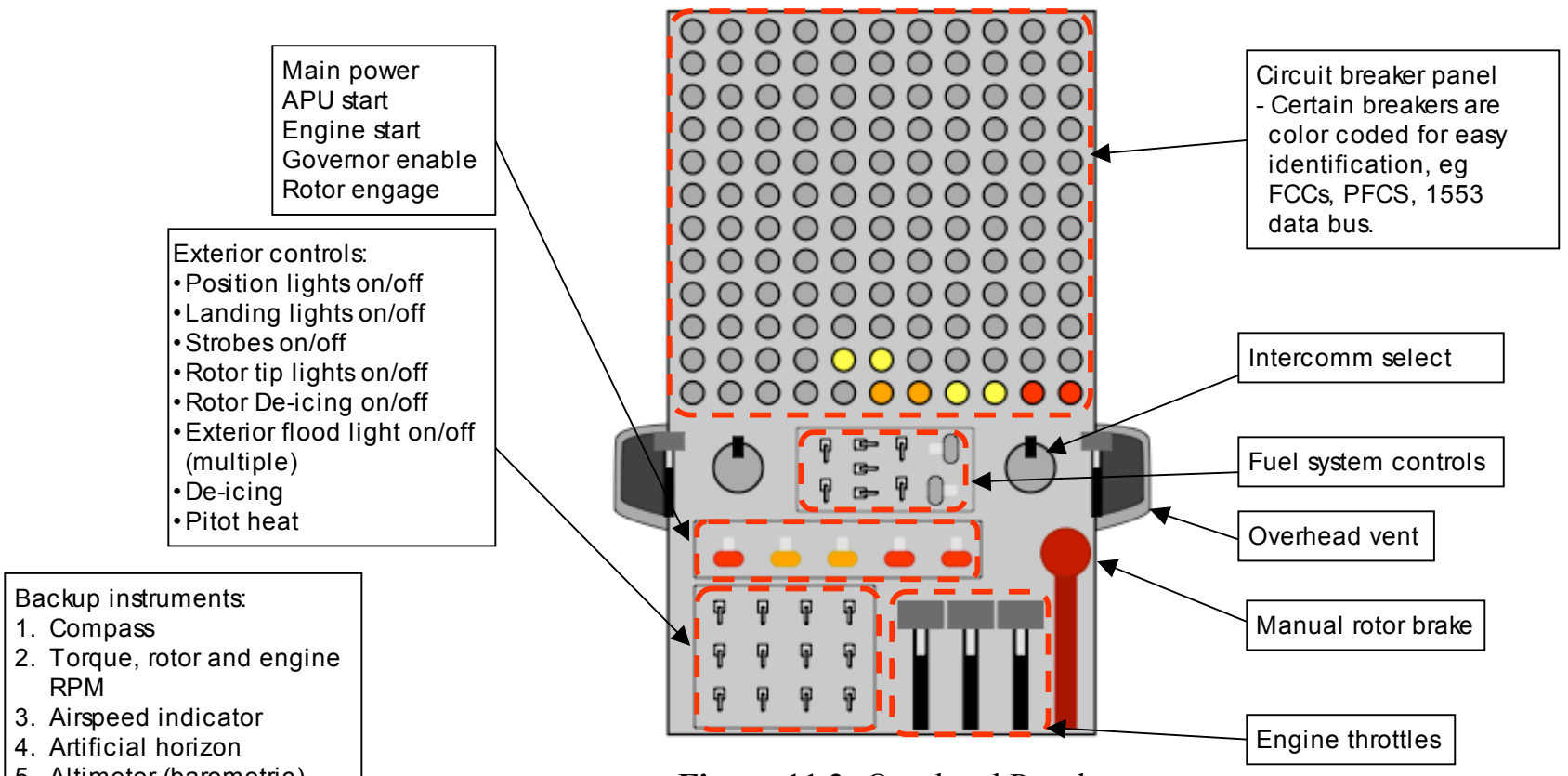

Figure 11.2: Overhead Panel

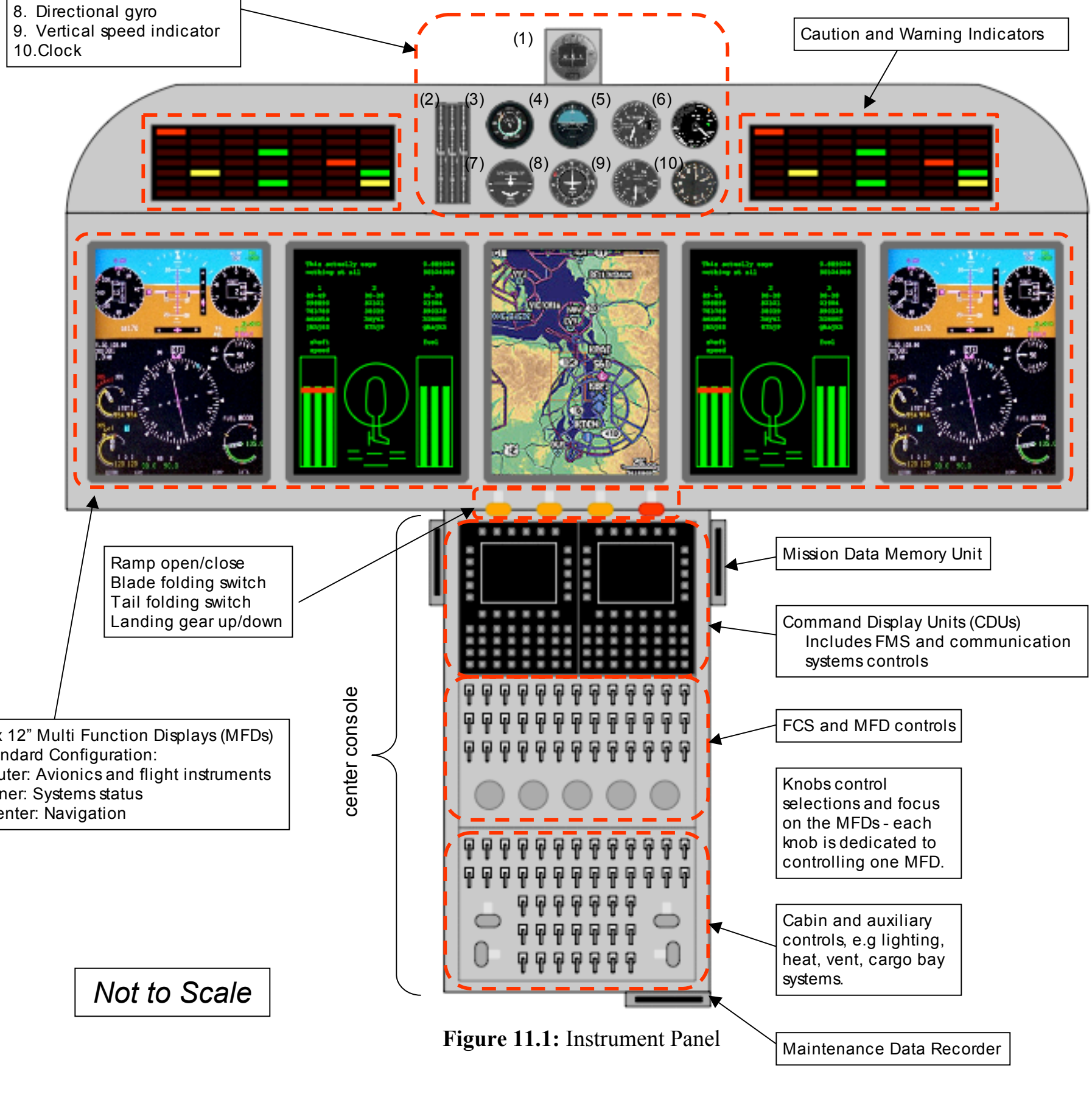

Figure 11.1: Instrument Panel

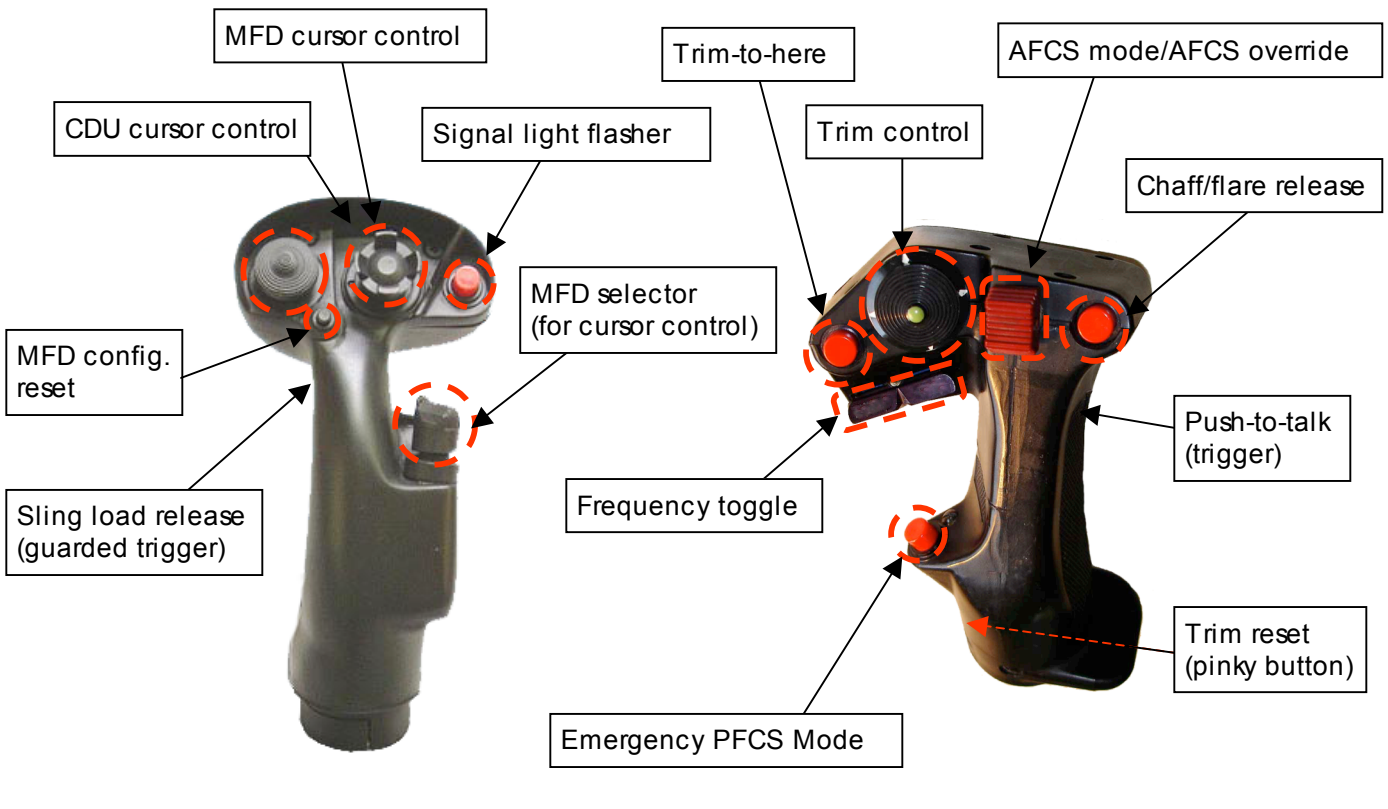

Figure 11.4: Collective Stick Grip

Figure 11.3: Cyclic Stick Grip

Mode, and manual chaff/flare release.

The collective grip (Foldout 11, Fig. 11.4) includes navigation, cockpit, and mission systems controls. Two hat switches act as selectors or a mouse for the MFDs and CDU. The MFD hat will also slew the Forward Looking Infrared (FLIR) sensor. A toggle switch selects which display or control the MFD hat switch affects, and a button resets the MFDs to a selected configuration. A twist grip throttle control allows the entire grip to rotate, though a feedback actuator locks the grip while the rotor speed governor is enabled.

The pedals steer the nose gear and actuate the brakes in addition to controlling the tail rotor or yaw channel.

11.1.2 Cockpit Systems and Avionics: As the Atlas will enter service in 2018, the systems and avionics for production are not currently available. For this proposal, current technologies in use are referenced for size and weight.

As a result of the shipboard environment, the Atlas will be exposed to large amounts of electromagnetic interference (EMI). MIL-STD-464A is the current set of requirements for EMI vulnerability and contribution. To meet the specifications electrical wiring and components will be shielded as needed to prevent interference issues. Technology such as Liquidmetal [Liqu05] casings will protect sensitive components from EMI.

In order to make replacement of failed parts as quick as possible, any Line Replaceable Unit (LRU) is located behind an access hatch. The cockpit systems are also designed to be easily removed for maintenance.

Multi-Function Displays (MFDs): Five 9”x12” MFDs are the main displays for the pilot and copilot. They are anti-glare, night vision goggle (NVG) capable, and touch enabled. The Rockwell Collins MFD-2912 has these specifications, except for touch control [Rock05]. While each MFD is configurable in-flight to suit the mission and pilot preference, standard layout is shown in Fig. 11.1 on Foldout 11. The central MFD is used as the primary navigation and situational awareness display. It displays a moving map and programmed waypoints. Radar data such as terrain and weather, and force information from the data link are also displayed. This MFD can further show FLIR images supplemented by radar data for a complete visualization of the terrain ahead. The outermost MFDs display flight instrumentation. An artificial horizon is the primary feature and includes information such as airspeed, heading, barometric and radar altitudes, vertical speed, and load factor. This display can also provide visual drift cues for manual station holding. The inner MFDs provide systems status and monitoring information including the engine, transmission, rotor, fuel, and HUMS data. The pilot may also inspect any system for more detailed information. In addition to the displays discussed, the MFDs can show video from cameras in the cargo bay and on the tail boom while loading or unloading.

Backup Instruments: In the event that the primary systems fail, backup analog instruments are included, allowing the pilot to fly safely in instrument conditions. The backup instruments are placed centrally in the instrument panel so both pilots can use them if necessary.

MIL-STD 1553B Data Bus: The data bus is the electronic backbone of the aircraft. All systems tie into the bus which is the

only means to move data. For this reason, there are two identical busses, physically separated. While the busses normally share the data throughput load, either can take over. Typically one bus can handle the entire load. If it were to become saturated, a prioritization scheme ensures critical data is moved first, cueing or discarding other data. Note that primary flight controls do not use the 1553B bus, but rather a dedicated system for uninterrupted communication within the FCS.

Flight Management System: The Flight Management System (FMS) integrates the individual avionics, presents their information, and provides a means to interact with the systems. The FMS also commands the AFCS operating in Flight Track Following mode or cues a pilot manually maintaining a flight plan. The Command Display Unit (CDU) in the center console is the interface to the system. The Rockwell Collins CDU-7000 currently fulfills these functions [Rock05].

The FMS communicates with the Mission Data Memory Unit where the pilots can save any information entered in the cockpit. The pilots also have the ability to load data such as maps, images, waypoints, flight plans, and frequencies prior to flight on a Joint Mission Planning System station so as not to waste time in the cockpit.

Communications Systems: A secure, reliable communications and data relay system is necessary for effective warfighting and to maintain situational awareness. A communications system conforming to the Joint Tactical Radio System specifications is the desired approach. This system will allow direct communications with Army, Navy, and Air Force assets in the air, on the ground, or at sea. It is a secure, jam resistant, and can transmit data. This system can link one asset with the entire theater of operations. Additionally, it can operate on civil frequencies for use in civil controlled airspace [USAr05]. The Atlas is equipped with two radio units integrated with the CDUs through the 1553B bus.

Navigation Systems: High performance navigation systems are crucial to successful operations. Using a combined inertial, radio, and GPS solution, a highly accurate and robust system is possible. GPS with differential capability (DGPS) is used for primary position determination. In the event that the Atlas enters a GPS Denied area or loses satellite tracking capability, TACAN (TACtical Air Navigation) is available and the Inertial Navigation System (INS) can maintain a "dead reckoned" navigation solution. The navigation systems are integrated with and controlled by the CDUs through the 1553B bus. As a backup means for navigation, dual VOR (VHF Omnidirectional Range) receivers and an ADF (Automatic Direction Finder) are available. There are several combined navigation units currently available with these capabilities, such as the Honeywell Embedded GPS Inertial [USNa05].

Mission Systems and Sensors: To operate in low light or poor visibility, augmented vision and terrain avoidance systems are necessary. Using NVGs, Multi-Mode Radar (MMR), and Forward Looking Infrared (FLIR), the pilot has multiple methods with which to visualize the surroundings. The MMR also provides information to the AFCS for safe nap-of-the-Earth flying. The Raytheon AN/APQ-186 MMR provides all these capabilities [Rayt05]. FLIR systems such as the Raytheon AN/AAQ-16 [Rayt05] can give pilots a clear view in most meteorological conditions. The single turret FLIR displays its image on an MFD and is aimed with a hat switch on the collective. Along with the navigation systems, these systems offer

the needed information for single pilot operation in instrument conditions.

Landing aboard a ship is one of the most critical operations for a pilot. As the Atlas is so large, the margin for error while landing on a ship deck is quite small and precision is of the utmost importance. To minimize risk during shipboard landings, the Energy Index pilot aid indicates deck quiescence calculated from the radar, radar altimeter, and FCC air data, which analyzes deck motion and wind to determine the relative safety of landing on the deck [Ferr05].

Hardened Flight Data Recorder: Were the Atlas to crash, a hardened data recorder provides information critical for accident reconstruction. The recorder is self-contained, maintenance-free, and is capable of surviving extreme loads and conditions. The DRS Technologies Deployable Flight Incident Recorder Set [DRST05] integrates with the 1553B bus and maintains a recording of the last 30 minutes of flight. In addition, it contains an Emergency Locator Transmitter, automatically activated when deployed. It is located on the underside of the tail boom.

Optional Equipment: Adding a second FLIR and integrating each to a Helmet Mounted Display (HMD), such as the Rockwell Collins EyeHUD [Rock05], would give the pilots greater situational awareness in low light or poor visibility. Each FLIR would be slaved to head position allowing the pilot to scan easily. The HMDs would also provide information typically found on a Heads Up Display, as well as obviating the need for NVGs.

11.2 Cabin and Cargo Area Systems

Intercom ports are located throughout the aircraft in order for the loadmaster to plug in and communicate with the flight crew. Video cameras located both inside the cargo bay and on the tail boom allow pilots to monitor loading.

The Atlas may optionally be fitted for increased capabilities managed by the loadmaster. The UAV Command System directs UAVs for reconnaissance or securing the landing zone. Weapons are also controlled by the loadmaster. These systems mount in front of the loadmaster, as this area has 1553B access and mounting points.

Section 12 - Fault Detection and Health and Usage Monitoring System (HUMS)

Aircraft health is monitored in two ways: through on-board real-time data processing and post-flight analysis and trending. In-flight, a Built-In Test, or BIT, system is used to report faults. The HUMS computer monitors each system with a number of sensors. The computer analyzes this data and determines whether a fault occurred. While each BIT is a relatively simple Boolean test, combining many BITs indicates system status. Each failed BIT is written to the maintenance data recorder and if a system is determined to be malfunctioning, the error is reported to the pilot. For a system such as this to be effective, care must be taken to minimize false BITs [Bain00].

In addition to fault information, the maintenance recorder saves time history data for post-flight analysis on a ground-based computer that uses a neural network to determine usage of life-limited parts. The neural network is “taught” how the recorded data impacts components. Ideally, a neural network uses all data in the analysis of each part. Parts such as the pitch links,

which historically must be replaced after a number of hours, will be monitored and replaced according to their computed usage. As the Atlas is a bussed aircraft, all of the sensors and computers are integrated with the existing 1553B bus, allowing for simple repair, replacement, and upgrading. Further gains may be realized by coupling the HUMS to wireless data transmission system. By wirelessly transmitting the data, maintainers can be ready with parts as soon as the vehicle is secured minimizing down time and maximizing operational readiness.

12.1 Main Rotor and Rotating Components

The main rotor is monitored primarily with feedback from the control system, load factor, and vibration data from accelerometers mounted in the tail, cockpit, and transmission deck. Most monitoring is through post flight analysis to calculate the use of life-limited components, though BITs are set for vibration at certain key frequencies.

12.2 Engines and Main Gearbox

Each engine's FADEC (Fully Automated Digital Electronic Control) system will interface with the aircraft's HUMS, and any information will be reported to the pilots and recorded to the maintenance data card through the HUMS. The main gearbox is monitored with chip detectors, thermocouples, and accelerometers. Torque and shaft speeds are also monitored. BITs set based on exceedances detected are responsible for most HUMS actions. Post flight analysis, using algorithms such as Harmonic Wavelet analysis and CAL4 developed at the University of Maryland [Samu05], calculates predicted transmission usage and safe torque limits based on actual use history.

12.3 Flight Control System and Avionics

All of the avionics systems contain built-in error checking. These checks correspond to BITs in the HUMS. Faults are reported, as well as self-corrective actions such as enabling a redundant system. For the actuators, feedback from the actuator control system is monitored. If an actuator's performance falls short of the preset limits, a fault is detected. Continuity checks are used to verify the function of the data bus and flight controls data paths.

12.4 Tail Rotor and Tail Gearbox

To minimize the number of sensors required, many sensors will provide information for monitoring multiple systems. The vibration sensors mounted to the tail boom detect abnormal motion from the tail system as well as those due to the main rotor. Thermocouples are used in tail gearbox, and control system feedback is used as well.

12.4 Structure

As with the tail rotor, structural monitoring will utilize vibration sensors already placed. Additional sensors will be used if needed based on the actual modal response of the structure. Information from the FCS, such as attitude, load factor, and rates, will supplement the vibratory information to provide additional inputs to the neural network aiding in the estimation of structural loads. Of particular note, the aircraft gross weight can be estimated using the neural network such that structural and rotor loads may be more accurately estimated.

Section 13 - Self-Defense Equipment/Countermeasures

As a military helicopter, the Atlas will be subject to threats from hostile forces. While heavy transport aircraft do not have significant self-defense capabilities due to the weight penalty of such systems, they should have a minimum of equipment to, at the very least, detect an imminent threat.

Sensors: The Atlas is equipped with a Missile Warning System that includes radar, laser, and infrared missile detection capabilities. If a launch is detected, a missile warning is indicated and a tone is sounded. The newest systems with these capabilities are the Litton AN/ALR-93 ECM Threat Warning Receiver, Raytheon AN/AVR-3 Laser Warning System, and Northrop Grumman AN/AAR-65 Missile Approach Warning System [Desi05, Noi05]. Systems such as the BAE AN/AAR-57 Common Missile Warning System (CMWS) integrate the individual components [Colu05].

Threat Evasion: Response to threats is based on the type of threat detected. For a radar guided missile, chaff is expelled. For infrared guided missiles, flares are expelled and the infrared jammer is activated. The Marconi AN/ALE-47 Threat Adaptive Countermeasures Dispenser System (TACDS) is a combined chaff and flare dispenser, providing one unit to suppress multiple threats [Desi05]. Dispensers are located on each side and underneath the tail boom, just aft of the clamshell doors. The AN/ALQ-212 Advanced Threat Infrared Countermeasures works with the CMWS and TACDS to actively and passively attempt to defeat infrared missiles. If autopilot is enabled when a threat is detected, it is disabled when the pilot moves the cyclic and the PFCS may be set to Emergency Mode for evasive action.

Weapons: Due to the weight, the Atlas will not be armed unless operations require return-fire capability. The Atlas can carry three .50 caliber automatic guns: mounted to each sponson and the underside tail boom. Each gun has infrared and visual targeting and can be slaved to the MMR. The guns mount on computer-controlled gimbals, directed by the Weapons Control Station, which can automatically aim and fire the guns, or the loadmaster can assume manual control.

Section 14 – Mechanical Subsystems (Engine / Transmission)

14.1 Engine Design

14.1.1 Current Engine Technology: The operational requirements of the Atlas demand an installed power far in excess of current rotorcraft. A survey of existing turboshaft engines revealed that no currently-available engine possesses the horsepower range and fuel consumption rate necessary to satisfy the mission for which the Atlas is designed. A new turboshaft engine will be developed in conjunction with the Atlas, which will use emerging technologies to provide substantial performance improvements over current engines.

14.1.2 Evaluation of Technology Initiatives: The new engine will use technology developed for the Integrated High-Performance Turbine Engine Technology (IHPTET) program [Hirs01]. IHPTET's Joint Turbine Advanced Gas Generator (JTAGG) program is a three-phase development of turboshaft engine technology to be completed during this decade. The

goals of the JTAGG program are a 120% increase in power-to-weight ratio and a 40% reduction of specific fuel consumption (SFC) from a 1987 baseline.

A survey of 3750+ HP Western turboshaft engines was conducted to evaluate the progress of available technology during the timeframe of the IHPTET program. The Honeywell T55, General Electric T64, and Rolls-Royce AE1107 (represented in 1987 by its predecessor, the Allison T701) were chosen for this survey. Figure 14.1 shows the power-to-weight ratios of the most advanced models of these engines at 1987, 1995, and 2004 [Tayl87, Jack95, Jack04]. Figure 14.2 shows the SFC of the same engines at 1987 and 1995; data was not available for 2004.

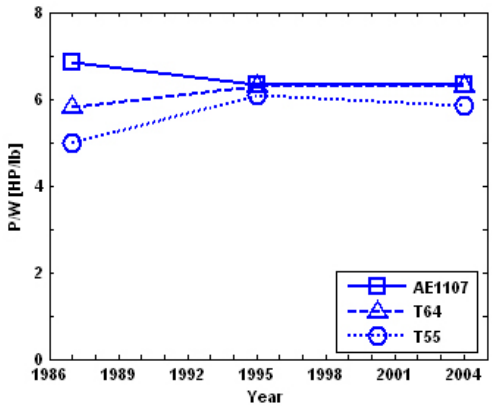

Figure 14.1: Recent Advances of Heavy Turboshaft Power-to-Weight Ratio

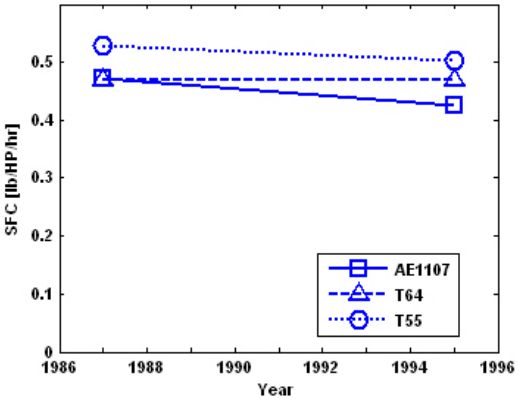

Figure 14.2: Recent Advances of Heavy Turboshaft Specific Fuel Consumption

The survey showed that the performance of large turboshafts has not improved significantly since the beginning of the IHPTET program. Additionally, Hirshberg shows that demonstration of IHPTET goals lag behind the original IHPTET timeline [Hirs01]. Therefore, the Atlas engine is modeled on more conservative recent IHPTET goals and NASA's Heavy Lift Study Engine large turboshaft model [NASA05], and the state-of-the-art LHTEC T800 light engine.

14.1.3 Gross Engine Sizing: A 2003 Runway Independent Aircraft (RIA) roadmap sets a goal of increasing turboshaft power-to-weight by 20% over the current state-of-the-art by 2009 using IHPTET and Versatile Affordable Advanced Turbine Engine (VAATE) technology. This reasonable increase was accepted for our analysis.

Current state-of-the-art trends were established with a survey of operational American, European, and other international turboshafts [Jack04]. The engines range from the 1,000-HP Rolls-Royce Gem 42 to the 6,150-HP Rolls-Royce AE1107. The most advanced model of each engine was included in the survey. Rated power, dry weight, length, and width were tabulated for each engine. The trendlines for weight as a function of power, and length and width as a function of weight follow exponential laws:

$$W\,[lb] = 5.60 \times \left(P\,[HP]\right)^{0.585}$$
$$L\,[in] = 2.24 \times \left(W\,[lb]\right)^{0.501}$$
$$w\,[in] = 6.67 \times \left(W\,[lb]\right)^{0.201}$$

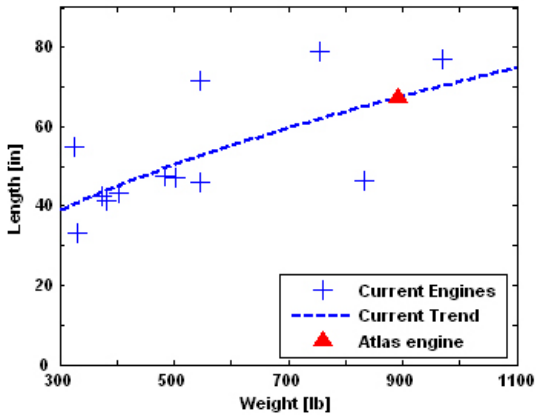

Figure 14.4: Length Envelope of Current Turboshafts

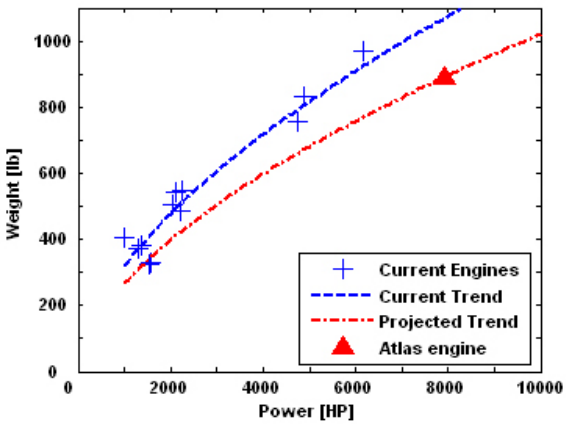

Figure 14.3: Dry Weight of Current and Projected Turboshafts

Technology advances are modeled as a decrease in weight at a given power:

$$W_{projected}\,[lb] = 4.67 \times \left(P\,[HP]\right)^{0.585}$$

This projection gives a power-to-weight ratio increase of 20% over the current trend at the power of the largest surveyed engine, the AE1107.

IHPTET goals do not specify an improvement in engine density. Current length and width trends were used to size the Atlas engine, which fixed engine density to the current state-of-the-art. Figures 14.3, 14.4, and 14.5 plot the surveyed data and trend lines. Two light engines—the LHTEC T800 and Rolls-Royce Gnome—correspond to the projected P/W trendline in Fig. 14.3, indicating that this trend is already achievable for smaller engines. Table 14.1 provides a sizing comparison between the Atlas engine and the AE1107.

14.1.4 Power Ratings: Power ratings for the Atlas engine are modeled on the relative power ratings of the T800 engine and the NASA Heavy Lift Study Engine relative power ratings, which are identical. Table 14.2 gives the relative power ratings of the Atlas engine, the T800 and the NASA Heavy Lift Study Engine. Table 14.3 gives the sea-level power output of the Atlas engine at ISA and ISA+20.

Table 14.1: Atlas Engine vs. AE1107

	Atlas Engine	AE1107
Power	7,916 hp	6,150 hp
P/W	8.88 hp/lb	6.33 hp/lb
Length	67.3 in	77.1 in
Width	26.1 in	26.4 in
SFC	.34 lb/hp/hr	.42 lb/hp/hr

14.1.5 Temperature and Altitude Losses: Losses from change in temperature and pressure are modeled as linear functions of temperature and pressure altitude. The lapse rates of the Atlas engine are identical to the T800:

$$P = P_0\left(1 - k_T \times \Delta T\,[°C]\right)\left(1 - k_h \times h\,[ft]\right)$$
$$k_T = 7 \times 10^{-3}\,[1/°C]$$
$$k_h = 2 \times 10^{-5}\,[1/ft]$$

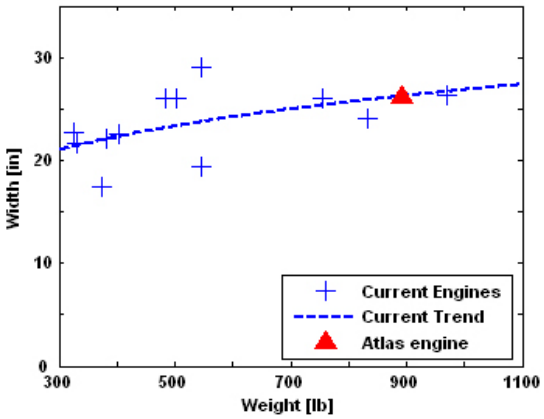

Figure 14.5: Width Envelope of Current Turboshafts

Table 14.2: Relative Power Rating Comparison, Non-dimensionalized by Rated Power			
	Atlas engine	T800-LHT-801	NASA Study Engine
Emergency (30 sec)	1.15	1.15	(not given)
Contingency (2 min)	1.05	1.05	1.05
Rated (5 min)	1	1	1
Intermediate (30 min)	0.93	0.93	0.93
Max. Continuous	0.79	0.79	0.79

Table 14.3: Atlas Engine Uninstalled Power Output at Sea Level		
	ISA	ISA+20
Emergency (30 sec)	9,103 HP	7,829 HP
Contingency (2 min)	8,312 HP	7,148 HP
Rated (5 min)	7,916 HP	6,808 HP
Intermediate (30 min)	7,362 HP	6,331 HP
Max. Continuous	6,254 HP	5,378 HP

where P_0 is power at sea-level, ISA. Linearization of the NASA Heavy Lift Study Engine produced lapse rates of the same order of magnitude, $k_T = 8\times10^{-3}\ [1/°C]$ and $k_h = 3\times10^{-5}\ [1/ft]$. Power variation with altitude is plotted in Fig. 14.6.

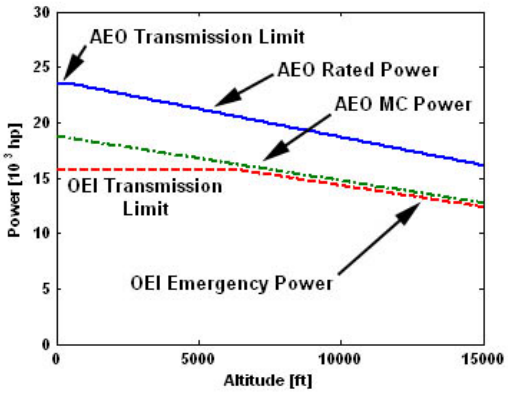

Figure 14.6: Atlas Power Variation with Altitude (ISA)

14.1.6 Specific Fuel Consumption

For an engine in the range of 6,000–8,000 HP, the NASA model gives a SFC of 0.33 lb/HP/hr. The expected SFC of the ZMKB Progress D-127, being developed for the Mi-26, is 0.36 lb/HP/hr. The Atlas engine's SFC of 0.345 lb/HP/hr at rated power is selected as the median of these values.

The value of the SFC is dependent on the engine's power output. The change in SFC with power output is linearly scaled from the trend of the T800 engine. The Atlas engine's SFC is

$$SFC\,[lb/HP/hr] = 0.264 + \frac{0.081}{\bar{P}}, \qquad \bar{P} = P/P_{MRP}$$

where P_{MRP} is rated power. Figure 14.7 plots the variation of fuel flow with engine power.

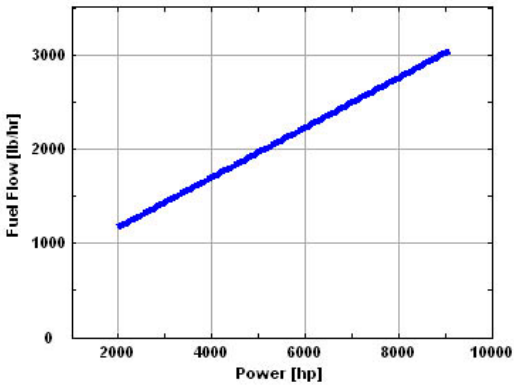

Figure 14.7: Atlas Engine Fuel Flow Rate

14.1.7 Number of Engines: Three 7,916-HP turboshaft engines power the Atlas. The stringent mission OEI requirement stipulates the ability to hover OGE at sea-level, ISA+20 with full payload and 60% fuel under emergency power. For the Atlas, the OEI power requirement is 15,658 HP at ISA+20. This condition requires more power output from each engine than any other flight condition, and was the main driver of the design. A trade study between two and three engines reduced weight, cost, and risk while meeting the OEI requirement.

A three-engine configuration minimizes powerplant weight. Four subsystems contribute to the weight of the powerplant: dry engine, main gearbox, equipment and installation weight. Table 14.4 gives relative subsystem weights. Using the power-to-weight trends from Section 14.1.3, total dry engine weight follows

$$W_{eng} \propto \frac{N_{eng}}{\left(N_{eng}-1\right)^{0.585}}$$

for a given OEI power requirement. For N_{eng} = 2 or N_{eng} = 3, dry engine weight remains constant. Selecting torque as the AEO transmission torque limit, main gearbox weight follows [Tish03].

$$W_{MGB} \propto \left(\frac{N_{eng}}{N_{eng}-1}\right)^{0.8}$$

Table 14.4: Engine configuration trade-offs

	3 engines	2 engines
Installed Power	23,748 HP	31,664 HP
Relative Engine Weight	1	1
Relative Gearbox Weight	1	1.26
Relative Equipment Weight	1.5	1
Relative Installation Weight	1	1

for a given OEI power and RPM. The weight of a two-engine gearbox is 1.26 times the three-engine gearbox weight. Equipment weight is assumed to be constant per engine. Installation weight is assumed to be constant since the reduced number of components for a two-engine installation will be offset by their increased bulk. The Atlas has a main gearbox weight of 6,614 lb and an equipment weight of 2,981 lb. An equivalent two-engine helicopter would have a gearbox weight of 8,325 lb and an equipment weight of 1,987 lb, a net increase of 717 lbs.

Reduction of installed power also influenced the selection of three engines. The Atlas's cruise performance is limited by blade stall limits, not power requirement. Because SFC decreases as an engine operates closer to its rated power, it is beneficial to set the rated power of the powerplant nearer to cruise power of 11,904 HP. This condition is better satisfied by the 23,748-HP three-engine configuration. Reduction of installed power will also decrease acquisition cost. The three-engine configuration mitigates development risks. The Atlas engine will be 29% more powerful than the AE1077. This represents a more realistic target than a two-engine configuration, requires a 160% increase over the AE1107. The AE1107 has similar envelope dimensions to the Atlas engine and can be fitted to initial Atlas prototypes despite being underpowered for the fully-loaded OEI requirement. This will reduce development time by allowing flight tests to occur concurrently with development of the Atlas engine. Since the Atlas engine is not significantly out of the range of current military and civilian heavy turbo shafts, manufacturing and development costs can be alleviated by commercial market sales.

14.1.8 Structural Integration: The Atlas engine's output shaft is located at rear of the engine. This simplifies the engine by eliminating the need to run the turbine output shaft forward through the compressor and helps to simplify the Atlas's transmission configuration. Two engines are mounted symmetricly to the side of the main gearbox. The offset between the aircraft centerline and centerline of each engine is 63-in. The third engine is mounted on the transmission deck, 94-in ahead and four inches port of the main rotor shaft. This geometry moves the engine CG forward of the main rotor to aid longitudinal CG balance.

The front of each engine is mounted on two A-frame supports. LIVE dampers at the hardpoints where the A-frames mount to the transmission deck isolate the engine from fuselage vibrations. The output shaft on the rear of each engine is housed inside a sheath that mates to the transmission gearbox housing and serves as a structural support, see Foldout 14.1. The engine shaft mates to the gearbox input shaft via a spherical gear to accept slight shaft misalignments.

14.1.9 Engine Installation: The Atlas's engines are installed with inlet particle separators and exhaust infrared (IR) suppressors. The inlet particle separator is a triple-filtration system to prevent ingestion of debris into the engine. The IR suppressor mixes exhaust air with ambient air and passes it through a heat absorber to reduce the engine heat signature. Inlet and exhaust ports direct the exhaust of the forward engine away from the inlets of the rear engines. Engine firewalls to confine fire and debris from the fuselage in the event of an engine failure. Power losses due to installation are assumed to be 6% of uninstalled power, primarily from exhaust and IR suppression.

14.1.10 Engine Subsystems: The Atlas engine is designed with full-authority digital engine control (FADEC) and oil subsystems that are integral to the engine. The FADEC system controls optimal engine performance based on flight-control inputs and internal sensor data. In the event of an engine failure, the FADEC will instantaneously initiate OEI engine operation. The FADEC outputs sensor data to the HUMS system for health monitoring. The engine has a self-contained oil system consisting of a pump, sump, cooler, filter, and particle detectors.

14.1.11 Auxiliary Power Unit: An Auxiliary Power Unit (APU) powers the Atlas avionics, electronic systems, and hydraulic systems and also provides power for main turbine start-up.

14.2 Transmission Design

Table 14.5: Gross Transmission Parameters	
Power to main rotor, per engine (OEI)	7,829 HP
Input shaft speed	18,300 RPM
Output shaft speed	118 RPM

14.2.1 Design Considerations: The high power requirements of the Atlas, particularly at the OEI condition, necessitate a transmission that is larger than any extant helicopter transmission. The transmission is rated at 23,487 HP and transmits a 7,829-HP input from each engine during OEI operation. Design studies and existing heavy-lift gearbox designs [Smir90] suggest that a path-splitting configuration, in which the power from each engine is transferred to the main rotor via multiple load paths, is not only beneficial but necessary for high-power transmissions [Cock85, Kran96]. Path-splitting reduces gear forces inversely with the number of load paths, reducing transmission weight. Only transmission configurations using multiple power paths per engine were considered. Gross transmission design parameters are given in Table 14.5.

14.2.2 Transmission Configuration:

Spur-gear Transmission Configuration: A configuration utilizing spur gears, similar to the Mi-26 Halo [Smir90], was considered as a "baseline" design. The Mi-26 configuration has proven its effectiveness through 30 years of continued operation. Power from each engine is turned though the first spiral bevel stage and split between two spur gears in the

Foldout 14.1: Transmission and Transmission Housing

Atlas Drivetrain Layout

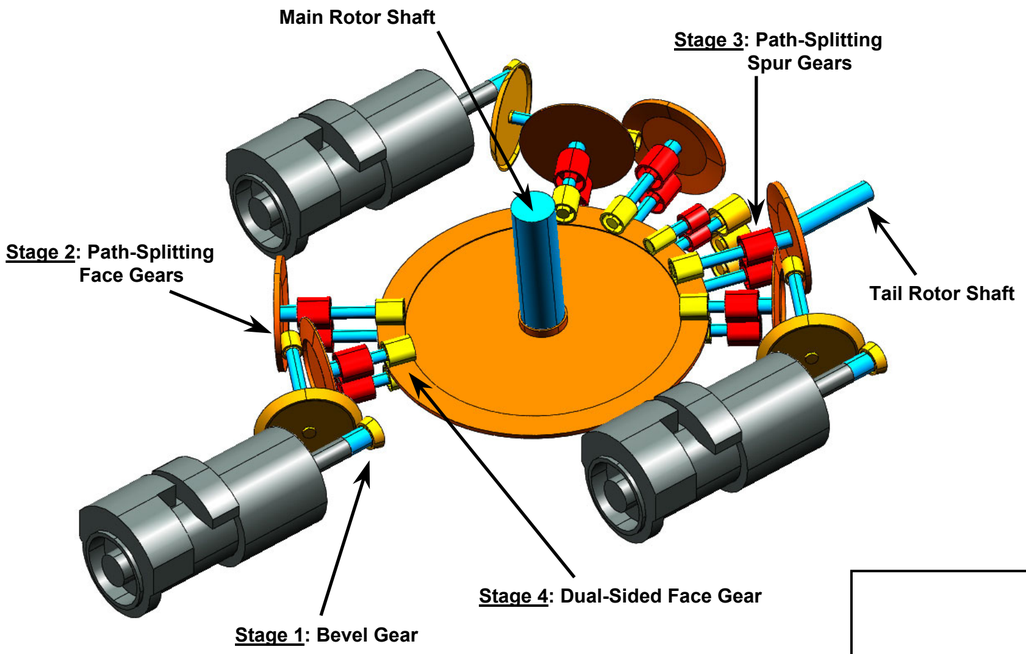

Transmission Details

Stage	Stage 1	Stage 2	Stage 3	Stage 4
Gear Type	Spiral Bevel	Face	Spur	Dual-Sided Face
Diametral Pitch	4	5	4.51	4
# of Teeth: Pinion / Gear	31 / 98	24 / 107	31 / 31	25 / 274
Reduction Ratio	3.16	4.49	1	10.96
RPM: Input / Output	18,300 / 5,789	5,789 / 1,298	1,298 / 1,298	1,298 / 118

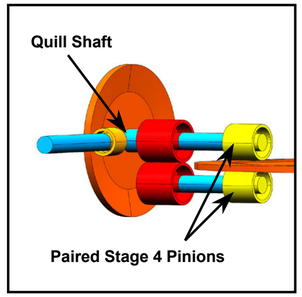

Detail of Stage 2, Stage 3, and Stage 4

Additional gears and shafts removed for clarity

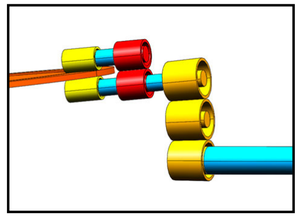

Detail of Tail Rotor Take-off

Additional gears and shafts removed for clarity

Atlas Transmission Housing

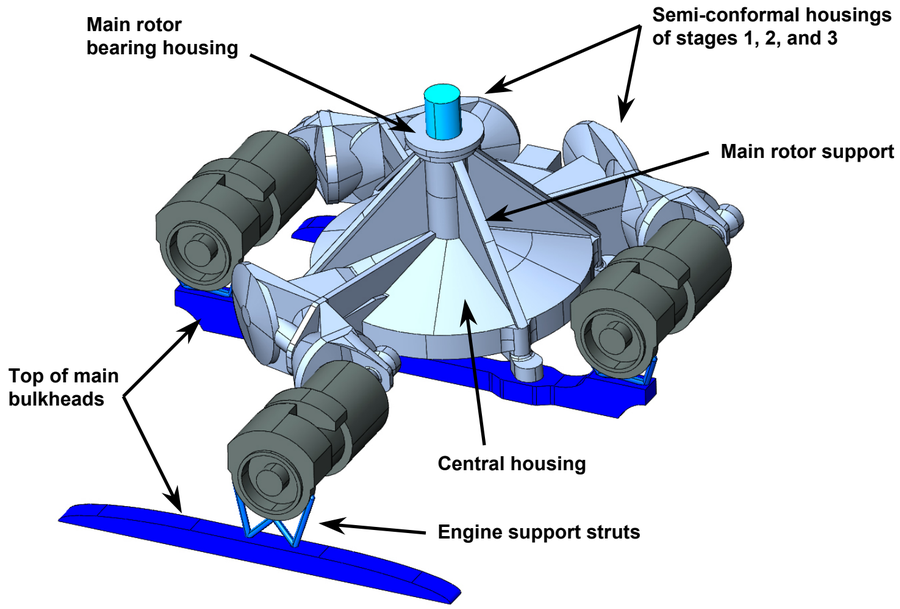

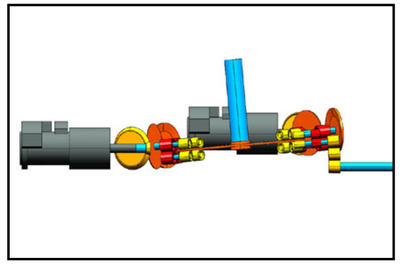

Side View of Drivetrain Layout

Port engine and gears removed to show MR shaft tilt

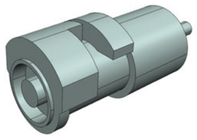

Atlas Engine

- 7,916 HP
- 8.88 HP/lb
- 67” length × 26” width
- 0.345 lb/Hp/hr SFC

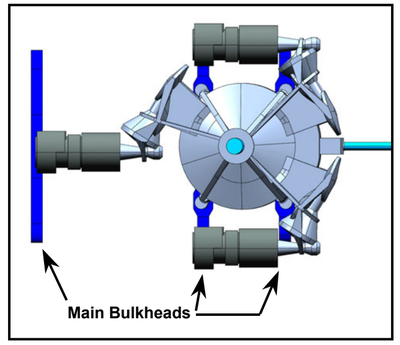

Top View of Transmission Housing

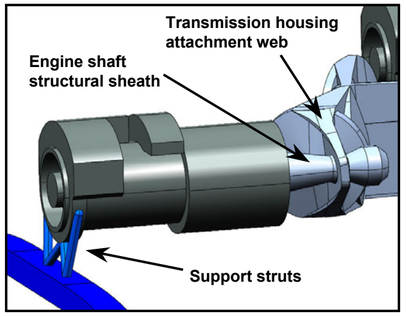

Detail of Engine Structural Support

Shown on Front Engine

second stage. Power is split again to dual bull gears in the third stage and collected via the main rotor shaft. Each engine thus transmits power to the main rotor through four separate paths. While this design is practical, a more innovative face gear design was chosen to save weight and space.

Face-gear Transmission Configuration: The Atlas uses a transmission layout based on the three-stage, two-engine RDS-21 gearbox developed by Sikorsky [Gmir04]. This layout reduces gearbox weight through the novel application of face gears. Similar to the spur-gear transmission, the Atlas face-gear transmission splits each engine input through four separate paths. Each engine drives an input spiral bevel stage (shaft angle = 58.9°, spiral angle = 35°) with a 4-pitch, 31-tooth pinion and a 98-tooth gear, both of which have a face width of 2.56 in. The first stage output drives a 5-pitch, 24-tooth spur pinion with a 4.8 in face width. This pinion simultaneously meshes with two 107-tooth face gears. The face gears evenly split the pinion torque and again the output of each face gear is split in a spur stage consisting of an identical 4.51-pitch, 33-tooth pinion and gear with a face width of 7.31 in. Quill shafts between the second and third stage ensure even torque distribution. The third-stage pinions and gears both drive input pinions that interface on the top and bottom of a dual-sided collector face gear. This final stage uses 4-pitch, 25-tooth spur pinions and a double-sided 274-tooth face gear, both with a tooth face width of 6.25 in. The main rotor shaft is splined to the center of the fourth-stage face gear. An additional upper-and-lower pinion pair extracts power from the collector gear to drive the tail rotor shaft. The second, third, and fourth stages are longitudinally oriented at 5° nose-down to accommodate the 5° forward tilt of the main rotor shaft. Foldout 14.1 shows the layout and gives relevant information about the powerplant and gives transmission details.

The Atlas's configuration represents an improvement in load management and layout over the baseline heavy-lift transmission. The second-stage face gear stage splits the torque evenly within ±2% of the input torque [Fill02], consequently canceling most net shear force on the second-stage pinion. The paired upper and lower fourth-stage pinions and tail rotor take-offs cancel the axial loads on the collector face gear. These configuration-based force cancellations reduce bearing loads and weight. The placement of the second stage face gear, third-stage pinion and gear, and fourth stage pinion on the same shafts also reduces bearing and lubrication system weights.

14.2.3 Weight Estimation: Research of face gears for rotorcraft transmissions has not progressed sufficiently to develop systematic weight estimation methods similar to Schmidt's method [Schm76]. A detailed weight estimation of the Atlas transmission's unconventional face-gear layout is not possible at this stage. Instead, a more general weight estimation was based on torque throughput. Gross transmission weight is proportional to $T^{0.8}$ [Schm76, Tish03]. The main gearbox weight can be calculated by Tishchenko's estimation [Tish03].

$$W_{MGB} = k_{MGB} T_{thru}^{\ 0.8}$$

where k_{MGB} is a main gearbox weight coefficient. The Atlas transmission's weight coefficient is the same as the OH-6A, the

most weight efficient helicopter transmission available. This represents a 10% decrease in weight coefficient from the Mi-26-type baseline. The main gearbox transmission weight is 6,614 lb.

14.2.4 Stress Calculations: Design of the Atlas transmission was performed using methods presented by Dudley and Schmidt [Dudl94, Schm76]. Engine installation losses were neglected to provide a safety margin in transmission design calculations. Initial gear size estimation was conducted using Schimdt's method based on assumed Hertz index K [Schm76]. Detail design was performed by matching two tooth-loading indices, Hertz index and unit load U_l, to existing designs. Hertz index parameterizes the compressive stress on a gear tooth face and unit load parameterizes bending stress at the gear tooth root. Equations for Hertz index and unit load for spur-gear and face-gear stages are derived from Dudley as

$$K = 126051\frac{P\left(m_g + 1\right)}{Fd^2 n_p m_g} \quad \text{and} \quad U_l = 126051\frac{PN_p}{Fd^2 n_p}$$

where P is the horsepower per load path, n_p is the pinion RPM, d is the pinion pitch diameter, F is the face width, m_g is the reduction ratio, and N_p is the number of teeth on the pinion [Dudl94]. Table 14.7 gives the Hertz index and unit load for each stage of the Atlas transmission and the existing stage estimate used for design reference.

Table 14.7 – Transmission Design Parameters

Atlas stage	K [psi]	U_l [psi]	Reference Stage	K [psi]	U_l [psi]
1 (spiral bevel gear)	462	15,419	Mi-26 spiral bevel gear	676	18,425
2 (split-path face gears)	994	18,498	RDS-21 split-path face gears	888	17,482
3 (spur gear)	972	16,036	RDS-21 spur gear	1,145	16,032
4 (collector face gear)	849	19,457	RDS-21 collector face gear	868	19,736

14.2.5 Structural Integration: Rotor mast loads are transmitted through the transmission housing to the main transmission deck bulkheads. A central housing surrounds the final face gear stage and serves as a load path for the mast forces. Semi-conformal housings enclosing the first, second, and third stages associated with each engine are cantilevered off of the main housing. The cantilevered housings support the structural sheath mounted to each engine, but do not transmit any main rotor loads. The transmission housing is mounted to the main bulkheads via four attachment feet. LIVE dampers at the bulkhead attachment points provide vibration isolation for the fuselage.

The transmission housing is constructed from magnesium-zirconium alloy castings. The central housing is constructed from separate upper and lower casts, and each engine-path housing is cast as individual inner and outer sections. A surface coating protects the housing from corrosion. The Atlas transmission housing is shown in Foldout 14.1.

14.2.6 Transmission Losses: Estimating 1% loss of input power per stage, transmission efficiency is 96%. Operating at the AEO transmission limit of 23,487 HP, transmission losses will be 939 HP dissipated as heat.

14.2.7 Oil System: The power and number of gears of the transmission requires an extensive oil system for lubrication and heat dissipation. Oil is transferred through cored passages in the transmission housing to internal jets, which lubricate each

gear mesh and bearing. The main housing, each engine housing, and the tail housing have independent oil pumps. Oil, from each housing, drains through a return line to a common sump in the central housing. Each return line is equipped with a chip detector and a magnetic particulate trap (MPT) to detect critical gear wear. The common sump is equipped with dual filters, each with a bypass valve. The transmission has a 30-minute dry-run capability in the event of an oil system failure. The usable capacity of the oil system is estimated as 45.2 gal by F.A.R. §27.100 guidelines. Oil flow rate necessary for cooling is estimated as 46 gal/min, assuming a sump temperature of 230°F and an outlet oil temperature of 450°F [UMCP99].

14.2.8 Tail Rotor Drive System: The Atlas tail rotor requires 2,137 HP at a nominal speed of 614 RPM at maximum operating conditions. Paired upper and lower 17-tooth spur pinions extract power from the collector gear at 1,909 RPM. Spur gears combine the inputs from the upper and lower pinions. Output power is transmitted through a quill shaft a series of helical bevel gears to achieve the change in angle for the tail rotor shaft. The tail gearbox consists of a 4-pitch, 32-tooth spur pinion driving a 99-tooth face gear, providing a 3.11 reduction to the tail rotor. The tail gearbox is equipped with an independent lubrication system.

Section 15 - Performance Analysis

15.1 Drag Estimation

Frontal areas of the Atlas were calculated from the CAD drawings and were combined with empirical data from Prouty given in Table 15.1 [Prou86]. A factor of 20% has been added for uncertainties, leakages, and protuberances.

The flat plate area of the Atlas is comparable to that of other helicopters in its class, such as the Mi-26 which has a flat plate area of 96 ft^2. The flat plate area is relatively high compared to smaller helicopters for several reasons: First, the rotor hub is large because it needs to accommodate 7 blades. The folding mechanism on each blade is located at 10% radius in order to facilitate blade folding, and increases the hub drag. Second, the fuel sponsons located on the sides of the fuselage

Table 15.1: Drag Estimation

	Flat Plate Area (ft^2)	Flat Plate Area (m^2)	Percent
Fuselage	24.60	2.270	32.60
Sponsons	3.10	2.246	4.11
Nacelles	1.70	0.158	2.25
Main Rotor Hub & Shaft	25.18	2.340	33.40
Tail Rotor Hub & Shaft	3.15	0.293	4.18
Main Landing Gear	1.68	0.156	2.23
Nose Landing Gear	0.00	0.000	0.00
Horizontal Stabilizer	1.20	0.111	1.59
Rotor/Fuselage Interference	10.30	0.957	13.66
Exhaust Drag	3.60	0.334	4.77
Miscellaneous Drag	1.00	0.093	1.33
Subtotal	75.41	7.006	100.00
20% Increase	15.08	1.401	
Total	90.50	8.407	

have a thickness to chord ratio of 24% and an aspect ratio of 0.15. Third, the rear clamshell doors have a high upsweep angle, increasing vortex drag in this area. Note from Table 15.1 that the drag from landing gear is relatively low because the nose gear is fully retracted and the main gear is partially retracted.

15.2 Hover Performance

Helicopter design generally focuses on hover performance because power requirements are usually largest in hover. The Atlas rotor geometry was designed for good hover performance through the use of twist, taper, and anhedral at the tips. These measures effectively reduce the takeoff power required by increasing the figure of merit, which results in a smaller engine, transmission, and aircraft size.

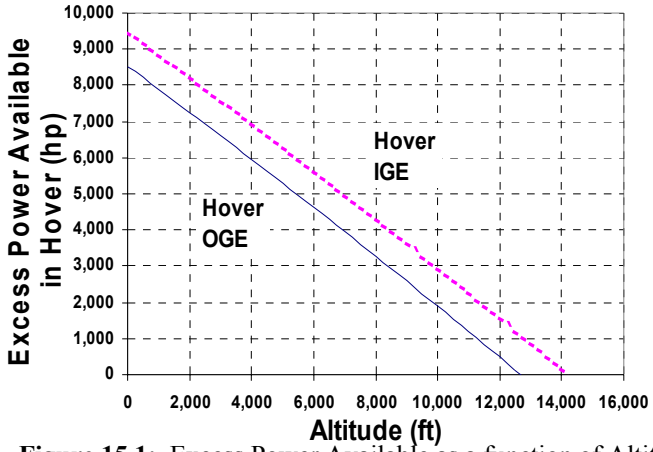

Figure 15.1: Excess Power Available as a function of Altitude

The RFP states that the helicopter must hover out of ground effect (HOGE) at 3000 feet density altitude. This requirement demands a large amount of power, which is also available in all flight regimes. Figure 15.1 shows the amount of excess power available at different altitudes for the Atlas in hover out of ground effect (OGE) and in ground effect (IGE). IGE was calculated for a height of one rotor radius above the ground.

From Figure 15.1, it can be seen that the Atlas has a good high-altitude capability, with a hover ceiling of about 12500 ft. For the same reason, the helicopter has a high rate-of-climb in hover for vertical takeoff. This is advantageous from a mission standpoint because the helicopter will be able to depart quickly from the ship deck and also from the objective landing zone once the FCS has been delivered.

The power loading was calculated to be 6.85 lb/hp [40.93 N/kW] and the disk loading is 10.21 lb/ft^2 [49.97 kg/m^2]. The power loading is relatively high while the disk loading is relatively low for a helicopter of this size, mainly due to the low design C_T/σ which gives a large main rotor diameter. These characteristics allow the Atlas to provide a large amount of lift for a relatively low power [Leis00].

15.3 Forward Flight Performance

The power requirements in forward flight decrease because of the decrease in induced power. As the helicopter increases speed, the parasitic power dominates the power requirements. Figure 15.2 shows the variation of power required with the airspeed. The Atlas was designed for a high cruise

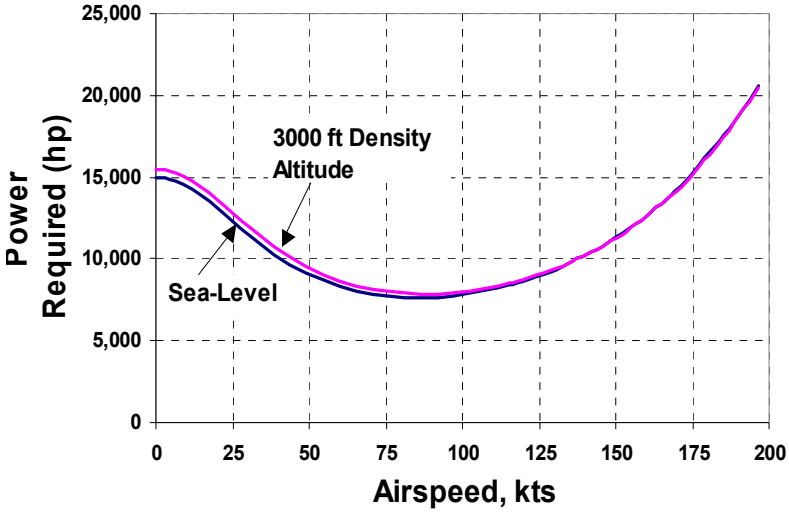

Figure 15.2: Power Curve as a function of airspeed

speed while fulfilling the maneuver requirement. Because the rotor is able to produce enough lift to meet the maneuvering requirement, it has a high stall margin in level flight.

The specific fuel consumption (SFC) changes with increasing speed as a function of power setting. SFC is lowest at the highest power setting relative to takeoff power. Using the value of SFC for each airspeed, along with the power required curve in Figure 15.2, the fuel flow can be calculated for each airspeed. These results are plotted in Figure 15.3. The speed for best range (V_{BR}) and best endurance (V_{BE}) can be derived from the results in Figure 15.3. V_{BR} is calculated at the minimum fuel per mile, or can be graphically found by drawing a line tangent from the origin to the fuel flow. At a density altitude of 3000 feet, V_{BR} is 145 knots. V_{BE} occurs where the helicopter is operating at the best lift-to-drag ratio and lowest power and fuel consumption per unit time [Leis00]. V_{BE} can be found by calculating the minimum fuel flow rate, based on the results from Figure 15.3. At 3000 feet density altitude, V_{BE} is 91 knots.

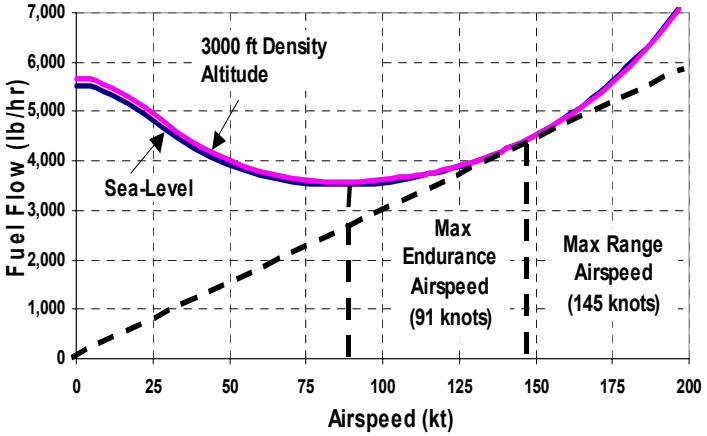

Figure 15.3: Fuel Flow vs. Airspeed at 3000 ft

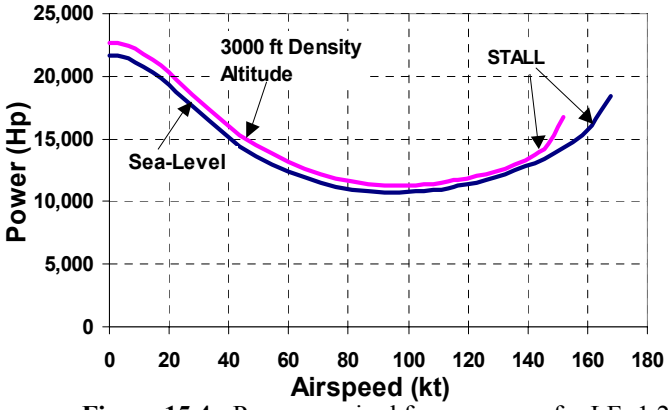

Figure 15.4: Power required for maneuver for LF=1.28

To ensure that the helicopter can meet the maneuver requirement while cruising at 99% V_{BR}, the helicopter characteristics were input to the performance code. From the SC1095 data, it was known that the blades stall around 15° local blade incidence [Bous03]. Thus, the stall speed was taken as the speed at which any blade element is operating above 15°. By multiplying the takeoff weight by a load factor of 1.29 at 145 kt., the performance code is able to predict the helicopter performance and trim in the maneuver condition. The power required to maneuver at this load factor is plotted in Figure 15.4. The helicopter was found to stall at 151 knots at a density altitude of 3000 ft, indicating that the helicopter will be able to complete the maneuver at cruise speed without stalling. The never-exceed

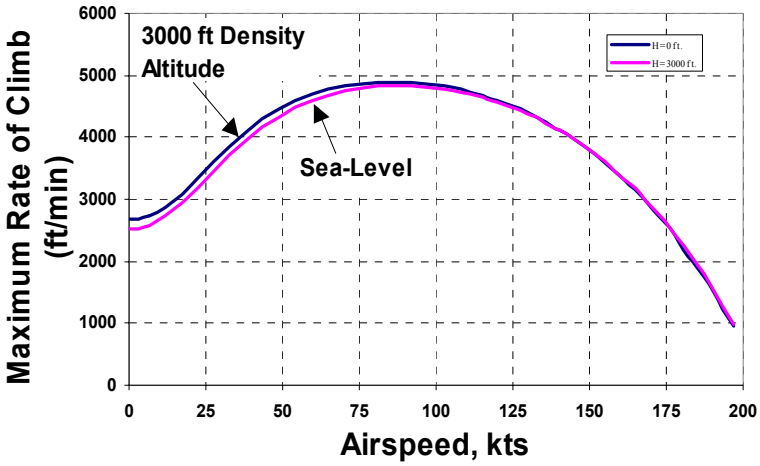

Figure 15.5: Maximum rate of climb as a function of airspeed

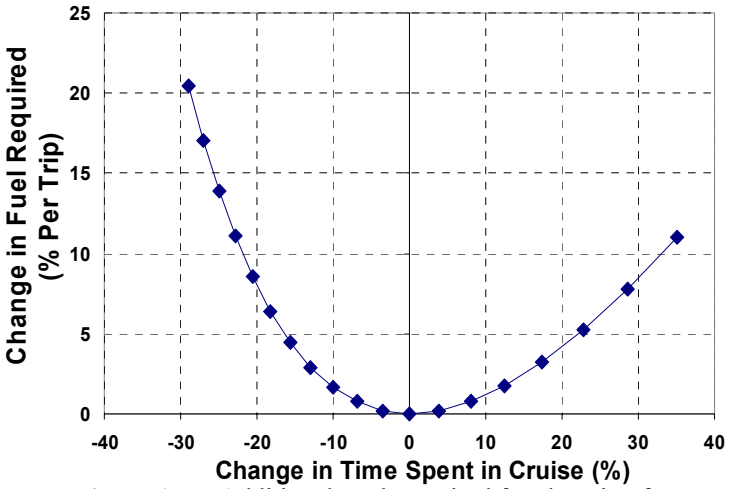

Figure 15.7: Additional Fuel Required for changing from Optimal Cruise Speed

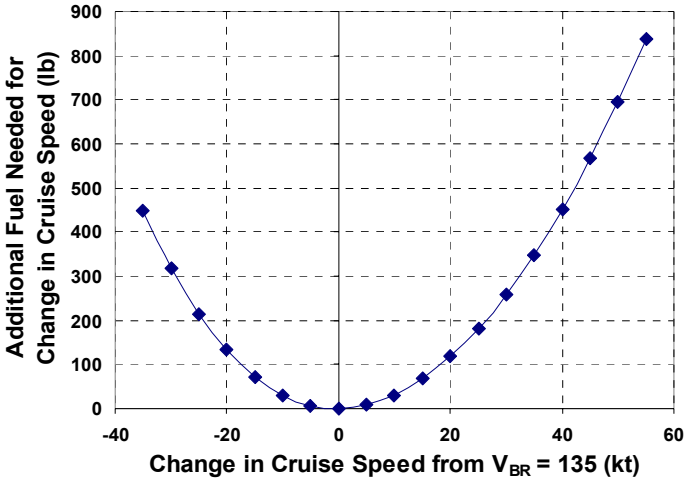

Figure 15.6. Additional Fuel Required for changing from Optimal Cruise Speed

speed is governed by swashplate limits as mentioned in handling qualities (section 9).

The maximum rate of climb (ROC) is estimated by dividing the excess power available by MGTOW. This ROC coincides with the speed for maximum endurance, and is plotted in Figure 15.5. At sea level, the maximum ROC at MGTOW is 4820 ft/min at 81 knots. This exceptional ROC does not take into account changes in fuselage attitude, which in reality changes with climb rate and airspeed. It should be noted that the maximum ROC marginally decreases and the speed for maximum endurance increases as the helicopter is climbing due to the change in density altitude.

15.3.1 Return trip (Without FCS)

For the return trip from the objective landing zone, the helicopter will be flying without the 20-ton payload and with 55% less fuel. Under these conditions, the Atlas will be flying at 58% MGTOW, which leads to a smaller V_{BR} of 135 kt. The speed is reduced because in level flight, without payload, the lift to drag ratio of the helicopter is significantly reduced. The rotor must provide more propulsion to lift, thereby decreasing the efficiency of the rotor. Additionally, the cruise speed is low due to the lower power setting, which results in a high specific fuel consumption. The amount fuel required is higher when the cruise speed is different from V_{BR}. Figure 15.6 shows the additional fuel required for the return trip for different cruise speeds. Figure 15.7 shows the impact on the mission time from cruising at a higher speed. It is seen that an increase in cruise speed from 135 kt to 160 kt results in an increase of fuel of about 190 lb per 125 nm (4% increase) per return trip. However, increasing the speed results in a

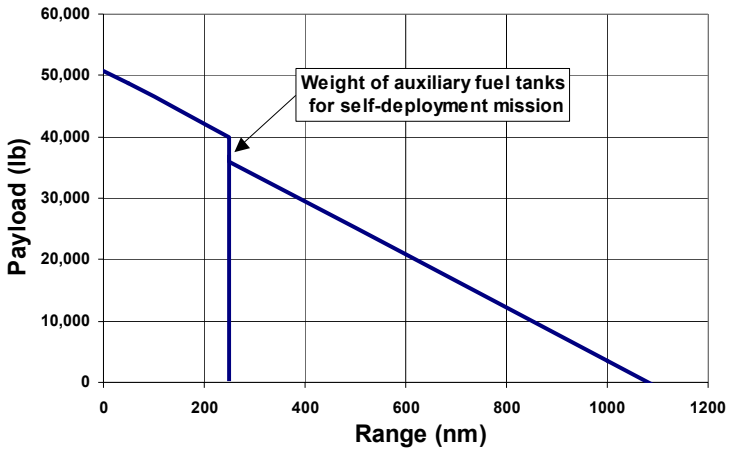

Figure 14.8: Payload-Range Diagram

reduction of 0.75 hr (15%) of the mission time spent in cruise, including the time to cruise between the CVN and L-Class ships at the beginning and end of the mission. Thus, a return cruise speed of 160 kt is recommended for this mission.

15.4 Mission Capability

The RFP requires that the design have a self-deployment capability up to 1000 nm for intra-theater combat. Using a total auxiliary fuel tank weight of 4000 lb, it was calculated that the Atlas can fly 1079 nm at 3000 ft density altitude without refueling, with a 20-minute fuel reserve at V_{BR} (Figure 15.8). The power and fuel requirements are also calculated for each segment of the defined mission. The results are shown in Table 15.2.

Table 15.2: Power and Fuel Requirements

	Power Setting (% installed)	Airspeed (kt)	Altitude (ft)	Time (hr)	Rate (ft/min)	SFC (lb/hp/hr)	Power (hp)	Fuel Flow (lb/hr)	Fuel Used (lb)
Outbound Segment									
HOGE	63%	0	0	0.02		0.371	14948	5538.5	92.3
Climb	63%	81	0	0.03	4890	0.371	14948	5538.5	138.5
Cruise	45%	145	3000	0.86		0.407	10755	4380.6	3776.4
Loiter	32%	81	3000	0.25		0.456	7863	3581.8	895.4
HOGE	65%	0	3000	0.05		0.368	15426	5670.7	283.5
							Outbound Fuel		**5143.4**
Return Segment									
Climb	32%	70	0	0.01	5870	0.461	7640	3520.3	62.1
Fast Cruise	44%	160	3000	0.78		0.412	10349	4268.4	3334.7
HOGE	32%	0	0	0.03		0.461	7640	3520.3	117.3
Loiter Res.	19%	70	500	0.33		0.594	4444	2637.4	879.1
			Total	**2.30**			**Inbound Fuel**		**4353.6**
							Total Fuel		**9497.0**
							% Fuel for OB		**54.2**

Section 16: Additional Applications and Capabilities

The Atlas can be equipped to perform many other potential missions, such as firefighting, medical evacuation, troop transport, high altitude logistics, minesweeping and can also be modified for civil cargo and passenger transport.

For future naval mine detection, the helicopter may be equipped with an Airborne Laser Mine Detection System (ALMDS). This system employs an externally-mounted solid-state laser a receiver system, and a power monitor circuit for real time laser health monitoring [Kush03].

The cargo bay may be reconfigured for emergency medical evacuation as well. Stoke's stretchers, frequently used in military applications, can be attached to hard points on the floor and fixed to the fuselage bulkheads. Additional medical equipment, such as life support and cardiac monitors, can be attached to hard points on the cargo bay floor. In a double-stack configuration, the Atlas can carry 12 litters. As a troop transport, the Atlas can carry 44 Category II fully- equipped soldiers, each weighing 300 lb. Seats (17.75" deep, 21" wide) may be fastened to hard points in the cargo area, while 24" wide aisles separate the rows (Foldout 7.2). The cabin is large enough to accommodate civil cargo and can be retrofit for civil

passengers. Because the Atlas has a hover ceiling of 12,500 ft and 23,000 ft in the loaded and unloaded condition, respectively, the aircraft is perfect for high altitude missions, such as operations in Afghanistan.

The Atlas also has the capability of sling loading. Sling load paths are carried through attachment points on the primary cargo bulkheads In this configuration, the Atlas can perform fire suppression missions by employing 20-ton Bambi Buckets or the 15-ton VSU-15 bucket, developed for the Mi-26 [Bamb05][VSU05]. The system has a lower operating cost as compared to that of a fixed wing firefighting aircraft. An electronic control system allows for hook rotation and simultaneous or independent release of the loads. The system provides aerial delivery of up to 5,200 USG of water, or may be equipped with automatic foam injection for increased capability. Overall, the Atlas is a versatile aircraft that can efficiently perform numerous civil and military missions.

Section 17: Conclusions

The Atlas is a heavy lift military transport helicopter designed for safe shipboard operations and flexible cargo-handling capability, both internal and external. The design proposal has focused on low acquisition and operating costs by minimizing empty weight and maintenance with high-value components. The Atlas features a three-engine power plant, an innovative, compact, lightweight face-gear transmission system and a robust rotor design capable of a high turn rate in cruise and continuous OEI capability. The compact elastomeric hub, active trim system and HUMS integration provide drastic improvement in maintenance costs over current helicopters. The all composite main rotor blades utilize tailored couplings to significantly reduce both vibrations and power in flight. Both the main rotor and tail boom employ push-button, fail-safe automatic folding. A low-vibration cabin environment is provided by LIVE MR dampers, incorporated throughout the airframe. The lightweight composite fuselage integrates state-of-the-art Electromagnetic polymer armor for the cockpit. The helicopter cargo area is rear loading with adequate clearance for care-free loading of any FCS vehicle, while roller and tread ways provide a flexible cargo loading platform. The mission equipment, including advanced auto-navigation, MMR, FLIR and IR/RF countermeasures gives the pilot unsurpassed situational awareness, minimal workload in all weather and night operations and security from hostile action.

The Atlas provides performance at and above the RFP requirements, including: (i) continuous OEI HOGE with payload, (ii) Ceiling of 12,500 ft, (iii) Cruise speed of 145 kt at 3000 feet with full payload, (iv) Intra-theater deployment range of 1000 nm, (v) Endurance of 2.8 hours with full payload, (vi) Maximum rate of climb of 4800 ft/min, (vii) Capable of transporting one FCS vehicle or two 463L pallets, (viii) Shipboard compatibility with CVN hangar deck access.

A high degree of modularity from efficient design may allow the helicopter to perform a range of other civil and military missions, such as cargo and personnel transport, mine sweeping, firefighting, medical evacuation and high altitude logistics. The innovative and economical Atlas helicopter is the ideal platform for present and future heavy lift operations.

Appendix A: MIL-STD-1374 Weight Summary

MIL-STD-1374 PART 1 PAGE 1
NAME UMD MODEL ATLAS
DATE 30 MAY 2005 REPORT

GROUP WEIGHT STATEMENT
AIRCRAFT
(INCLUDING ROTORCRAFT)
ESTIMATED – CALCULATED – ACTUAL
(CROSS THOSE NOT APPLICABLE)

CONTRACT NO

AIRCRAFT, GOVERNMENT NO.

AIRCRAFT, CONTRACTOR NO.

MANUFACTURED BY

	MAIN	AUX
ENGINE QUANTITY	3	
ENGINE MANUFACTURED BY		
ENGINE MODEL		
ENGINE TYPE		
PROPELER QUANTITY		
PROPELLER MANUFACTURED BY		
PROPELLER MODEL		

PAGES REMOVED PAGE NO.

MIL-STD-1374 PART 1 **GROUP WEIGHT STATEMENT** PAGE 2
NAME UMD **WEIGHT EMPTY** MODEL ATLAS
DATE 30 MAY 2005 REPORT

15	ROTOR GROUP						
16	BLADE ASSEMBLY			5942			
17	HUB & HINGE	(FOLD WT _____LBS)		3803			
19	EMPENNAGE GROUP	CANARD	HORIZ. STAB.	VERTICAL FIN	VENTRAL FIN	TAIL ROTOR	
20	TOTAL						
21	BASIC STRUCTURE		115	250			
22	SECONDARY STRUCTURE						
23	CONTROL SURFACES						
24	(INCL. BALANCE WEIGHTS)	( )	( )	( )			
25	BLADES					368	
26	HUB & HINGE					452	
27	ROTOR / FAN DUCT & ROTOR SUPTS						
30	FUSELAGE GROUP				FUS./HULL	BOOMS	
31	TOTAL						
32	BASIC STRUCTURE				13309	1000	
33	SECONDARY STRUCTURE						
34	ENCLOSURES, FLOORING, ETC.						
35	DOORS, RAMPS, PANELS & MISC.				1250		
38	ALIGHTING GEAR GROUP TYPE TRICYCLE	MAIN	NOSE / TAIL		ARR. GEAR	CAT. GEAR	
39	TOTAL	2696	675				
40	RUNNING GEAR / FLOATS / SKIS						
41	STRUCTURE						
42	CONTROLS						
57	TOTAL STRUCTURE						21895

* LANDING GEAR "TYPE": INSERT "TRICYCLE", "TAIL WHEEL", "BICYCLE", "QUADRICYCLE", OR SIMILAR DESCRIPTIVE NOMENCLATURE.
** WING, FUSELAGE, ETC.

MIL-STD-1374 PART 1 **GROUP WEIGHT STATEMENT** PAGE 3
NAME UMD **WEIGHT EMPTY** MODEL ATLAS
DATE 30 MAY 2005 REPORT

58	PROPULSION GROUP		AUXILIARY		MAIN		
59	ENGINE				906	906	906
60	ENGINE INSTALLATION				2991		
68	LUBRICATING SYSTEM						
69	FUEL SYSTEM				950		
70	TANKS - PROTECTED				250	250	
74	DRIVE SYSTEM						
75	GEAR BOXES, LUB SYS & RTR BRK				8737		
76	TRANSMISSION DRIVE						
77	ROTOR SHAFT						
78	GAS DRIVE						
80	FLIGHT CONTROLS GROUP				1396		
81	COCKPIT CONTROLS						
84	AUXILIARY POWER GROUP				115		
85	INSTRUMENTS GROUP						
86	HYDRAULIC GROUP				271		
	FIRE PROTECTION GROUP				886		
88	ELECTRICAL GROUP				2357		
89	AVIONICS GROUP						
90	EQUIPMENT				1200		
91	INSTALLATION						
92	ARMAMENT GROUP	(INCL. PASSIVE PROTECTION (			LBS.)		
93	FURNISHINGS & EQUIPMENT GROUP						
94	ACCOMODATION FOR PERSONNEL				145.5		
95	MISCELLANEOUS EQUIPMENT						
98	ENVIRONMENTAL CONTROL GROUP				1144		
99	ANTI-ICING GROUP						
114	TOTAL WEIGHT EMPTY PG. 2 - 3						55375

* LANDING GEAR "TYPE": INSERT "TRICYCLE", "TAIL WHEEL", "BICYCLE", "QUADRICYCLE", OR SIMILAR DESCRIPTIVE NOMENCLATURE.
** WING, FUSELAGE, ETC.

SAWE RP NO. 8A - PART 1 **GROUP WEIGHT STATEMENT** PAGE 4
NAME UMD **USEFUL LOAD AND GROSS WEIGHT** MODEL ATLAS
DATE 30 MAY 2005 REPORT

115	LOAD CONDITION						
117	WEIGHT EMPTY	55375					
118	CREW (QTY 3)	600					
119	UNUSABLE FUEL (TYPE ____) (GALS ____)	100					
120	OIL (TYPE ____) (GALS ____)						
121	TRAPPED	50					
122	ENGINE	686					
140	CHAFF (QTY _____)	50					
141	FLARES (QTY _____)	50					
150	OPERATING WEIGHT						
151	PASS. / TROOPS (QTY 2) (WT. EA. 220)	440					
153	CARGO	40000					
164	ZERO FUEL WEIGHT						97859
165	USABLE FUEL TYPE LOC GALS						
166	INTERNAL	10868					
167							
168	EXTERNAL						
169							
170	TOTAL USEFUL LOAD	53352					
171	GROSS WEIGHT						108727

References:

[Airc02] *Aircraft Tire Data Book*. Goodyear Corporation. 2002.

[AirF00] Air Force Instruction 11-2C-130. *C-130 Operations Configuration/Mission Planning*. Apr 2000.

[Alde03] Aldemir. *J. Sound and Vibration*, Vol. 266 (4), Sept 2003. pp 847–874.

[Alex86] Alex and McCoubrey. *J. American Helicopter Society*. Apr 1986. pp 345–359.

[AR5670] *AR-56: Structural Design Requirements (Helicopters)*. Naval Air Systems Command. 1970.

[Bain00] Bain and Orwig. *3rd Annual System Engineering & Supportability Conf*. Aug 2000.

[Bamb05] http://www.sonnet.com/usr/wildfire/varidump.html . May 2005.

[Bao03] Bao *et. al*. *Proc. 44th AIAA/ASME/ASCE/AHS/ASC Conf*. Apr 2003.

[Beau05] Beauclair. *J. Air & Cosmos*, No. 1980. Apr 2005.

[Berg98] Berg and Wellstead. *J. Intelligent Material Systems and Structures*. Vol. 9 (8). 1998. pp 592–600.

[Bous03] Bousman. *NASA TP-2003-212265, AFDD/TR-04-003*. Dec 2003.

[Bryn98] Byrnes and Milne. US Patent 5810562. Sept 1998.

[Chab93] Chabot and Brescia. *25th Intl. SAMPE Technical Conference*. Oct 1993. pp 431–443.

[Chai96] Chai and Mason. *6th AIAA/NASA/ISSMO Symp*. 1996. pp 525–540.

[Choi03] Choi and Wereley. *J. Aircraft*. Vol. 40 (3). 2003. pp 432–439.

[Cock85] Cocking. *Vertica*. Vol. 10 (2). 1986. pp 213–225.

[Colu05] Colucci. *Aviation Today*. May 12, 2005.

[Covi81] Covington *et. al*. US Patent 4527739. 1981.

[Crib99] Cribbs and Friedmann. *Proc.40th AIAA/ASME/ASCE/AHS/ASC Conf*. Apr 1999.

[Curr88] Currey. *Aircraft Landing Gear Design.* AIAA Education Series. 1988.

[Desi05] http://www.designation-systems.net/. 2005.

[DRST05] http://www.drs.com/products/index.cfm?gID=21&productID=367. 2005.

[Dudl94] Dudley, D. W. *Handbook of Practical Gear Design*. CRC Press LLC. 1994.

[Engi74] *Engineering Design Handbook: Helicopter Engineering Pt. 1*. AMCP 706-201. 1974

[Epps01] Epps and Chopra. *Smart Materials and Structures*. Vol. 10 (1). Feb 2001.

[Ferr05] Ferrier, *et. al*. *AHS Specialists Meeting on Unmanned Rotorcraft Design, Control and Testing*. 2005.

[Fill02] Filler, *et. al*. *Proc. 58th American Helicopter Society Intl. Forum*. June 2002.

[Giur97] Giurgiutiu and Rogers. *Proc. 38th Structures, Structural Dynamics and Materials Conference*. 1997.

[Glob05] http://www.globalsecurity.org/military/. 2005.

[Gmir04] Gmirya, *et. al*. *Proc. 60th American Helicopter Society Forum*. June 2004. pp 1221–1228.

[Harr97] Harris and Scully. *Proc. 53rd American Helicopter Society Forum*. May 1997. pp 1575–1608.

[Hess01] Hess, *et. al*. *Proc. IEEE Aerospace Conference*. 2001.

[Hirs01] http://www.vtol.org/IHPTET.HTM. May 2005.

[Hunt97] Hunter, *et. al*. US Patent 5601408. 1997.

[Jack95] Jackson, P. *Jane's All the World's Aircraft 1995–96*. Jane's Publishing Co Ltd. 1995.

[Jack04] Jackson, P. *Jane's All the World's Aircraft 2004–05*. Jane's Publishing Co Ltd. 2004.

[Keys79] Keys. *Rotary-Wing Aerodynamics: Volume II*. NASA Contractor Report 3083. 1979.

[Key98] Key. *Proc. 54th American Helicopter Society Forum.* May 1998.

[Kohl98] Kohlgruber and Weissinger. DLR-IB 435-98/22, June 1998.

[Kran96] Krantz and Delgado. NASA TM-107202. 1996.

[Kubo01] Kubo, *et. al*. *Proc. 57th American Helicopter Society Intl. Forum*. 2001.

[Kush03] Kushina, *et. al*. *Proc. SPIE*. Vol. 4968. 2003.

[Liqu05] http://www.liquidmetal.com/applications/dsp.defense.asp. 2005.

[Leis00] Leishman, J.G., *Principles of Helicopter Aerodynamics*, Cambridge University Press. 2000.

[Lord05] http://www.lord.com. May 2005.

[Lynn69] Lynn, *et. al*. *J. American Helicopter Soceity*. Vol 15 (4). 1969.

[Mass88] Massey and Wells. *Rae Soc. Conf. on Handling Qualities and Control*. Nov 1988.

[Math01] Mathews, *et. al*. *J. Guidance, Control, and Dynamics*, Vol. 25 (2). Mar-Apr 2002.

[MB01] Data sheet #006 S92. Martin-Baker Design Office. Aug 2001.

[McLe90] McLean. *Automatic Flight Control Systems*. Prentice Hall International. 1990.

[Milw53] Milwitzky and Cook. "Analysis of Landing Gear Behavior." NACA Report 1154, 1953.

[Moog05] http://www.polysci.com. May 2005.

[NASA05] "NASA Heavy Lift Study Engine." NASA Heavy-lift Rotorcraft Systems Investigation. 2005.

[Niu88] Niu. *Airframe Structural Design*. Conmilit Press Ltd. 1988.

[NOI05] http://www.chinfo.navy.mil/navpalib/policy/vision/vis04/top-v04.html. 2005.

[Padf96] Padfield. *Helicopter Flight Dynamics*. AIAA Educational Series, 1996.

[Prou98] Prouty. *Helicopter Stability and Control*. PWS Engineering. 1986.

[Rayt05] http://www.raytheon.com/. 2005.

[Rich03] Richardson, *et. al*. *Intl. J. Rotating Machinery*. Vol. 9 (1). 2003. pp 35–40.

[Rock05] http://www.rockwellcollins.com/. 2005

[Rosk04] Roskam, J., *Airplane Design Part IV*. DAR Corporation, 2004.

[Samu05] Samuel and Pines. *J. Sound and Vibration*. Vol. 282. 2005. pp 475–508.

[Schm76] Schmidt. *Proc. 35th Annual International Conference of SAWE*. May 1976.

[Sehg99] Sehgal. *Proc. 55th American Helicopter Society Forum*. May 1999.

[Shen04] Shen, *et. al*. *Proc. 45th AIAA/ASME/ASCE/AHS/ASC*. Apr 2004.

[Sing02] Singh. Master's Thesis. University of Maryland. 2002.

[Smir90] Smirnov, G. *Vertiflite*. Vol. 36 (3). Mar-Apr 1990. pp 20–23.

[Smit98] Smith. *Proc. 54th American Helicopter Society Forum*. May 1998.

[Smit99] Smith. *Proc. 55th American Helicopter Society Forum*. May 1999.

[Snap05] http://www.snap-titequickdisconnects.com/index.asp. June 2005.

[Stra04] Straub, *et. al*. *J. Intelligent Material Systems and Structures*. Vol. 15. Apr 2004. pp 249–260.

[Tate94] Tate and Padfield. *Proc. 50th American Helicopter Society Forum*. May 1994.

[Tayl87] Taylor. *Jane's All the World's Aircraft 1987–88*. Jane's Publishing Co. Ltd. 1987.

[Thui99] Thuis. Report NLR-TP-99026. National Aerospace Laboratories, The Netherlands, 1999.

[Tish76] Tishchenko and Radin. *Helicopters Selection of Design Parameters*. Mashinostroyeniye Press. 1976.

[Tish00] Tishchenko. *Vertiflite*. Summer 2000.

[Tish03] Tishchenko, *et. al*. *J. American Helicopter Society*. Vol. 48 (2). Apr 2003. pp. 71–79

[Tish05] Tishchenko. "ENAE 634 Class Notes." University of Maryland. May 2005.

[Ubel02] Ubels and Wiggenraad. *1st European Workshop on Survivability*. Feb 2002.

[UMCP99] American Helicopter Society Student Design Competition entry. U. Maryland. 1999.

[UMCP04] American Helicopter Society Student Design Competition entry. U. Maryland. 2004.

[USAr05] http://jtrs.army.mil. 2005.

[USNa05] http://enterprise.spawar.navy.mil/pmw156/int-sys.htm. 2005.

[Venk99] Venkatesan and Udayasankar. *J. Aircraft*. Vol 36 (2). Mar-Apr 1999.

[VSU05] http://www.mtu-net.ru/mosseev/firetank.htm , May 2005.

[Whit05] http://www.whitehydraulics.com. May 2005.

[Will89] Wille. *Proc. 48th Annual International Conference of SAWE*. 1989.